

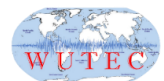
Wutec Geotechnical International

**FINITE ELEMENT DYNAMIC ANALYSES  
OF  
AUSTRIAN DAM**

Prepared by

G. Wu, Ph. D., P.Eng.

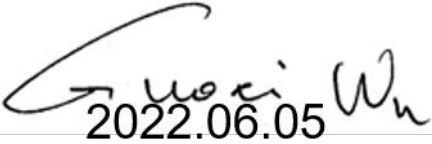
February 24, 2022



Report No. WGI-220224  
February 24, 2022

*Not to be reproduced without the permission of WGI*

WGI-220224  
2022-02-24



2022.06.05  
by

Guoxi Wu, Ph.D., P.Eng.

Wutec Geotechnical International  
Email: [gwu@wutecgeo.com](mailto:gwu@wutecgeo.com)

Report No. WGI-220224  
February 24, 2022

# FINITE ELEMENT DYNAMIC ANALYSES OF THE AUSTRIAN DAM

## TABLE OF CONTENTS

Section	Subject	Page
1.0	INTRODUCTION.....	- 1 -
2.0	AUSTRIAN DAM AND THE DAMAGES IN LOMA PRIETA EARTHQUAKE .....	- 2 -
3.0	EMBANKMENT DAM FILLS AND THE UNDRAINED SHEAR STRENGTH .....	- 5 -
4.0	STATIC STRESSES OF THE DAM PRIOR TO THE EARTHQUAKE	- 8 -
5.0	DYNAMIC ANALYSIS OF AUSTRIAN DAM: A TOTAL STRESS APPROACH.....	- 13 -
	5.1 General Methodology .....	- 13 -
	5.2 Input Ground Motions .....	- 14 -
	5.3 VERSAT-2D Soil Constitutive Models.....	- 16 -
	5.4 Results of Total Stress Dynamic Analysis: Case 1a.....	- 21 -
6.0	RESULTS OF PARAMETRIC ANALYSES .....	- 26 -
	6.1 Suitability of Input Ground Motions .....	- 27 -
	6.2 Dam Crest Acceleration Response Spectra .....	- 30 -
	6.3 Sensitivity of Phreatic Surface and Other Parameters .....	- 33 -
	6.4 Selection of Undrained Shear Strength Values .....	- 34 -
	6.5 Methods of Using Undrained Shear Strengths in Analysis ....	- 35 -
	6.6 Effect of Dam Foundation Rock Stiffness on Response .....	- 37 -
	6.7 Effect of Shear Wave Velocity of the Dam Fills on Response-	40 -
7.0	DISCUSSION.....	- 40 -
8.0	CONCLUSIONS.....	- 41 -
	ACKNOWLEDGMENTS 致谢.....	- 42 -
	REFERENCE .....	- 42 -
APPENDIX A	BACKGROUND INFORMATION .....	
APPENDIX B	INPUT EARTHQUAKE RECORDS: LEX & CLS.....	
APPENDIX C	SECTION A-A' GEOMETRY AND PHREATIC SURFACES .....	
APPENDIX D	VERSAT-2D INPUT AND OUTPUT FILES .....	
	Input File 1 Build the Dam in Dry .....	
	Input File 2 Add Reservoir Water.....	
	Output from Input File 2.....	
	Input Files 3 and 4 for Earthquake Loading .....	
	Output File from Input File 4 for Earthquake Loading .....	
APPENDIX E	FULL SIZE FIGURES .....	

|

## FINITE ELEMENT DYNAMIC ANALYSES OF THE AUSTRIAN DAM

### 1.0 INTRODUCTION

The Austrian dam, constructed in 1950, is a 55-m high compacted earthfill dam in California; the dam was heavily damaged by the 1989 Mw = 6.93 Loma Prieta earthquake. The earthen embankment dam consisted primarily of low plasticity clayey sands and clayey gravels; subjected to earthquake ground motions with estimated peak horizontal bedrock accelerations of 0.55-0.6g, the dam settled 0.76 m on average at its crest, developed extensive longitudinal cracks (up to 300 mm wide in one location) on both the upstream and downstream faces of the dam. The observed and measured dam displacements suggested that the dam had earthquake-induced internal movements related to lateral spreading of dam (Wahler Associates 1990; Harder et al. 1998). Earthquake ground motions were recorded in two nearby sites. This case history is of great value and can be used to calibrate current engineering procedures for nonlinear dynamic response history analysis and to evaluate currently available soil constitutive models for clayey soils.

In current study, the dynamic responses of the Austrian dam in the 1989 Loma Prieta earthquake were analyzed using the finite element computer program VERSAT-2D (WGI 2019), and undrained response of the saturated dam fills was modelled using a total stress approach. The total stress method of analysis, using the Mohr Coulomb failure criterion and various forms of hysteretic stress-strain relations, is a common method for dynamic analysis of undrained response involving clayey or cohesive soils; it is widely used in geotechnical engineering (Wu et al. 2006; Wu 2010; Ryan et al., 2013; Hadidi et al. 2014; Sweeney and Yan 2014; and others). The effective stress method of analysis, including calculation of earthquake-induced pore water pressure (PWP) during shaking and impact of the PWP on soil stiffness and strength, is becoming a standard approach for undrained response history analysis of sandy soils involving soil liquefaction and its induced large ground deformations (Wu 2001, 2015, 2018, 2021; Finn et al. 1986; Wu and Chen 2002; Sherstobitoff et al. 2004; Finn and Wu 2013; and many others), and it was adopted for clayey soils (Boulanger 2019) although it is less available than for sandy soils.

The difference between the VERSAT approach and other more complicated approaches (e.g., Boulanger 2019) is that the VERSAT analysis does not require

calibration of soil parameters ahead of a dynamic analysis, but it uses more fundamental parameters of soils such as  $V_s$  for stiffness, undrained shear strength  $S_u$ , friction angle ( $\phi'$ ) for shear strength, normalized SPT blow count  $(N_1)_{60}$  for liquefaction resistance, and residual strength if soil liquefies. The VERSAT approach is, in terms of soil parameters required, in kind of what an engineer would do when a limit equilibrium slope stability analysis is to be performed.

By presenting the analysis methodology and results of the analyses, this paper demonstrates the merits of using the VERSAT approach and its capability of capturing the key features of seismic performance for earthen dams in earthquakes, even in large earthquakes. The VERSAT approach would be more suitable for engineering analysis than for academic studies. Dynamic analyses of the dam were performed using the base-case model and the proposed  $S_u/\sigma'_m$  approach for calculating in-situ undrained strengths as well as sensitivity analyses on input ground motion, phreatic surface, undrained strength, and dam bedrock foundation stiffness on dynamic response of the dam. The computed responses are found to be in good agreement with the measured dam crest settlements and the observed lateral spreading deformation pattern. Limitations associated with the total stress analysis model, the input ground motions, the input soil parameters, and their potential implications on the analysis results are discussed.

## **2.0 AUSTRIAN DAM AND THE DAMAGES IN LOMA PRIETA EARTHQUAKE**

Austrian Dam, constructed in 1950, is a 55-m-high compacted earthfill dam located on Los Gatos Creek in Santa Clara County of California. At about 11 km from the earthquake epicenter as shown in Fig. 1, the dam was heavily damaged by 1989 Loma Prieta earthquake. As shown on the plan view of the dam (about 230 m in length) in Fig. 2, the earthfill dam experienced extensive cracking and deformation during the earthquake. Roughly parallel longitudinal cracks in the upper 15 m of the upstream and downstream faces were up to 100 mm wide shortly after the earthquake; cracks widened to as much as 300 mm at the surface and 4.3 m deep after a few of weeks. Noticeably, the standpipe for piezometer P-1 (located midway down the downstream face) was observed to be significantly deformed between elevations 291.1 and 292.6 m (or about 7.6–9.1 m above the bedrock), and the standpipe for piezometer P-6 (located at the dam crest) was deformed between elevations 310.2 and 317.2 m (about mid-height of the

dam). These movements were suggestive of earthquake-induced internal and deep deformations related to lateral spreading of the earthfill dam (Harder et al. 1998).

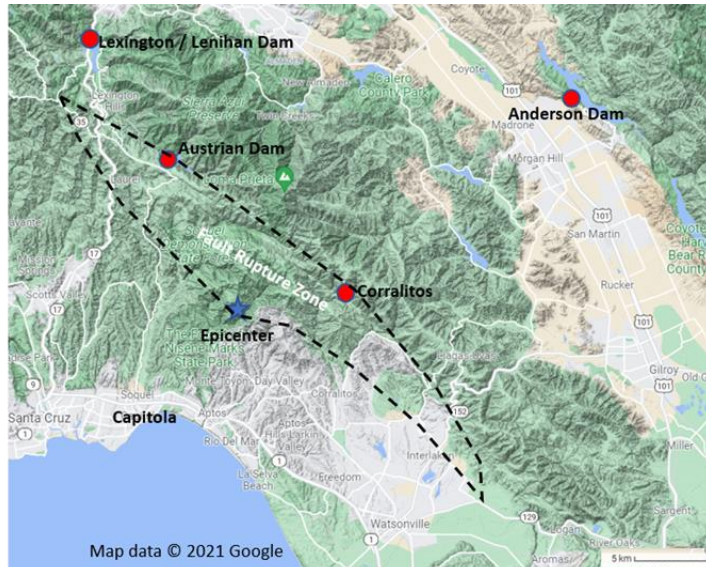


**Fig. 1.** The 1989 Loma Prieta earthquake fault rupture zone by Harder et al. (1998.) in relation to ground motion recording stations (the Lexington station and the Corralitos station) and the Austrian dam in California, US. (Map data © 2021 Google.)

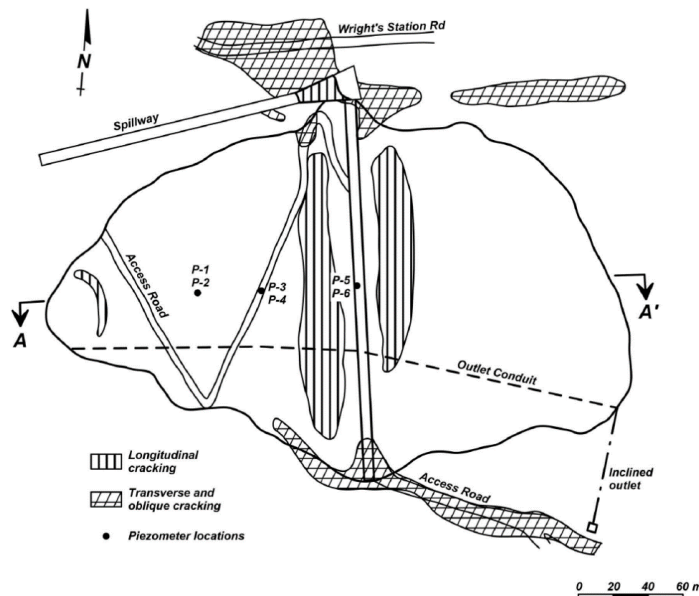


**Fig. 2.** Plan view with areas of cracking induced by the 1989 Loma Prieta earthquake and locations of piezometers at that time. (Adapted from Wahler Associates 1990; Harder et al. 1998; Boulanger 2019.)

Post-earthquake survey of survey monuments on the dam crest indicated an average dam crest settlement of 0.76 m (2.5 ft) along the central 170 m of the crest length (Harder et al. 1998). Because the survey monuments were not tied into a stationary benchmark, only relative horizontal displacements along the dam crest were measured; the survey results indicated that the right abutment appeared to move downstream horizontally 458 mm (1.5 ft) relative to the left abutment (Harder et al. 1998). In other words, the right end of the dam may have moved 305 mm (1 ft) in the downstream direction, while the left end of the dam could have moved 153 mm (0.5 ft) in the upstream direction.

The maximum cross section (A-A') of the dam is shown in Fig. 3. The dam was founded on bedrocks with crest width of 6.1 m and crest elevation of 343 m. The dam's upstream and downstream slopes range from 2.5:1 (horizontal to vertical) near the crest, transitioned to 3:1 in the middle of the slopes, and further flattened to 3.5:1 near the toes. Construction of the dam fills was carried out (with a compaction effort of DWR 20,000 ft · lb/ft<sup>3</sup>) by selective borrowing in an attempt to build an upstream impervious zone, a downstream pervious zone, and a gravel strip drain (see Fig. 3). However, post construction study and sampling of the dam fills indicated that there was no appreciable difference between the two zones, and the gravel drain was not completely effective in relieving the downstream seepage pressures (Harder et al. 1998). As such, it was considered reasonable to treat the entire dam consisting of homogeneous materials for analysis purpose.

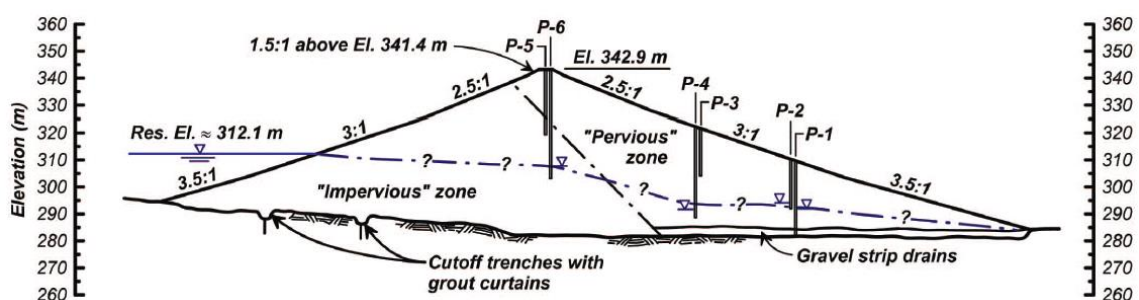


**Fig. 3.** Maximum cross-section (A-A') showing phreatic surface based on piezometer records. (Adapted from Wahler Associates 1990; Harder et al. 1998; Boulanger 2019.)



### 3.0 EMBANKMENT DAM FILLS AND THE UNDRAINED SHEAR STRENGTH

The dam fills of the Austrian dam consisted primarily of low-plasticity clayey sands (SC) and clayey gravels (GC) with gravel content (coarser than 4.75 mm) ranging from 26 to 72% (mean of 46%) and fines content (finer than 0.075 mm) ranging from 16 to 44% (mean of 32%). Soil classification, gradation, Atterberg limits and compaction test data are summarized in Table 1. Details of the dam construction and material properties were originally provided in Wahler Associates (1979, 1981) and then summarized in Harder et al. (1998) and also used in Boulanger (2019). The data were mostly based on field and laboratory investigation conducted in 1979 when undisturbed tube samples were taken from boreholes drilled on the dam faces; laboratory tests performed included soil index tests, grain size gradation analysis, isotropically consolidated undrained (ICU) triaxial compression tests for shear strength and resonant column tests for low-strain (or maximum) shear modulus.

During the repair work to the dam after the 1989 Loma Prieta earthquake, relative degree of compaction of the dam fills was further measured in the upstream shell of the dam and the results were compared with the dry densities determined by tests performed during the 1950 construction. The average compaction of 93% obtained from the 1989 verification testing indicated that compaction efforts of the 1950 construction were reasonable for the embankment dam fills (Wahler Associates 1990).

Of particular interest to the current study are the data from the ICU triaxial tests conducted in 1979 on six undisturbed tube samples. From the ICU triaxial test data, undrained shear strength ( $S_u$ ) was calculated and plotted in Fig. 4 against the consolidation stresses; a similar plot was also shown in Boulanger (2019). The  $S_u$  is defined as the shear stress on the eventual failure plane at failure, and failure occurs when the principal stress ratio ( $\sigma'_1 / \sigma'_3$ ) reaches its peak in shearing (Boulanger 2019). In common language, this is the shear stress of the point on a Mohr circle that touches the failure envelope; it is less than the maximum shear stress in the Mohr circle. In current study, the undrained shear strengths of the saturated dam fills are related to the consolidation stresses (the Lower and Middle strength lines);  $\sigma'_{3c}$  in Fig. 4 are the consolidated stresses used in ICU triaxial tests.

**Table 1.** Geotechnical properties of dam fills of the Austrian dam

Geotechnical Property	Range	Mean
USCS classification	SC, GC	-
Percent coarser than 4.75 mm (%)	26–72	46
Percent finer than 0.075 mm (%)	16–44	32
Specific gravity, $G_s$	2.60–2.78	2.70
Liquid limit	28–32	31
Plasticity index (PI)	11–15	13
Water content as compacted in 1950 (%)	9.5–19.5	14.5
Dry unit weight as compacted in 1950 (kN/m <sup>3</sup> )	16.9–20.8	19.0
Dry unit weight of samples in 1989 (kN/m <sup>3</sup> )	19.1–20.7	19.9
$K_{2max}^a$	106–128	122
Effective stress, $c'$ (kPa)	-	0
Effective stress, $\phi'$ (°)	-	44
Total stress failure envelope, $c$ (kPa)	-	14
Total stress failure envelope, $\phi$ (°)	-	21

Sources: Data from Wahler Associates (1979, 1981, 1990) and Harder et al. (1998).

<sup>a</sup> $K_{2max}$  is related to  $K_g$  in equation (3) as  $K_g = 21.7 K_{2max}$ ; thus  $K_g$  (mean) = 2647.

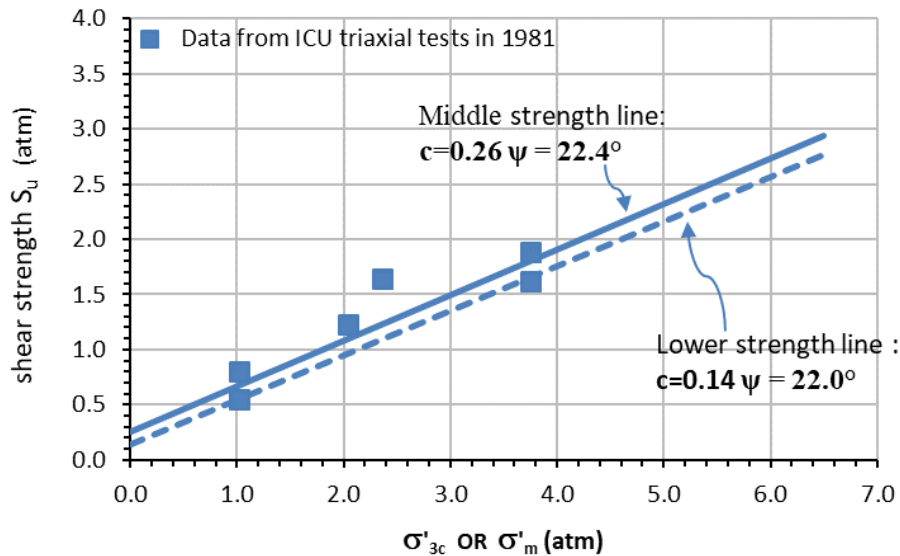


**Fig. 4.** Undrained shear strengths and the mean consolidation pressure ( $\sigma'_m$ ) derived from test data of the ICU triaxial test specimens (Data from Wahler Associates 1979, 1981; Boulanger 2019.)

For the in-situ pre-earthquake stress conditions, except these with  $K_0$  of 1.0, the soils are not isotropically consolidated. In the current study using the finite element method, the undrained shear strength of a saturated soil element is calculated using the following equation,

$$S_u = c + \sigma'_m \tan(\Psi) \quad (1)$$

$$\sigma'_m = (\sigma'_x + \sigma'_y + \sigma'_z) / 3 \quad (2)$$

where  $S_u$  is the undrained shear strength of a soil element;  $\sigma'_m$  is the mean consolidation pressure or stress at the soil element center prior to earthquake loading;  $\sigma'_x$  and  $\sigma'_y$  are the horizontal and vertical effective stresses, respectively, in two-dimensional (2D) plane strain finite element analysis presented in this study;  $\sigma'_z$  is the horizontal effective stress in the direction perpendicular to the 2D plane. The cohesion ( $c$ ) and the friction angle ( $\Psi$ ) are undrained strength parameters that would either be obtained from in-situ shear tests or determined from undrained direct simple shear tests; for the current study, they are derived as shown in Fig. 4 from the ICU triaxial compression test data.

Using the proposed  $S_u/\sigma'_m$  method, the computed  $S_u$  that are based on or anchored at the mean consolidation pressure ( $\sigma'_m$ ) are compared in Fig. 5 with the  $S_u$  calculated using the procedure adopted by Boulanger (2019). The Duncan and Wright (2005) procedure for evaluating slope stability with limit equilibrium method was extended and applied by Boulanger (2019) for his finite difference dynamic analysis of the Austrian dam. In general,  $S_u$  calculated using the proposed  $S_u/\sigma'_m$  method are lower (and thus more conservative) than  $S_u$  calculated using the procedure adopted in Boulanger (2019). The undrained shear strength  $S_u$  is about 10.5% lower at  $K_0 = 0.5$  regardless of the stress level. The difference narrows as  $K_0$  increases; at  $K_0 = 0.8$  the difference in  $S_u$  reduces to about 3% regardless of stress level. The proposed  $S_u/\sigma'_m$  approach might be more suitable for engineering practice as shown in the following dynamic analysis. The SHANSEP approach (Ladd and Foote 1974; Ladd and DeGroot 2004) or the  $S_u/p'$  approach (Duncan and Wright 2005) are often used for heavily over-consolidated fine-grained soils.

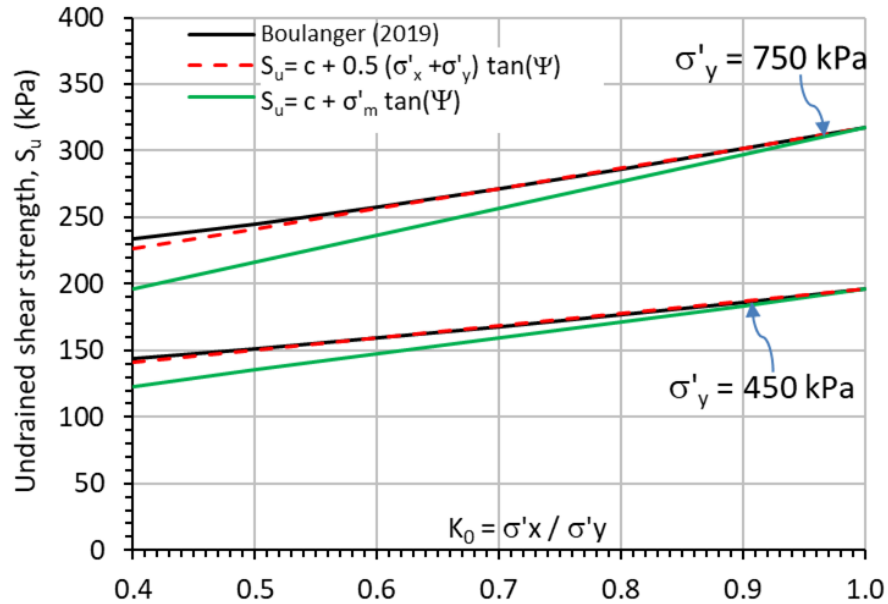


**Fig. 5** Undrained shear strength  $S_u$  of saturated dam fills illustrated for two stress levels:  $\sigma'_y = 450$  kPa and  $\sigma'_y = 750$  kPa. Note that  $c = 14$  kPa and  $\Psi = 22^\circ$  are used for all three methods;  $\sigma'_m$  is calculated with  $\sigma'_z = \sigma'_x$ ; and  $\phi' = 44^\circ$ ,  $K_f = 5.0$  and shear stress  $\tau_{xy} = 0$  are used in Boulanger (2019)

#### 4.0 STATIC STRESSES OF THE DAM PRIOR TO THE EARTHQUAKE

The total stress method of analysis is often adopted for evaluating seismic stability and deformation of embankment dams consisting in whole or in part of fine-grained soils (clays, silts), clayey sands or gravels (e.g., the Austrian dam fills), or glacial till core of low permeability in other dams. The advantage of performing a total stress analysis, by using  $S_u$  or the  $c-\phi$  parameters, is that there is no need to evaluate or determine the amount of earthquake-induced dynamic pore water pressures (PWP) and their impact on shear strengths of these soil materials. However, in order to adequately determine the undrained shear strengths of saturated soils, the method requires a sound evaluation of the past maximum consolidation pressure,  $\sigma'_p$ ; this is more relevant to foundation soils (than to dam fills) as they are more likely to be over-consolidated due to their long geological history.

The dam fills at the Austrian dam are considered to be normally consolidated or lightly over-consolidated with an over-consolidation ratio (OCR) of less than 2 to 4; it is adequate to estimate the undrained shear strength of the saturated dam fills from the ICU

triaxial tests by relating the current in-situ effective stresses to the consolidation pressures applied in the ICU triaxial tests.

At the time of Loma Prieta earthquake in 1989, the reservoir water level was about 30 m below the dam crest, and the water levels measured on October 16, 1989 (one day before the earthquake) in piezometers (P-1, P-2, P-4 and P-6) were low as shown on Fig. 3. The other two piezometers (P-3 and P-5) were dry in 1989. The reservoir level had been at similarly low for 3-4 years prior to the earthquake because of drought conditions.

The post-earthquake piezometer recordings indicated that the earthquake-induced pore water pressures (PWP heads increased 15.2 m in P-6 and 16.8 m in P-1 two days after the earthquake) dissipated relatively slowly; the PWP heads dropped about 7.5 m from 15.2 m in P-6 and about 1.3 m from 16.8 m in P-1. The PWP reduction in P-1 was only about 8% over a period of 10 days. The water level at P-2 rose about 3.2 m after the earthquake and the level remained almost the same over a period of approximately two months (Wahler Associates 1990; Harder et al. 1998). The observed slow rate of PWP dissipation suggest that the PWP immediately after the earthquake may have been 0%–10% greater than the values measured two days after the earthquake, and that essentially undrained loading conditions existed during the earthquake loading (Boulanger 2019). These piezometer data provide a basis for assumptions to be made on the phreatic surface of the dam at the time of earthquake for assessing the in-situ effective stresses of the dam.

The static stresses of the dam were calculated using the finite element computer program VERSAT-2D for 2D plane strain analysis (WGI 2019). For static stress analysis, VERSAT-2D employs an elastic perfectly plastic model with the Mohr-Coulomb failure criterion. Prior to failure, the shear modulus is modelled as linear and strain-level independent; however, the stress-level dependency of soil stiffness (shear and bulk moduli) is allowed by using equations (3) and (4) for calculating the two moduli as are used for the dynamic analysis (see the following sections). The shear and bulk modulus constants ( $K_g$  and  $K_b$ ) have much lower values than these for dynamic analyses; these constants for static analysis are equivalent to the elasticity parameters (e.g., Young's modulus and Poisson's ratio) that can be obtained from laboratory oedometer compression tests and sometime from triaxial shear tests.

The finite element model of the maximum cross section (see Fig. 3) is shown in Fig. 6 that included the finite element mesh grid size (generally 1 m vertical by 1.5 m horizontal), soil material zones, and the phreatic surface used in analysis. The finite

element mesh has a total of 7258 nodes and 7072 elements with 4 nodes in each element. Soil material MAT-1 (in yellow color) is for dam fills that are above the phreatic surface and unsaturated with a unit weight of  $21.0 \text{ kN/m}^3$ ; MAT-3 has identical mechanical properties as MAT-1 but is shown in blue color to represent the dam crest. MAT-5 (in orange color) is used for dam fills below the phreatic surface and thus saturated with a unit weight of  $22.4 \text{ kN/m}^3$ ; MAT-4 has identical mechanical properties as MAT-5 but is shown in green color to identify the location and extent of the gravel strip drain. MAT-2 (in red color) is used to model the portion of foundation bedrocks that is higher than the model base at elevation 282 m.

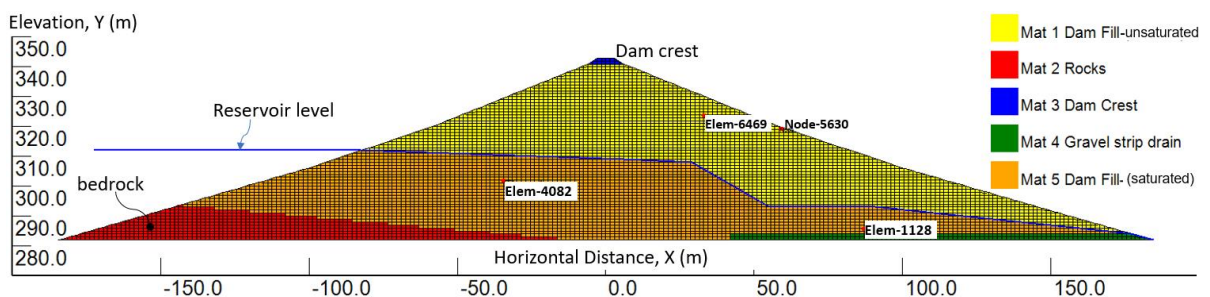


**Fig. 6** VERSAT-2D finite element model of the Austrian dam with finite element grids, soil and rock zones, reservoir water level and phreatic surface

In the static stress analysis of the Austrian dam,  $K_g = 530$ ,  $K_b = 2650$ , and parameters  $m = n = 0.5$  in equations (3) and (4), were used for all dam fills (i.e., MATs 1, 3, 4 and 5). The adopted ratio of the bulk and shear moduli ( $K_b/K_g = 5.0$ ) implies that a Poisson's ratio of 0.41 has been applied to the dam fills. The drained shear strength parameters with zero cohesion ( $c' = 0 \text{ kPa}$ ) and a friction angle of  $\phi' = 44^\circ$  were used for the dam fills associated with the Mohr Coulomb failure criterion.

The analysis steps taken in VERSAT-2D static stress analysis were as follows:

- Step 1, build the dam in layers (5 m thick each layer, vertically consisting of five 1-m high soil elements in the layer and horizontally including all elements across the dam) to simulate the fill placement sequence and the compaction loads applied in each layer. The stress-level dependent elasticity moduli (soil stiffness) are updated after each 5-m thick layer is added onto the model.
- Step 2, apply the reservoir water level (at elevation 312 m) and the phreatic surface (elevation 309 m at  $X = 3 \text{ m}$ ; elevation 308 m at  $X = 29 \text{ m}$ ; elevation 293 m at  $X = 55 \text{ m}$ ; elevation 293 m at  $X = 91 \text{ m}$ ; and El 284 m at  $X = 177 \text{ m}$ )

that is near the downstream toe of the dam). This included hydrostatic water pressures in soils and the water loads from reservoir water on the upstream face of the dam. In order to maintain adequate stability of the embankment dam slope, the hydrostatic water pressures and water loads were applied in increments (nine increments were used in this study). The incremental loading process (or unloading due to water buoyancy) is an essential analysis element needed to achieve the required convergence in a nonlinear analysis involving plasticity and flow rule. Each of the load increment was considered complete if the total unbalanced force of the entire model is less than 0.5 kN.

The phreatic surface (water table) was applied as a piezometric surface; the pore-water pressure was computed as the vertical distance from the piezometric line to the point of interest, multiplied by the unit weight of water. When there is no vertical seepage gradient, this approach is a reasonable approximation (USBR 2019). The phreatic surface used in here are these measured water levels in the piezometers P-6, P-4 and P-1 (one day before the earthquake); an assumption was made that the large drop in phreatic water level between P-6 and P-4 occurred at the midway between the two piezometers as there was no measurement.

The calculated static stresses in the 2D plane are shown in Figs. 7(a, b, c) for vertical effective stresses  $\sigma'_y$ , coefficient of horizontal stress  $K_0$  ( $=\sigma'_x / \sigma'_y$ ), and shear stresses ( $\tau_{xy}$ ), respectively. The vertical effective stresses are about 600-750 kPa for the upper half of the saturated dam fills under the dam crest below the water table, the lower half of the saturated dam fills are about 750- 900 kPa. The horizontal stress coefficients ( $K_0$ ) are between 0.48 and 0.52 for the same upper part and increase to about 0.55-0.65 for the lower part; in general, the  $K_0$  increase with depth and from the center (directly under the crest) to the areas under the upstream and downstream slopes. For saturated soils in the downstream slope, the  $K_0$  are mostly about 0.7-0.8 (in yellow color); on the reservoir side in the upstream slope, the  $K_0$  are slightly higher at about 0.7-1.0.

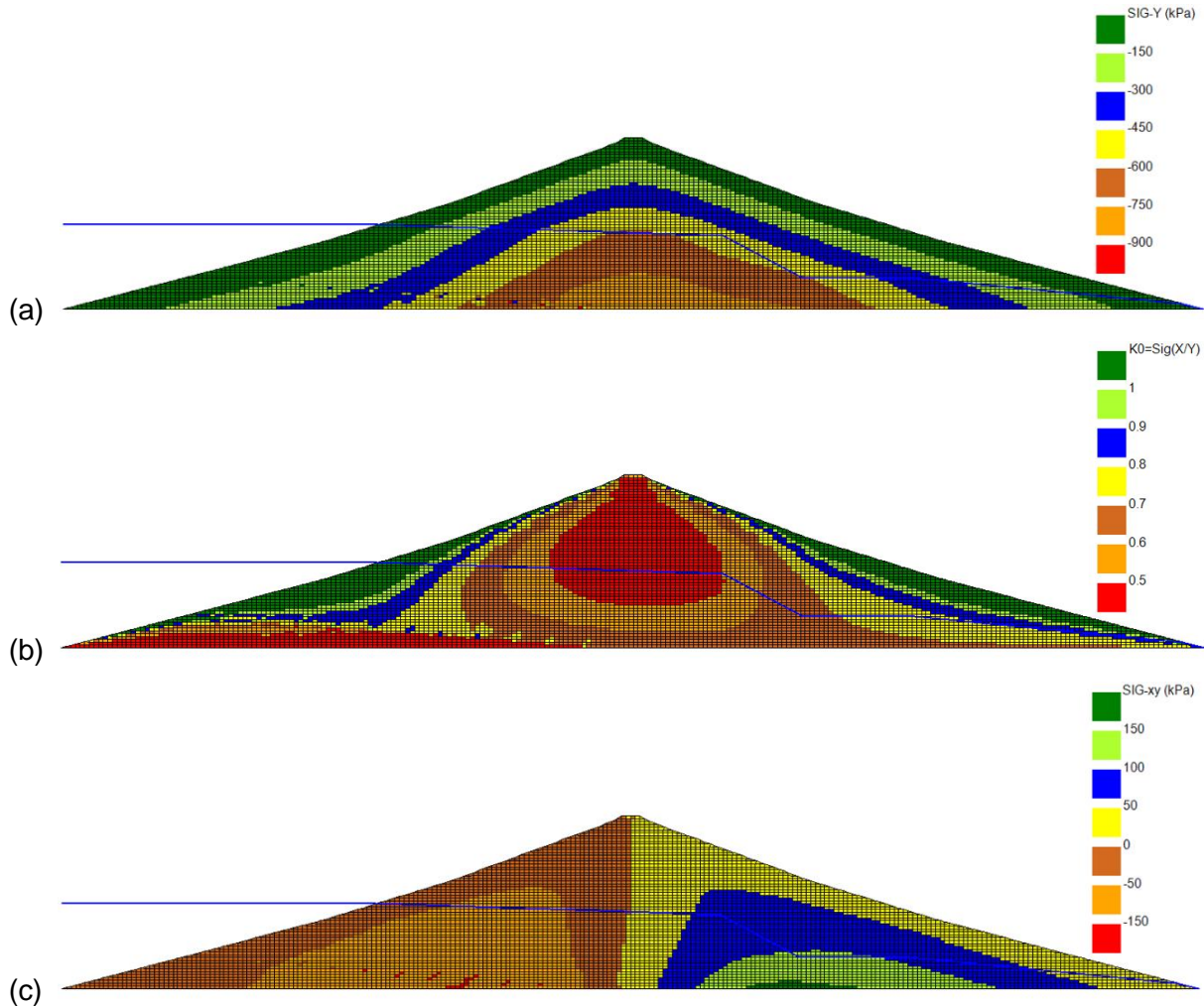


**Fig. 7** Static stresses of the Austrian Dam as calculated from VERSAT-2D: (a) vertical effective stresses  $\sigma'_y$  (negative sign represents compressive stresses); (b) horizontal stress coefficient  $K_0 (= \sigma'_x / \sigma'_y)$  where  $\sigma'_x$  is horizontal effective stress; and (c) shear stresses  $\tau_{xy}$  in the 2D plane XY

The undrained shear strengths of the saturated soils (the soils that are underneath the water table) were calculated using the proposed  $S_u/\sigma'_m$  approach in equation (1) where the  $\sigma'_m$  were calculated using the  $\sigma'_x$ ,  $\sigma'_y$ , and  $\sigma'_z$  directly computed from the VERSAT-2D static analysis. Note that VERSAT-2D has the capability of computing the static stresses  $\sigma'_z$ . The computed  $S_u$ -ratios ( $=S_u/\sigma'_y$ ) are plotted in Fig. 8. The  $S_u$ -ratios are about 0.29-0.3 for the upper portion of the saturated dam fills underneath the dam crest and about 0.3-0.35 for the lower portion. For the saturated soils in the downstream slope, the  $S_u$ -ratios are mostly about 0.35-0.4 (in yellow color); in the upstream slope, the  $S_u$ -ratios are slightly higher at about 0.35-0.5 (greater than 0.5 near the surface due to higher  $K_0$ ).



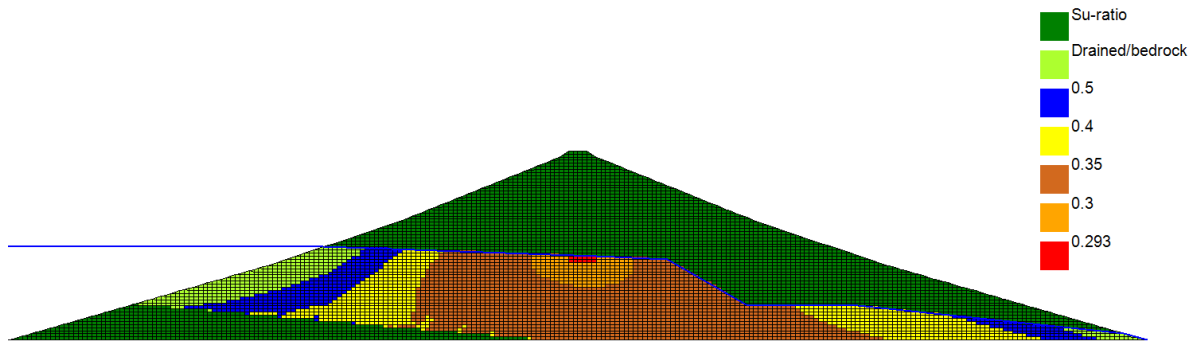


**Fig. 8** Undrained shear strength ratio ( $S_u$ -ratio) using the proposed  $S_u/\sigma'_m$  approach and the Lower strength line in Fig. 4:  $S_u$ -ratio =  $S_u/\sigma'_y$ .

## 5.0 DYNAMIC ANALYSIS OF AUSTRIAN DAM: A TOTAL STRESS APPROACH

The VERAST-2D finite element model as used for the static stress analysis and shown in Fig. 6 are also used for the 2D nonlinear dynamic analyses of earthquake-induced deformations of the Austrian dam using the total stress approach. The static stresses from VERSAT-2D static analysis were used as the starting point for the nonlinear dynamic analysis.

### 5.1 General Methodology

The VERSAT-2D (WGI 2019) dynamic analyses of seismic response are always carried out in an undrained condition, whereas a total stress analysis is performed for clayey soils using the VERSAT-CLAY model or an effective stress analysis is conducted for sandy soils using the VERSAT-SAND model; the latter can take into account the effect of PWP on shear strength of sandy soils (i.e.,  $c'$  and  $\phi'$ ) as the effective stresses decrease with the increase of PWP, and ultimately can model liquefaction of sandy soils. The VERSAT-SAND model had been adopted for modelling liquefaction of the hydraulic fills in the dynamic analysis of the Upper San Fernando dam (Wu 2001). When the VERSAT-CLAY model is used, the  $S_u$  are calculated using the pre-earthquake stresses (i.e., the static stresses), after which they are kept unchanged throughout the entire duration of earthquake loading.

This type of analysis approach was adopted and applied by Professor Finn (Finn et al., 1986) in early 1980's when seismic deformation analyses were still in the early stage and when numerical calculations or finite element dynamic analyses were not so easy or

so convenient to perform. The simple and straight-forward analysis method was further enhanced to become the VERSAT method and then applied in research and engineering design analysis, including simulation of soil liquefaction and its induced large ground deformation (Wu 2001; Finn and Wu 2013). The PWP models that were developed (Wu 2001) for effective stress analysis of sandy soils are not described in here as they are not relevant to the current total stress analysis of the Austrian dam.

The fundamental difference between the VERSAT approach and other more complicated approaches (e.g., Boulanger 2019) is that the VERSAT method of analysis does not require calibration of soil parameters ahead of a dynamic analysis, but it uses the more fundamental parameters of soils such as  $V_s$  for stiffness, undrained shear strength  $S_u$ , friction angle ( $\phi'$ ) for shear strength, normalized SPT blow count  $(N_1)_{60}$  for liquefaction resistance, and residual strength if soil liquefies. The approach is in fact very similar to what an engineer would do when a limit equilibrium analysis is to be performed using a slope stability analysis program such as the program SLOPE/W developed by GEO-SLOPE International of Canada.

## 5.2 Input Ground Motions

The Austrian dam was located on the north side of the epicenter for the 1989 Loma Prieta earthquake, while a nearby strong motion recording station at Corralitos was located on the east side of the epicenter. In particular, both the Austrian dam site and the Corralitos station were situated near the top edge of the Loma Prieta fault rupture zone (a reverse oblique fault) as shown in Fig. 1. Therefore, the Austrian dam site and the Corralitos station are to have similar input parameters for the purpose of ground motion intensity evaluation, except source directivity and the site geologic condition that are to be discussed later in the following sections. Using the NGA West2 seismic models (Bozorgnia et al. 2014), the Austrian dam site was assigned a closest distance to surface projection of coseismic rupture ( $R_{jb}$ ) of 0.16 km and a closest distance to coseismic rupture ( $R_{rup}$ ) of 3.85 km, the same  $R_{jb}$  and  $R_{rup}$  values listed for the Corralitos station (PEER 2021). In this ground motion calculation, the Austrian dam site was considered as a hang-wall site, while according to PEER (2021), the Corralitos station was a footwall site. However, these two sites are very close to the surface projection of the top of the fault rupture, a line that represents the separation between the footwall and hanging wall sides of the rupture. The horizontal distance from a site to this line is denoted as  $R_x$ , which is negative for footwall

sites and positive for hanging wall sites; the  $R_x$  value for the Corralitos station is  $-0.16$  km (PEER 2021), and the  $R_x$  value for the Austrian dam site was assumed to be  $+0.16$  km. Thus, because these  $R_x$  values are small, the ground motions at these two sites are not expected to be significantly affected by the fact that one site is on the footwall and the other site is on the hanging wall.

For the Austrian dam there was no reported data on shear wave velocities of the foundation bedrock, consisting of highly fractured sandstone, graywacke, cobble conglomerate, shale, and serpentine (Harder et al. 1998), but unpublished data from a limited number of other projects in the region have shown shear wave velocities ranging from 760 to 2,700 m/s in the upper 30 m of the Franciscan formation (Boulanger 2019). The motions at the Austrian Dam site were not recorded; they were estimated to have peak horizontal accelerations between 0.55 and 0.60g (Harder et al. 1998).

The other nearest strong motion recording station was located at the abutment of the Lexington dam (latterly renamed the Lenihan dam). The Lexington station was located further away from the epicenter than the Austrian Dam site (see Fig. 1); it was outside of the surface projection area of the Loma Prieta fault rupture zone. In current ground motion calculation, the Lexington was considered to be a foot-wall site, and it had  $R_{fb}$  of 3.22 km and  $R_{rup}$  of 5.02 km (PEER 2021). On Franciscan formation rocks with an inferred  $V_{s30}$  of 1,070 m/s, the recorded Lexington motions had an Arias intensity (AI) of 1.9 cm/s, peak horizontal accelerations of 0.41g in  $90^\circ$  and 0.44g in  $0^\circ$  (PEER 2021).

For analysis of seismic deformations of the Austrian dam in 1989, it is considered appropriate to linearly scaling up the ground motions recorded at the Lexington station and use the scaled motions as the input ground motions at the Austrian dam. The use of ground motions recorded at the Corralitos station directly on Austrian dam may not be as suitable as the scaled Lexington motions for reasons to be discussed in the following sections.

Using the input parameters discussed above and others ( $M_w = 6.93$ ,  $Z_{TOR} = 3.8$  km,  $R_x = -3.22$  km for foot-wall site,  $V_{s30} = 1000$  m/s which is the highest  $V_{s30}$  value allowed in the GMPEs), peak horizontal ground acceleration (PGA) at the Lexington station (the median value at 5% damping) was estimated to be 0.38g from the NGA West2 ground motion prediction equations (GMPE) and the associated weight of 0.12 for Idriss model and 0.22 for other four models (Bozorgnia et al. 2014). When the same calculation was carried out for the Austrian Dam site (a hanging-wall site), a PGA (also the median value at 5% damping) of 0.52g was estimated. The PGAs at the two sites predicted by the

GMPEs of NGA West 2 are remarkably consistent with the measured 0.41-0.44g at the Lexington station or the estimated 0.55-0.60g at the Austrian dam; the predicted median PGAs at both sites are lower by about 11% than the recorded (or estimated) PGAs. The predicted PGA at the Austrian dam is approximately 36% higher than the predicted PGA at the Lexington station; therefore, the measured ground motions at the Lexington station were linearly scaled up by a factor of 1.36 and applied as the input motions at the Austrian dam.

Time histories of the scaled horizontal (both the 0° and 90° components) accelerations and the associated displacements are shown in Fig. 9. The scaled acceleration record has a peak ground acceleration (PGA) of 0.56g and 0.60g for 90° and 0°, respectively. The scaled vertical acceleration record (not shown in here) has a PGA of 0.19g. For finite element models having a rigid base, acceleration time histories (horizontal and vertical) are applied directly at the rigid base, i.e., assuming the input motions were recorded at the rigid base.

### 5.3 VERSAT-2D Soil Constitutive Models

Soil constitutive models employed in VERSAT-2D dynamic analysis are comprised of the Mohr Coulomb failure criteria for simulation of soil shear strengths and the 2-parameter hysteretic shear stress-strain relationship for modelling of soil stiffness including shear modulus reduction and hysteretic damping increase with the increase of shear strains.

VERSAT-2D (WGI, 2019) uses the hyperbolic stress - strain model to simulate the nonlinear and hysteresis shear stress - strain relationship for soils. The low-strain shear modulus,  $G_{max}$ , and the bulk modulus,  $B$ , are stress level dependent as defined in the following:

$$G_{max} = K_g P_a \left( \frac{\sigma'_m}{P_a} \right)^m \quad (3)$$

$$B = K_b P_a \left( \frac{\sigma'_m}{P_a} \right)^n \quad (4)$$

where  $P_a$  is the atmospheric pressure, 101.3 kPa

$K_b$  is bulk modulus constant

$K_g$  is shear modulus constant;  $m$  and  $n$  are shear and bulk modulus exponentials, respectively;  $\sigma'_m$  is defined in equation (2).

The relationship between the shear stress,  $\tau_{xy}$ , and the shear strain,  $\gamma$ , for the initial loading condition is modelled to be nonlinear and hyperbolic as follows:

$$\tau_{xy} = \frac{G_{max} \gamma}{1 + \frac{G_{max}}{\tau_{ult}} \bullet |\gamma|} \tag{5}$$

$$\tau_{xy} = \frac{G_{max} \gamma}{1 + R_f \bullet |\gamma|} \tag{6}$$

where  $\tau_{ult}$  is the ultimate shear stress in the hyperbolic model;  $G_{max}$  is the low-strain shear modulus ( $G_{max} = \rho V_s^2$  with  $\rho$  being the soil density and  $V_s$  being the shear wave velocity).

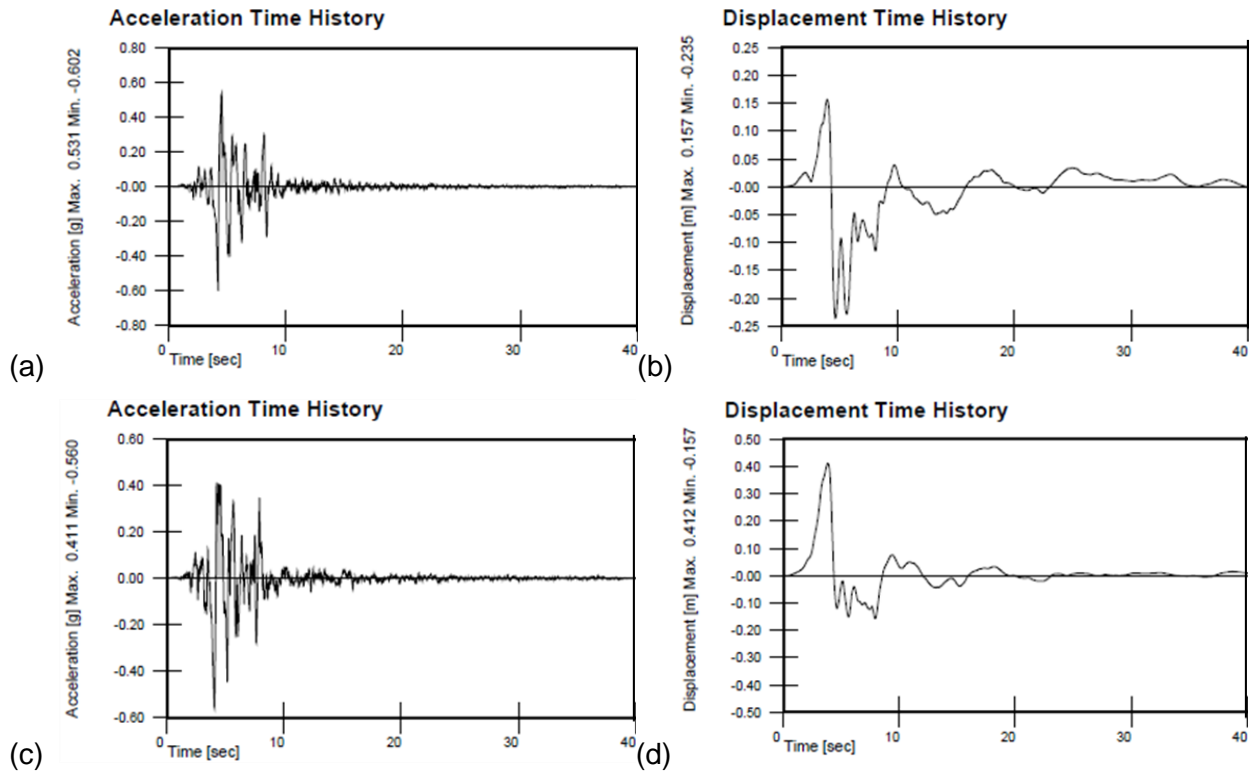


**Fig. 9** Time histories linearly scaled from records at the Lexington dam (showing only 40 s): (a) horizontal accelerations for 0°; (b) horizontal displacements for 0°; (c) horizontal accelerations for 90°; (d) horizontal displacements for 90°.

The  $\tau_{ult}$  is conveniently determined by introducing a modulus reduction factor  $R_f$ , which is shown in equation (6) and detailed in Wu (2001). As shown in Fig. 10 and noted in Finn and Wu (2013), the use of  $R_f$  enhances the hyperbolic stress-strain model so that the model can provide a better match to the target dynamic modulus ( $G$ ) and damping data. For an example, at a shear strain of 0.1%, the  $G/G_{max}$  ratio is 0.5 and the hysteretic

damping is 14.5% when  $R_f$  value is 1000; they become 0.33 and 22.4%, respectively, when  $R_f$  increases to 2000.

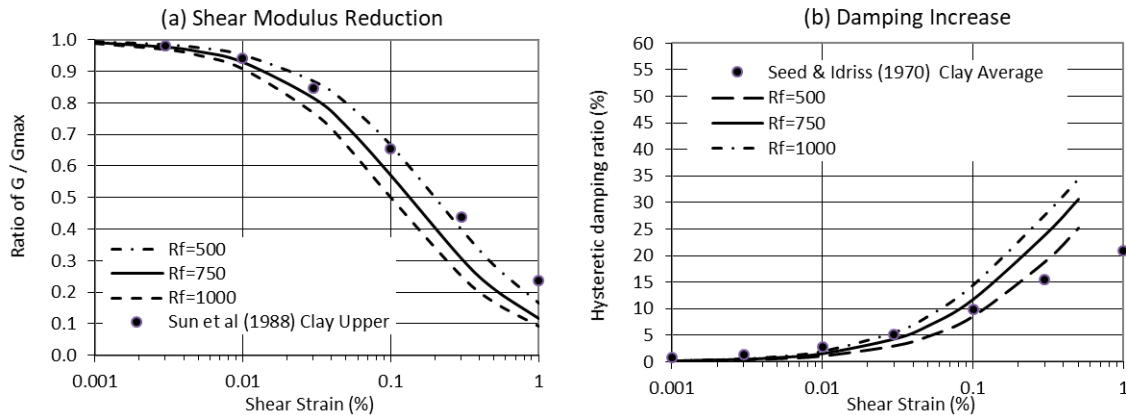


**Fig. 10** Shear modulus and hysteretic damping relation with shear strain in VERSAT soil constitutive models: (a) shear modulus decreasing with strain; and (b) damping ratio increasing with strain

The shear stress-strain hysteresis response (simulated using the VERSAT-CLAY model) of soil elements subject to cyclic (sine wave) undrained loading are presented in Figs. 11(a, b, c, d). These graphs illustrate the difference between the numerical modelling response and the observed true laboratory test response (or the field response in an earthquake) of soils subject to constant stress amplitude cyclic loading.

In Fig. 11(a), when there is no static shear stress (e.g., a generic soil element within a level ground), sine-type input shear stresses do not cumulate strains (or displacements) on the soil element if the applied shear stress amplitude is less than the shear strength. In other words, prior to failure, cyclic shear strains of the element are independent of number of loading cycles. Repetitive loading cycles (either constant stress amplitude or constant strain amplitude) do neither change the size of the stress-strain loops; nor cause more strains (or displacements) on the soil element. When failure of the soil element occurs by applying cyclic stresses with an amplitude of 185 kPa (higher than the  $S_u = 180$  kPa of the soil element), permanent shear strains (or displacements) cumulate. The portion of stress exceeding the strength (i.e.,  $\Delta$ -stress = 5 kPa) is redistributed to the adjacent soil elements. As shown in Fig. 11(a), the maximum shear stress of the soil element remains at 180 kPa after failure, the  $\Delta$ -stress causes the element to deform to a new permanent configuration.

The response of soil elements situated on soil slopes with initial static shear stresses is illustrated in Figs. 11(b, c, d) using soil elements 1182 ( $\tau_{st} = 122$  kPa,  $\sigma'_y = 489$  kPa,  $S_u = 171$  kPa) and 4082 ( $\tau_{st} = -71$  kPa,  $\sigma'_y = 508$  kPa,  $S_u = 164$  kPa) on the Austrian dam (see Fig. 6 for their locations on the dam). In the simulation, the dam is subject to two levels of sine-wave accelerations (frequency of 1.0 Hz) at its base, a low level with a PGA of 0.1g and a moderate level with a PGA of 0.3g. In Fig. 11(b), soil element 1128 fails in the direction of the static shear stress when a relatively small cyclic shear stress (i.e., an increment of about 29 kPa) is applied on the element; and the portion of stress exceeding the 29 kPa causes the element to deform to a new permanent configuration. The portion of stress exceeding the 29 kPa are redistributed to adjacent soil elements, and progressively carried on to other elements if the immediate soil element also fails in shear. The amount of irrecoverable shear strain  $\Delta$ -strain in Fig. 11(b) that is caused by a loading cycle depends on both magnitude and duration of the loading cycle. The incremental shear strains ( $\Delta$ ) in the third and subsequent fourth cycles of sine-wave loadings are relatively constant indicating stabilization of the loading condition. The pattern of irrecoverable displacement on soil elements with non-zero static shear stress is somewhat similar to that of a sliding block on inclined plane.

Figs. 11(c, d) shows the response of the soil elements 1128 and 4082 subject to a moderate level of sine-wave accelerations with a PGA of 0.3g. Note that only response of three cycles is shown in graphs. Soil element 1128 displaces, between the first and the second cycles, a lot more (with an incremental  $\Delta$ -strain of about 2.2%) under the 0.3g of shaking than that ( $\Delta$ -strain of about 0.15%) under the 0.1g of shaking. As the shaking level increases to 0.3g, the amplitude of cyclic shear stresses in the opposite direction of the static shear stress significantly increases; for soil element 1128, this opposite direction cyclic stresses reach an amplitude of about 170 kPa that indicates a near-failure stress condition. As soil element 4082 is located under the upstream slope of the dam (soil element 1128 is under the downstream slope), element 4082 displaces at the time when the first cycle of sine-wave accelerations hits the dam, causing an irrecoverable strain of about 0.8%. It is noted that element 4082 fails in shear in both directions of shaking, i.e., in the same and opposite directions of the static shear stress. When failure occurs in a loading cycle in both directions, the hysteresis loop of the cycle could be larger than a regular loop that closes without forming a failure plateau in the loop. For element 4082,

the hysteresis loop with a plateau has a double strain amplitude of about 0.3% with a reasonable amount of hysteretic damping.

The base assumption adopted in the VERSAT-CLAY model for simulating response of undrained loading on clays, silts, or the saturated dam fills of the Austrian dam is, the irrecoverable strains (ultimately expressed as permanent displacements of the dam) are controlled by the relative magnitude of the shear stresses ( $\tau_{cyc}$ ) in relation to  $S_u$  of soils. The shaking-induced pore water pressure (PWP) is irrelevant to the analysis. The total stress method used in dynamic finite element analysis is in fact consistent with or exactly same as that employed in limit equilibrium stability analysis; the merit of this approach is that it does not require calibration of the constitutive model. A more complicated constitutive model (often a plasticity model) would adopt the effective stress method of analysis for simulating the undrained response (Boulanger 2019); the response would be governed or greatly influenced by the amount of PWP predicted (or estimated) from the plasticity model. Calibration of such model will have a controlling effect on result of dynamic analysis; it could unfold in two ways: (a) unconservative if the predicted PWP is low and if the model uses the drained friction angle ( $\phi' = 42$  for the saturated fills of the Austrian dam) in the strength modelling; (b) sometimes quite conservative if a large reduction in vertical stresses (i.e., unloading) occurs because of large vertical input accelerations (e.g., the Corralitos input motion).



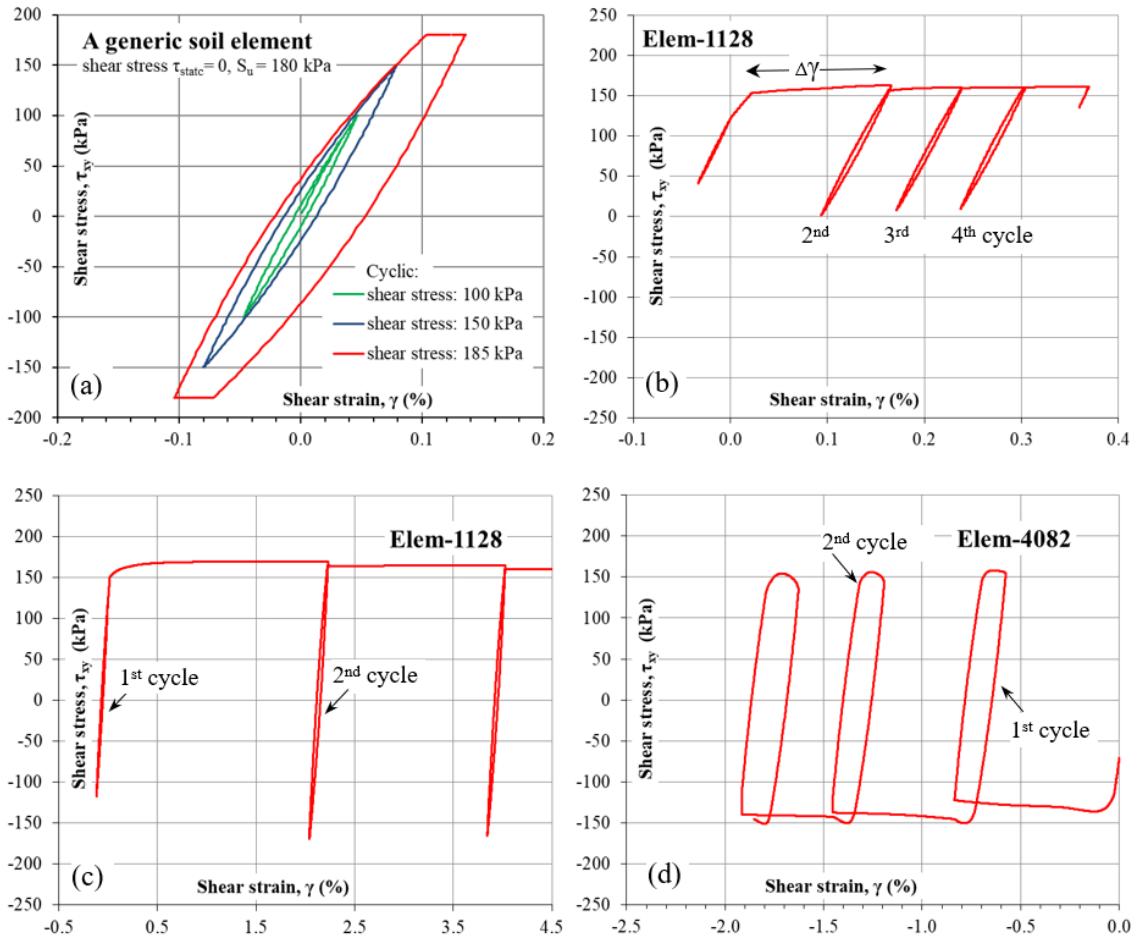


**Fig. 11** Shear stress-strain response of saturated dam fills in constant shear stress amplitude cyclic (sine wave) loading: (a) for a generic soil element at 3 stress levels; (b) for soil element 1128 under the 0.1g input accelerations; (c) for soil element 1128 and (d) for soil element 4082 under the 0.3g input accelerations.

#### 5.4 Results of Total Stress Dynamic Analysis: Case 1a

The Case 1a analyses included: (a) the measured phreatic surface; (b) the Lower strength line in Fig. 4; (c) using the  $S_u/\sigma'_m$  approach to calculate  $S_u$  of the saturated soils; (d) using default parameters ( $R_f = 500$ ,  $DT = 0.001$  s, rigid base input motions). The soil parameters for the Case 1a dynamic analyses are shown in Table 2. During dynamic loading, the bulk modulus of a soil element, once calculated from its static mean normal effective stress, is kept unchanged throughout the entire duration of earthquake loading.

**Table 2.** Total stress dynamic analyses of Austrian Dam: Case 1a Soil Parameters

No.	VERSAT model	$K_b$	$n$	$K_g$	$m$	Unit weight	Drained, $\phi'$ (°)	Undrained, strength
MAT-1	SAND	7942	0.5	2647	0.5	21.0	44	-
MAT-3	SAND	7942	0.5	2647	0.5	21.0	44	-
MAT-4	CLAY	20500	0	2647	0.5	22.4		$S_u^a$
MAT-5	CLAY	20500	0	2647	0.5	22.4		$S_u^a$
MAT-2	ELAS	18720	0	9360	0	25.5		

Note: Unit weight in  $kN/m^3$ .

<sup>a</sup> $S_u = c + \sigma_m' \tan (\Psi)$  where  $c = 14$  kPa,  $\Psi = 22^\circ$  (i.e., the Lower  $S_u$  in Fig. 4)

The end-of-earthquake deformations of the dam are presented in Fig. 12; the basic pattern of deformations is that the upstream part of the dam moves laterally toward the reservoir and the downstream part of the dam moves laterally but in the opposite direction. As shown in Fig. 12(a) the horizontal displacement contours indicate that the dam split in two directions from its vertical centerline. The lateral spreading movements of the dam body caused the dam to settle, as shown in Fig. 12(b). The dynamic analysis calculated a dam crest settlement of 0.77 m using the LEX-00° horizontal and its associated vertical input accelerations; the calculated crest settlement was 0.70 m using the LEX-90° horizontal and its associated vertical input accelerations. The VERSAT-2D computed dam crest settlements are in good agreement with the actual dam crest settlement of 0.76 m observed immediately after the 1989 Loma Prieta earthquake. The computed horizontal displacements are about 0.72-0.58 m (for LEX 00°-90°) on the upstream slope moving towards the reservoir; they are about 0.49-0.54 m (for LEX 00°-90°) on the downstream slope.

The deformation pattern of the dam is consistent with the computed shear strains of the dam, as shown in Fig. 13. Similar to observations of clay embankment in a limit equilibrium stability analysis, significant shear straining zone tends to develop first near the bottom of a slope due to high shear stresses. Shear strains between 5 and 10% were predicted to have occurred in the lower part of the upstream slope, i.e., in the saturated dam fills immediately above the bedrock; in it one soil element was predicted to have shear strain greater than 10%. The shear strains of the saturated dam fills in the downstream slope of the dam are of a similar order of magnitude, also about 5 – 10%; however, in a small zone near the base of the downstream slope, the shear strains are large at about 15-20% and greater than 20% at the zone’s bottom. This downstream

shear zone (i.e., the zone with shear strains larger than 10%) is in relatively lower ground (low elevation); the ground elevation in this shear zone is about 10 m lower than the shear straining zone in the upstream slope of the dam.

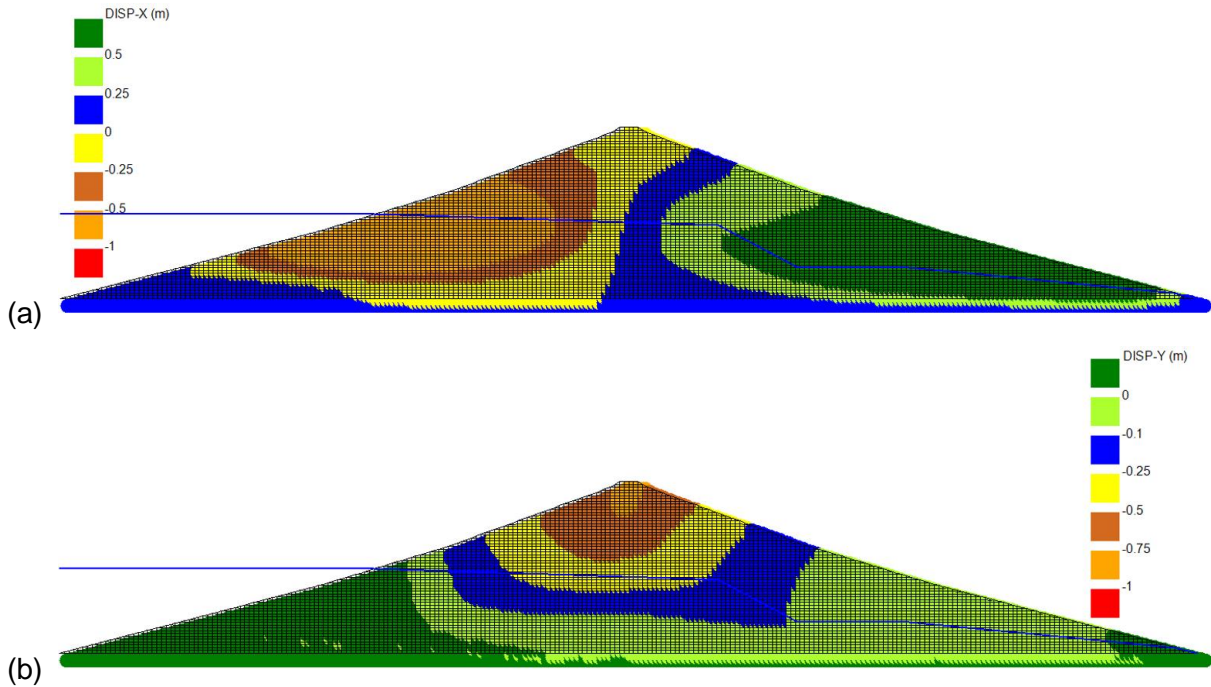


**Fig. 12** End-of-earthquake deformations of the Austrian dam calculated by VERSAT-2D using the Case 1a soil parameters and input accelerations (LEX-00°): (a) contours of horizontal displacements (m); and (b) contours of vertical displacements (negative sign represents settlement).

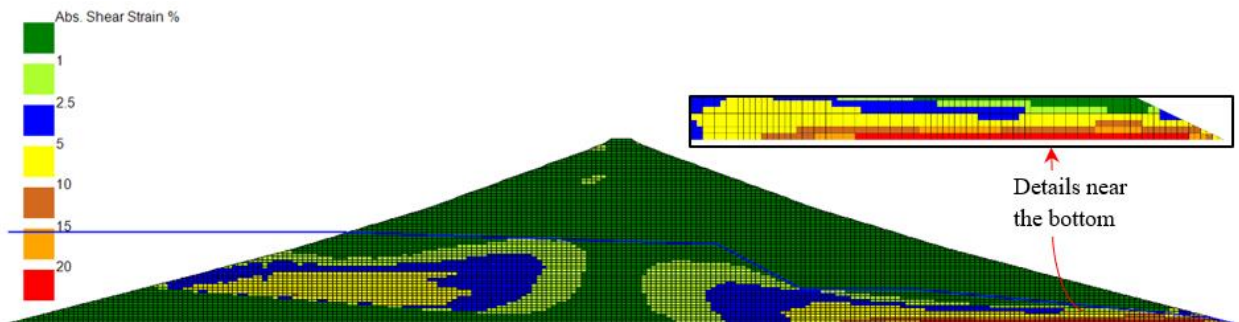


**Fig. 13** End-of-earthquake strains of the Austrian dam calculated by VERSAT-2D using the Case 1a soil parameters and input accelerations (LEX-00°): contours of absolute shear strains (%)

Shear stress-strain hysteresis response histories are of great interest and values in understanding a nonlinear dynamic analysis of soils. As shown in Fig. 14, the hysteretic stress-strain relation of soils provides an insight look of the model; it basically illustrates to a great extent how the soil material is modelled in a dynamic analysis. Shear stress-strain histories (or traces) obtained from the VERSAT-2D dynamic analysis of the Austrian dam are shown in Fig. 14(a) and in Fig. 14(b) for soil elements 1128 and 4082, respectively. The locations of the two elements in the cross section are shown in Fig. 6. Although the cumulative shear strains are about +5.5% and -3.2% in elements 1128 and 4082, respectively, the incremental strains in any hysteresis loops are less than or in order of 0.25%; the damping in the hysteresis loops is reasonable.

The shear stress-strain response of unsaturated dam fills, which was modelled using the VERSAT-SAND model and the drained shear strength parameters (i.e.,  $\phi' = 42$  and a cohesion of zero), is represented by the response of soil element 6469 (see Fig. 6 for its location on the dam) and shown in Fig. 14(c). The total cumulated shear strain of soil element 6469 is less than 1%; the incremental strain in any hysteresis loops is less than 0.05%.

The horizontal displacements and shear strains of the Austrian dam computed from VERSAT-2D dynamic analyses are consistent and in great agreement with the observed dam performance in the Loma Prieta earthquake in 1989, in terms of the magnitude and location of “lateral spreading of the embankment of the dam” (Harder et al 1998) and the apparent deformations observed in standpipe for piezometers P-1 and P-6. The computed displacement histories of the dam crest are shown in Fig. 15(a) (in the graph, horizontal displacement is named as DIS-X and vertical as DIS-Y). The graph also includes for comparison the computed horizontal displacements at the mid-height of the upstream and downstream slopes of the dam. Majority (about 0.76 m out of the 0.77 m) of the crest settlement (DIS-Y) was predicted to have occurred, as expected in an undrained total stress analysis, during the early 15 s of shaking; in reality, settling of the dam may have continued during shaking after 15 s. The horizontal acceleration response of the dam crest is shown in Fig. 15(b), which also includes the rigid base input accelerations.

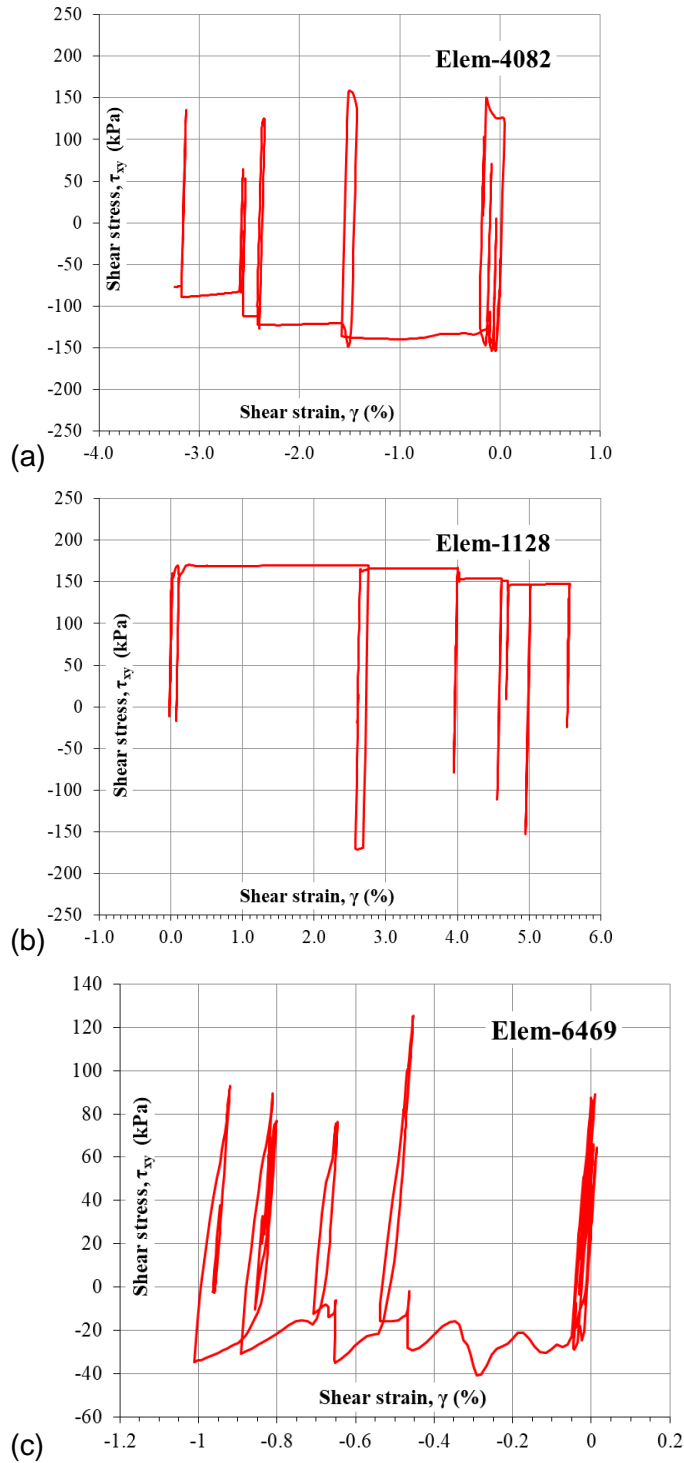
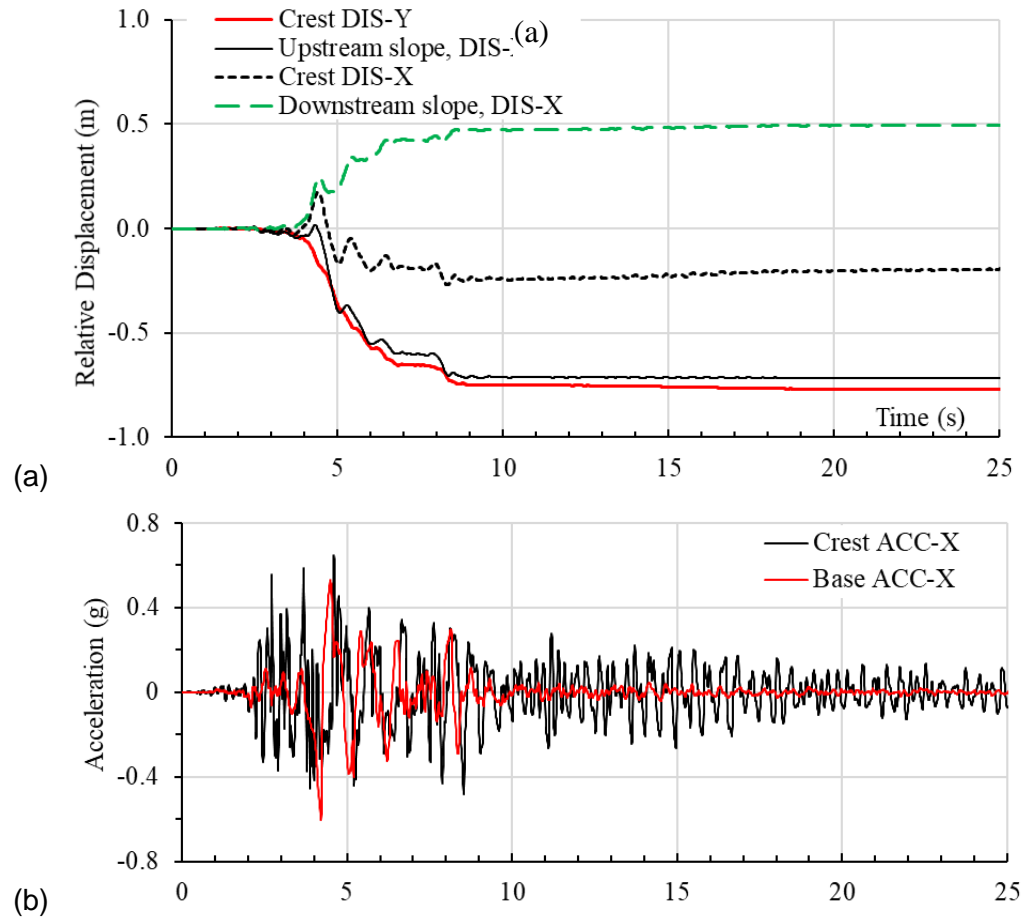


Fig. 14 Shear stress – strain histories calculated by VERSAT-2D using the Case 1a soil parameters and input accelerations (LEX-00°): (a) soil element 4082 (upstream saturated zone); (b) soil element 1128 (downstream saturated zone); and (c) soil element 6469 (in unsaturated zone).



**Fig. 15** Response histories of the Austrian dam calculated by VERSAT-2D using the Case 1a soil parameters and the LEX-00° input accelerations: (a) displacements at three locations on the dam – at mid-height of the upstream and downstream slopes and at the dam crest; (b) accelerations (X) at the dam crest versus the input accelerations at the base.

## 6.0 RESULTS OF PARAMETRIC ANALYSES

Parametric analyses of the Austrian dam included these scenarios: suitability of input ground motions using the Lexington dam record and the Corralitos station record; the sensitivity of phreatic surface on seismic deformations of the dam; the impact of undrained shear strengths between the Lower and Middle strength values; the methods of applying undrained shear strengths in dynamic analyses; and the effect of dam foundation stiffness (i.e., shear wave velocity  $V_{s30}$ ) on dynamic response of the dam.

## 6.1 Suitability of Input Ground Motions

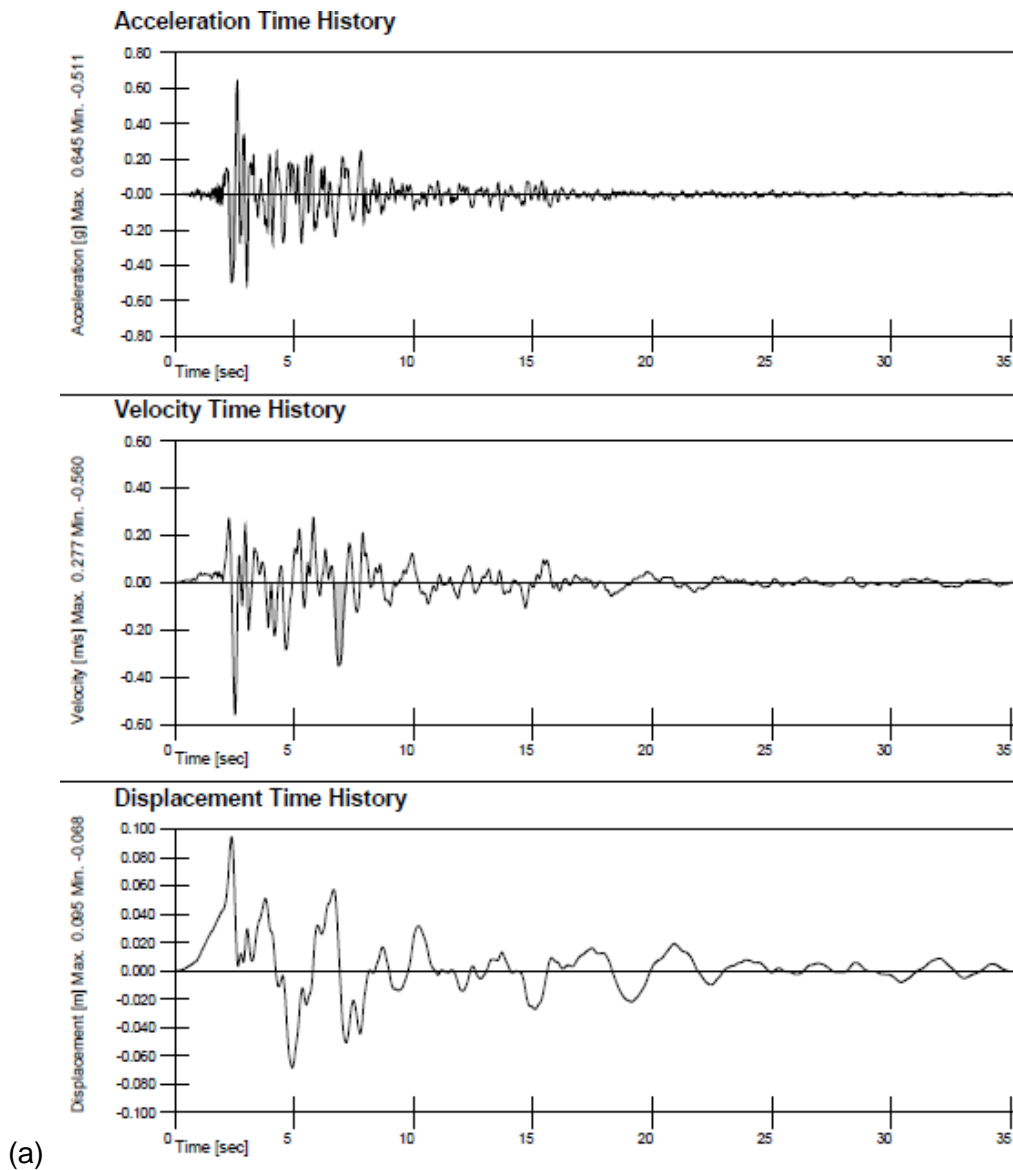
Although both sites were situated along the axis of the rupture fault, the Corralitos ground motion recording station was located on the southeast side of the Loma Prieta earthquake epicenter (see Fig. 1); the Austrian dam site was located on the northwest side of the epicenter. The two sites were in the opposite directions of the earthquake epicenter. As such, the ground motions generated by the earthquake at the two sites could be significantly different because of earthquake source directivity, which is the focusing of wave energy along the fault in the direction of rupture, moving outward from the earthquake epicenter. In other words, distance to the fault is not the only consideration for ground motion characteristic; the direction to the epicenter also matters.

The Corralitos station is on predominantly shale landslide deposits that have a  $V_{s30}$  (i.e., weighted average shear wave velocity to a depth of 30 m) of 462 m/s; the recorded ground accelerations have an Arias intensity (AI) of 3.2 cm/s, peak horizontal accelerations 0.483g in 90° and 0.645g in 0° [see Fig. 16(a)] and a high peak vertical acceleration of 0.46g [see Fig. 16(b)]. The low  $V_{s30}$  of a recording station can substantially alter the magnitude and frequency content of the ground motions. Based on analysis of the acceleration response spectra [see Fig. 16(c)], the 0° and 90° horizontal components of the Corralitos records have predominant frequencies of approximately 4.0 Hz and 1.4-2.0 Hz, respectively; these frequencies are close to the resonant frequencies of the Austrian dam. Modal frequency analysis of the Austrian dam conducted using VERSAT-2D revealed that the fundamental modes of the dam's maximum cross section (in Fig. 6) had frequencies between 2.5 Hz and 5.0 Hz (corresponding to periods from 0.4 and 0.2 s) between the first and the fifth modes.

In current parametric analyses, dynamic analyses of the dam were also conducted using the as-recorded Corralitos station accelerations (i.e., no alteration or scaling) as input motions (CLS-00° and CLS-90°, both with vertical accelerations), in part to compare with the results obtained by other studies (Boulanger 2019) where the Corralitos ground motions were used directly as input motions for dynamic analyses of the Austrian dam.

The parametric dynamic analyses on input ground motions were conducted using the Case 1a phreatic surface and its associated parameters; the results of the analyses are shown in Table 3. As shown in Fig. 17(a) dam crest settlement of 0.69 m was computed using the CLS-00° input accelerations, and crest settlement of 0.63 m was predicted using the CLS-90° input accelerations; these dam crest settlements are about

10% lower than those computed using the scaled Lexington accelerations as input motions. However, the computed peak horizontal ground accelerations (PGA) at the dam crest are high and between 1.13g (for CLS-00° ) and 1.21g (for CLS-90° ) which are about 80% higher than these calculated using the scaled Lexington accelerations; the computed acceleration history response at the dam crest is shown in Fig. 17(b) for CLS-00°. The calculated PGAs at the dam crest are 0.66g and 0.63g using the scaled Lexington accelerations, i.e., LEX-00° and LEX-90°, respectively.





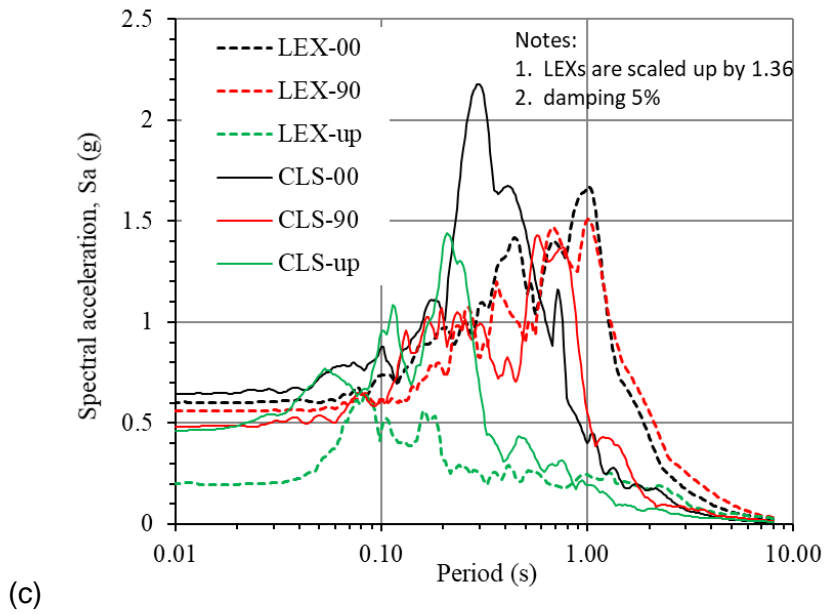
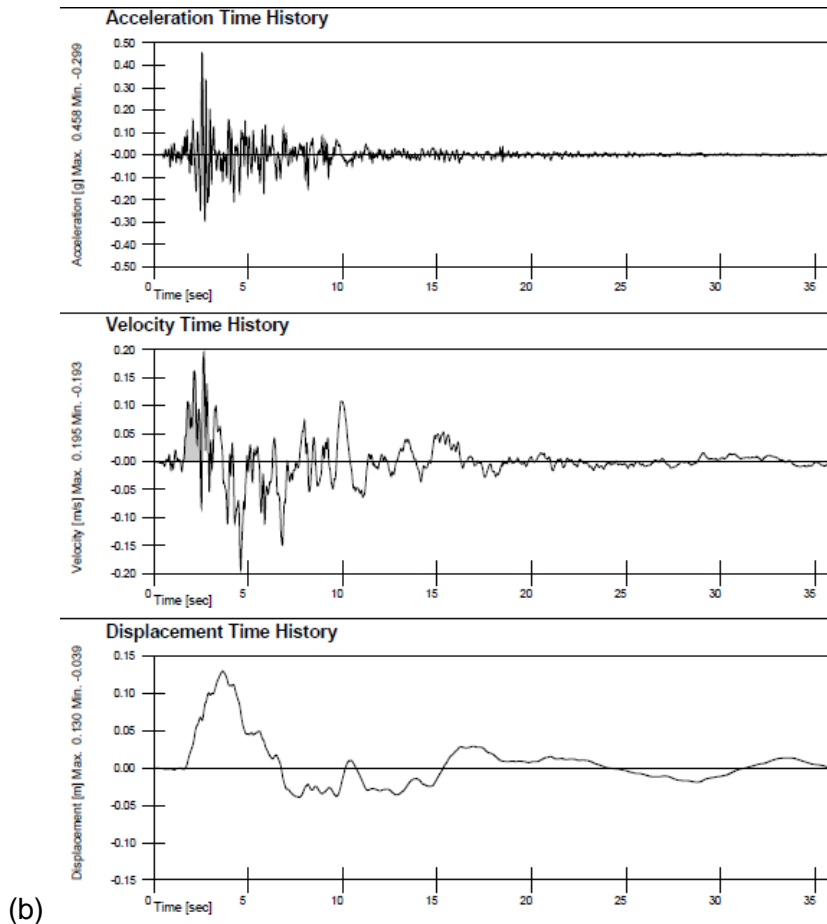


**Fig. 16** Time histories of recorded accelerations at Corralitos station (showing only 35 s): (a) horizontal accelerations for 0°; (b) vertical accelerations; (c) comparison of spectral accelerations between LEX and CLS accelerations

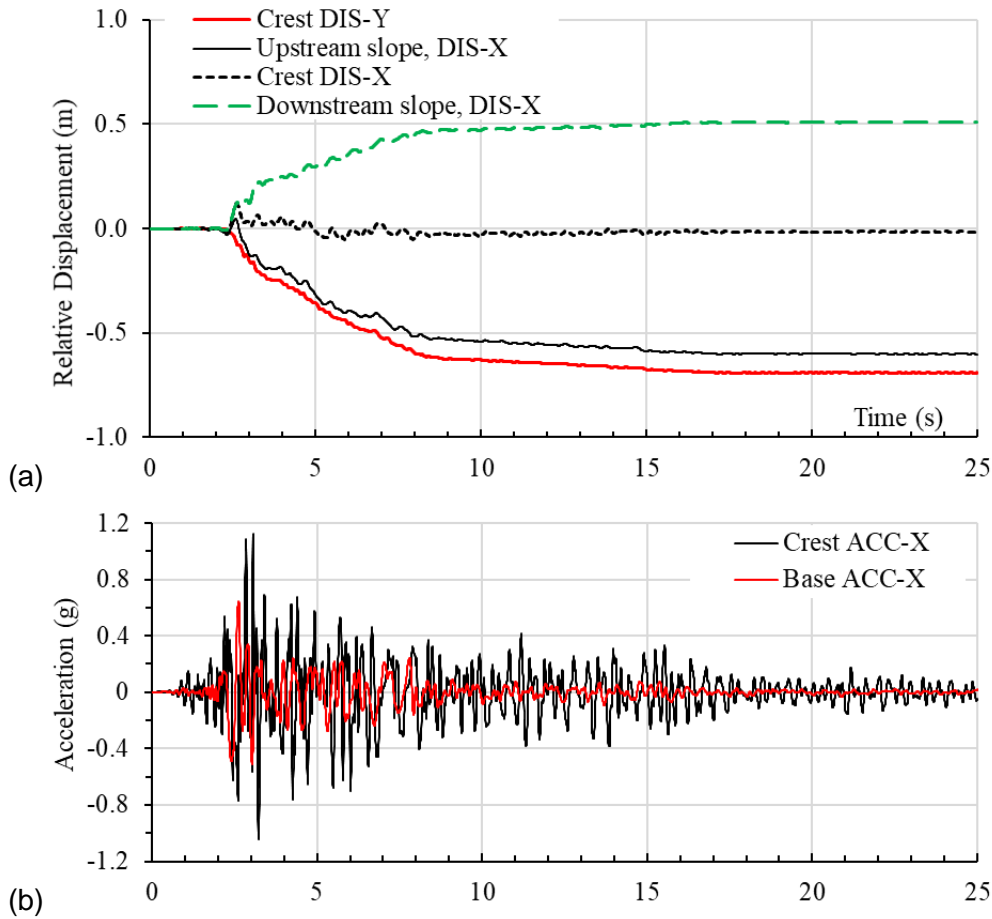


**Fig. 17** Response histories of the Austrian dam for Case 1a soil parameters and the CLS-00° input accelerations: (a) displacements at three locations on the dam; (b) accelerations (X) at the dam crest;

## 6.2 Dam Crest Acceleration Response Spectra

Seismic deformations of the dam are mostly controlled by the shear strength of the dam fills; permanent displacements of the dam occur when the earthquake induced shear forces exceed the shear resistance of soils. However, the shear stiffness of soils has a paramount impact on the acceleration response of the dam under earthquake loadings. Thus, the modulus reduction factor,  $R_f$ , is a governing contributor to the acceleration response of the dam. The use of a higher  $R_f$  value will result in more reduction of soil shear modulus as the shear strain increases; it will reduce the stiffness of the dam and elongate the response period of the dam.

As shown in Table 3, the use of  $R_f = 2647$  for Cases 1(b, c, d) instead of  $R_f = 500$  for Case 1a has resulted in deamplification of ground motions from the dam base to the dam crest; the response accelerations at the dam crest have an average PGA of 0.42 g for Cases 1(b, c, d) and a PGA of 0.66 g for Case 1a. With a PGA of 0.60g for the input base acceleration, the deamplification factor is 0.70 for Cases 1(b, c, d) and the amplification factor for Case 1a is 1.10. The response spectra of the computed accelerations at the dam crest for Cases 1(a, b, d) are shown in Fig. 18 together with the spectra of the input base accelerations. It is seen in Fig. 18 that the dam has much stronger acceleration response at high frequency (4 – 25 Hz) ground motions for a low  $R_f$  of 500 (Case 1a) than for a high  $R_f$  of 2674 (Cases 1b and 1d). The response periods of the dam listed on Fig. 18 show a first mode period increase from 0.38 s at beginning of shaking (0 – 1 s) to 0.84 s during strong shaking (4 – 6 s) for Case 1a, whereas for Cases 1(b, d) the corresponding period increase is from 0.38 s to 2.10 s indicating a much more elongated period when  $R_f$  of 2647 is used. These dam response periods are simultaneously calculated by VERSAT at specified time interval (e.g., 0.5 s or 1.0 s) when the dynamic analysis is progressing in the time domain.

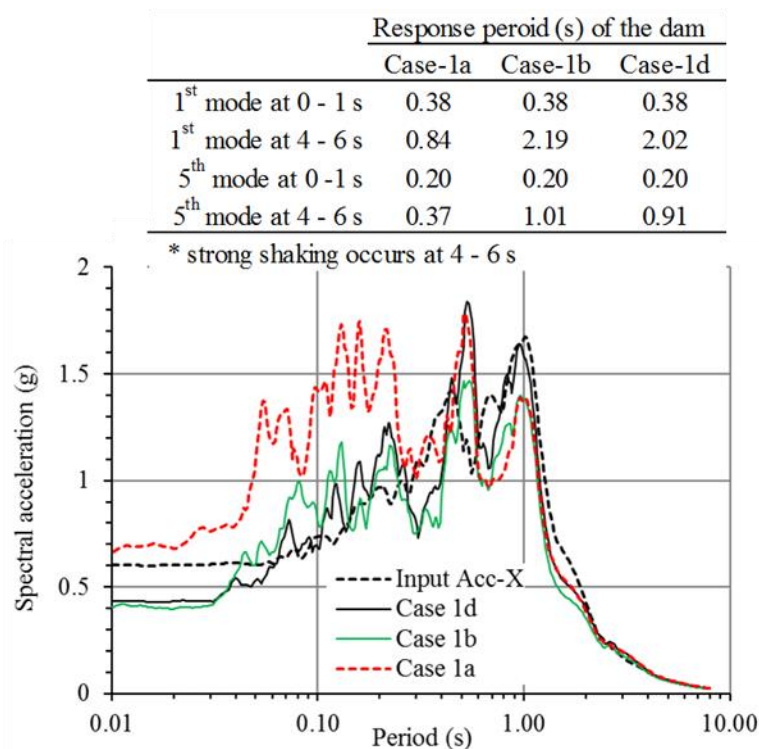


Fig. 18 Response periods of the dam and response spectra of dam crest horizontal accelerations for Cases 1(a, b, d) and input accelerations (LEX-00°)

Since there were no recorded ground motions at the Austrian dam crest, it had no definite evidence to point to a large deamplification of ground motions at the dam. However, recorded ground motions at the Lexington dam appear to indicate no ground motion amplification at the Lexington dam that was subjected to input motions with a PGA of about 0.44g. Because the Austrian dam had input motions with a higher PGA of 0.60g, it is reasonable to assume there was some ground motion deamplification occurred at the Austrian Dam. As such,  $R_f$  between 500 and 2647 (e.g., 2000) would be a more realistic value for the dam fills at the Austrian dam based on analyses of this case history.

**Table 3.** Accelerations and displacements of the Austrian dam computed by VERSAT-2D

Cases	Details	Input motions	Dam crest			Downstream DIS-X <sup>a</sup> , m
			ACC-X, g	DIS-X, m	DIS-Y, m	
CASE 1: phreatic surface as in piezometers P-6, P-4, P-1	1a. Lower $S_u$ in Fig. 4; undrained shear strengths $S_u$ applied using the $S_u/\sigma'_m$ approach	LEX-00	0.66	-0.19	-0.77	0.49
		LEX-90	-0.63	-0.03	-0.70	0.54
		CLS-00	1.13	-0.01	-0.69	0.51
		CLS-90	1.21	-0.06	-0.63	0.45
	1b. As 1a, $R_f = 2647$ (all soils)	LEX-00	0.40	-0.10	-0.92	0.63
	1c. As 1b, 2% viscous damping	LEX-00	0.41	-0.07	-0.80	0.55
	1d. As 1b, Middle $S_u$ in Fig. 4	LEX-00	0.43	-0.13	-0.77	0.50
CASE 2: Phreatic surface 4 m higher than measured at P-4	2a. Lower $S_u$ in Fig. 4 and the $S_u/\sigma'_m$ approach	CLS-00	1.12	0.01	-0.77	0.58
		CLS-90	1.15	-0.04	-0.68	0.50
		LEX-00	0.61	-0.18	-0.83	0.54
		LEX-90	0.57	-0.02	-0.75	0.58
	2b. Lower $S_u$ in Fig. 20; total stress $c-\phi$ approach	CLS-00	0.75	-0.59	-2.40	1.16
		CLS-90	0.98	-0.60	-1.30	0.53
		LEX-00	0.64	-0.42	-0.84	0.41
		LEX-90	0.67	-0.14	-0.78	0.52
	2c. As 2a, but 2% viscous damping. Direction of input accelerations was reversed for 00-r and 90-r.	LEX-00	0.63	-0.32	-0.72	0.38
		LEX-90	-0.55	-0.18	-0.61	0.38
LEX-00-r		0.51	0.06	-0.69	0.57	
LEX-90-r		-0.52	0.04	-0.63	0.52	
2d. As 2c, $DT = 0.0005$ s	LEX-00	0.63	-0.32	-0.73	0.38	
CASE 3 Phreatic surface 8 m higher than measured at P-4	3a. Lower $S_u$ in Fig. 4 and the $S_u/\sigma'_m$ approach	LEX-00	0.63	0.01	-0.83	0.65
		LEX-90	0.61	0.11	-0.76	0.67
	3b. Middle $S_u$ in Fig. 4 and the $S_u/\sigma'_m$ approach	LEX-00	0.78	-0.05	-0.63	0.47
		LEX-90	-0.67	0.05	-0.62	0.52
	3c. As 3a, elastic base with $V_{s30}$ $= 1070$ m/s	LEX-00	0.55	0.00	-0.84	0.64
		LEX-90	-0.48	0.09	-0.73	0.64
	3d. As 3c, $K_{2max} = 98$ for all dam fills	LEX-00	0.57	0.03	-0.92	0.72
		LEX-90	0.47	0.08	-0.79	0.67

Note: The dam crest after the 1989 Loma Prieta earthquake settled 0.76 m on average by measurement, and the right abutment, relatively to the left abutment, moved 458 mm horizontally and towards the downstream; except noted

otherwise, viscous damping of 1%,  $R_f = 500$  and  $DT = 0.001$  s were used in all dynamic analyses; for the rigid base model, vertical input accelerations were always applied with the horizontal input accelerations for both the Lexington and Corralitos input motions and for both the  $0^\circ$  and  $90^\circ$  components; for the elastic base model in 3c and 3d, only horizontal input velocities were applied as outcropping velocities; vertical input velocities were not applied.

<sup>a</sup>Downstream DIS-X is the horizontal displacements at the finite element node No. 5630 located at  $X = 58.5$  m and  $Y = 320.0$  m in Fig. 6.

<sup>b</sup>DT is the time increment (s) selected for numeric integration.

### 6.3 Sensitivity of Phreatic Surface and Other Parameters

Another parametric study of the dynamic analysis was to investigate the impact of the phreatic surface assumed in the downstream slope on seismic deformation of the Austrian dam. Based on results of steady seepage analyses, the phreatic surface in the dam in the vicinity of piezometer P-4 was estimated to be about 8 m higher than what was measured at P-4 (Boulanger 2019). As the dam deformations are mostly influenced by the undrained shear resistance of the saturated dam fills, it is expected that a larger saturation zone would result in larger deformations of the dam. Parametric analyses of phreatic surface were carried out for two scenarios as shown in Fig. 19: Case 2 (see Table 3) with the piezometric level at P-4 assumed to be at elevation 297 m (4 m higher than the measured at P-4) and Case 3 for 8 m higher than the measured at P-4. The calculated “Downstream DIS-X” (see Table 3) increase from 0.49-0.54 m (for Case 1a and LEX  $00^\circ$ - $90^\circ$ ) to 0.53-0.58 m (for Case 2a and LEX  $00^\circ$ - $90^\circ$ ); the displacements further increase to 0.64-0.67 m (for Case 3a and LEX  $00^\circ$ - $90^\circ$ ). The dam crest settlements increase from 0.77-0.70 m (for Case 1a and LEX  $00^\circ$ - $90^\circ$ ) to 0.83-0.75 m (for Case 2a and LEX  $00^\circ$ - $90^\circ$ ); the crest settlements remain largely unchanged at 0.83-0.76 m (for Case 3a and LEX  $00^\circ$ - $90^\circ$ ).

The sensitivity on analysis results of  $R_f$  (see Fig. 10), direction of input accelerations, and DT (the time increment selected for numeric integration) was conducted using the Case 2 phreatic surface. When  $R_f = 750$  was used for both saturated and unsaturated dam fills, the calculated dam crest settlements decrease from 0.83-0.75 m (for LEX  $00^\circ$ - $90^\circ$  and  $R_f = 500$  in 2a) to 0.72-0.61 m (for LEX  $00^\circ$ - $90^\circ$  and  $R_f = 750$  in 2c). Using the same  $R_f = 750$ , reversing the direction of input accelerations caused 0.02 m (about 3%) in difference of the calculated dam crest settlement; reducing DT from 0.001 s (the default value used in all analysis except this sensitivity check) to 0.0005 s resulted in essentially the same dam crest settlement and downstream slope displacements (see

2d in Table 3). These sensitivity analyses demonstrated the robustness of the VERSAT-2D dynamic analysis.

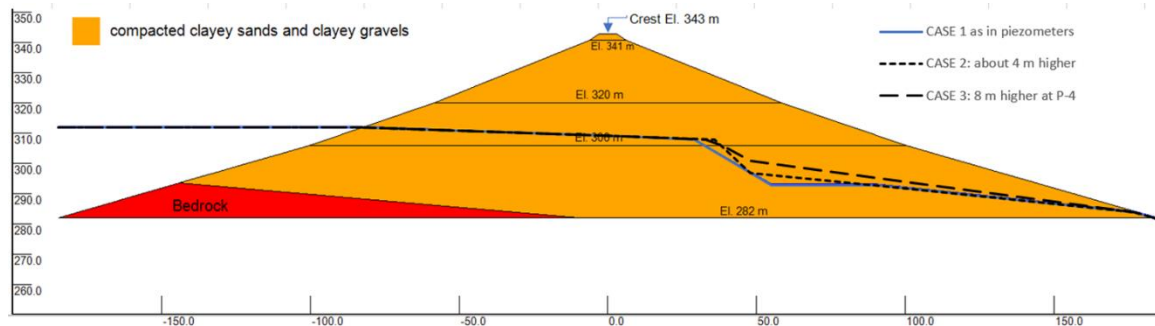


**Fig. 19** Comparison of phreatic surfaces used in parametric analyses

#### 6.4 Selection of Undrained Shear Strength Values

The significance of the undrained shear strength of the saturated dam fills on dam deformation was studied using Case 3 phreatic surface and the scaled Lexington input accelerations. This study of  $S_u$  was carried out using the Middle shear strength line in Fig. 4:

- Lower  $S_u$ : using the Lower strength line in Fig. 4 with  $c = 14$  kPa and  $\Psi = 22.0^\circ$  in equation (1). This is the  $S_u$  used in Case 1a and all other cases except Cases 1d and 3b
- Middle  $S_u$ : using the Middle strength line in Fig. 4 with  $c = 26$  kPa and  $\Psi = 22.4^\circ$ . This is the  $S_u$  applied for Cases 1d and 3b only.

As shown in Table 3, the dam crest settlements decrease from 0.83-0.76 m (for LEX  $00^\circ$ - $90^\circ$ ) using the Lower  $S_u$  (Case 3a) to 0.63-0.62 m (for LEX  $00^\circ$ - $90^\circ$ ) using the Middle  $S_u$  (Case 3b). It was estimated that in the critical shear zones (e.g., for soil elements 1128 and 4082) the undrained shear strength  $S_u$  increased by approximately 15 kPa from the Lower values of 160 kPa. The 9.4% increase in undrained shear strength has resulted in an increase in dam crest settlement of about 24%. Whenever possible, more data for soils shear strengths, either through in-situ shearing tests or by laboratory direct shear or triaxial tests, should be obtained and analyzed in order to make a sound determination on the undrained shear strengths of fine-grained soils for design or for stability and deformation assessment. In the current study, use of the Lower shear

strengths from the six ICU triaxial test data points appeared to be reflective of the in-situ undrained strength condition in the saturated dam fills.

## 6.5 Methods of Using Undrained Shear Strengths in Analysis

An interesting parametric study performed in here is the method of applying the undrained shear strength of the saturated dam fills in dynamic analysis. The  $S_u/\sigma'_m$  approach has been used as the default method for the foregoing analyses. In this sensitivity analysis, the total stress envelope parameters ( $c$ ,  $\phi$ ) will be used to represent the undrained shear strengths of the saturated dam fills. In here, the strength parameters ( $c$ ,  $\phi$ ) are derived from the total stress Mohr-Coulomb failure envelope; these parameters are sometimes reported in literature (Harder et al. 1998; Bray and Macedo 2019) to represent undrained shear strength of soils, and they are often used in static analysis of highly over-consolidated soils and less frequently for seismic stability evaluation of earthen dam (Ryan et al. 2013). The maximum shear stresses at failure from the ICU triaxial test data (Wahler Associates 1979) are shown in Fig. 20 against the mean principal total stresses at failure, i.e.,  $(\sigma_{1f} + \sigma_{3f})/2$ . Note that the measured pore water pressures in the ICU triaxial tests are not needed in the total stress method of analysis.

Similar to the analysis using the  $S_u/\sigma'_m$  approach, the total stress envelope parameters were derived in Fig. 20 as

- Lower strength line:  $c = 14$  kPa and  $\phi = 21^\circ$ . These are the strength parameters used in Case 2b with input accelerations of LEX-00°, LEX-90°, CLS-00°, CLS-90° and their associated vertical input accelerations.
- Middle strength line:  $c = 28$  kPa and  $\phi = 21^\circ$ . This set of strength is not used in this study.

Note that the total stress envelope parameters ( $c$ ,  $\phi$ ) for the Lower strength line were also reported in Harder et al. (1998) and referenced in Bray and Macedo (2019) in their illustrative example for estimating earthquake induced slope displacements.

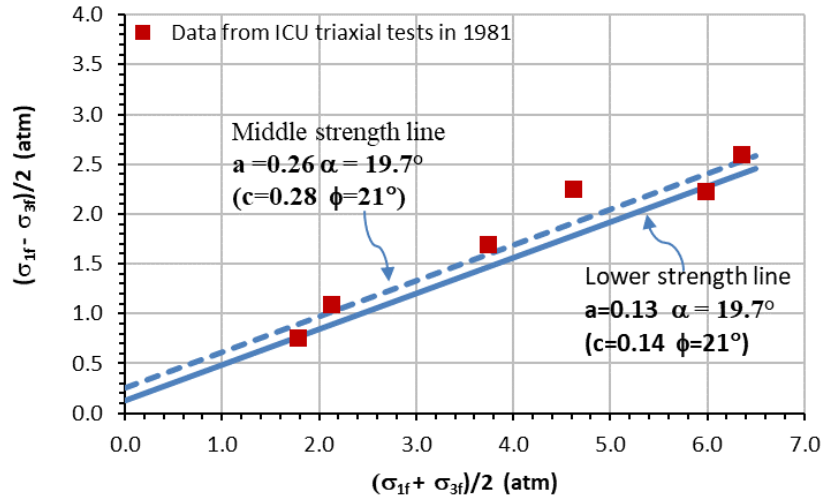


**Fig. 20** Undrained shear strength parameters ( $c$ ,  $\phi$ ) derived from the total stress Mohr-Coulomb failure envelope using the ICU triaxial test data (Data from Wahler Associates 1979, 1981; Boulanger 2019)

Dynamic analyses of the Austrian dam were carried out using the “Total Stress” analysis option in VERSAT-2D and the VERSAT-SAND constitutive model for the total stress envelope approach (i.e., the  $c$ - $\phi$  approach) of the saturated dam fill. The analyses were conducted using the Case 2 phreatic surface and the Lower strengths. Results of the two analyses are presented in Table 3; the calculated dam crest settlements are 0.84-0.78 m (for LEX 00°-90° in 2b) using the  $c$ - $\phi$  approach, that are in good agreement (about 1% difference) with 0.83-0.75 m (for LEX 00°-90° in 2a) using the  $S_u/\sigma'_m$  approach. This sensitivity analysis appears to indicate that the  $c$ - $\phi$  approach is equally applicable to the seismic deformation analyses. However, when the Corralitos input accelerations were applied in the  $c$ - $\phi$  approach, the calculated dam crest settlements increase to 2.40-1.30 m (for CLS 00°-90° and the  $c$ - $\phi$  approach in 2b) that are about 3-2 times the settlements of 0.77-0.68 m (for CLS 00°-90° and the  $S_u/\sigma'_m$  approach in 2a). The shear strain contours of the dam computed using the  $c$ - $\phi$  approach are shown in Fig. 21(a) (for CLS-00° input accelerations) for comparison of shear strain distribution in the dam in Fig. 13 (for LEX-00° input accelerations and the  $S_u/\sigma'_m$  approach). The color legend for shear strains in the two figures is purposely made different to be able to show the difference in magnitude of strains between the two analysis cases. For a large area in the upstream embankment slope of the dam, the shear strains increase to 20-30% when the  $c$ - $\phi$  approach was



adopted, see Fig. 21(a); in the same area the shear strains are about 5-10% (in the yellow color zone in Fig. 13) for the  $S_u/\sigma'_m$  approach.

The large dam crest settlement and large lateral displacement (up to 1.8 m) of the upstream slope calculated using the Corralitos input accelerations, as seen in Fig. 21(b), are mainly attributed to the high vertical accelerations with a PGA of 0.46g (i.e., 71% and 95% of the PGAs for the 0° and 90° horizontal accelerations, respectively) in the recorded Corralitos record. The high vertical input accelerations could significantly reduce the vertical total stresses ( $\sigma_v$ ), thus reduce the principal total stresses ( $\sigma_1$  and  $\sigma_3$ ) and ultimately reduce the shear resistance of the saturated dam fills, on both the upstream and downstream slopes of the dam.

This sensitivity dynamic analysis seems to suggest that the c- $\phi$  approach may be used in dynamic analyses of earthquake deformations of saturated cohesive soils, provided that the input motions don't contain large vertical accelerations such as the Lexington record. The Lexington record had vertical accelerations with a PGA of 0.19g that was 32%- 35% of the PGAs for the two horizontal accelerations. However, cautions must be taken in interpreting the data and analysis results when the c- $\phi$  approach is indeed adopted, even if it is a sensitivity analysis. The c- $\phi$  approach should be avoided whenever possible in dynamic analysis of dams and be excluded if the analysis involves large vertical input accelerations.

## 6.6 Effect of Dam Foundation Rock Stiffness on Response

This sensitivity analysis of foundation bedrock stiffness was completed using Case 3 phreatic surface, the Lower strength line and the  $S_u/\sigma'_m$  approach, and assuming that the input motion was the recorded ground motion on a free field surface of the same rock as the dam foundation. In here, a 1-m thick bedrock layer was included at the base of the model (see Fig. 6) to represent the elastic half space of bedrock with a shear wave velocity of 1070 m/s (i.e., assuming the Austrian dam has bedrock  $V_{s30}$  of the Lexington dam rock foundation); the entire base (all finite element nodes on the base) were set to have a viscous boundary that is based on the formulations developed by Lysmer and Kuhlemeyer (1969). The "Outcropping Velocity" input option (WGI 2019) in VERSAT-2D program was turned on; the recorded horizontal velocities (also downloaded from the PEER website) were applied as outcropping input velocities.

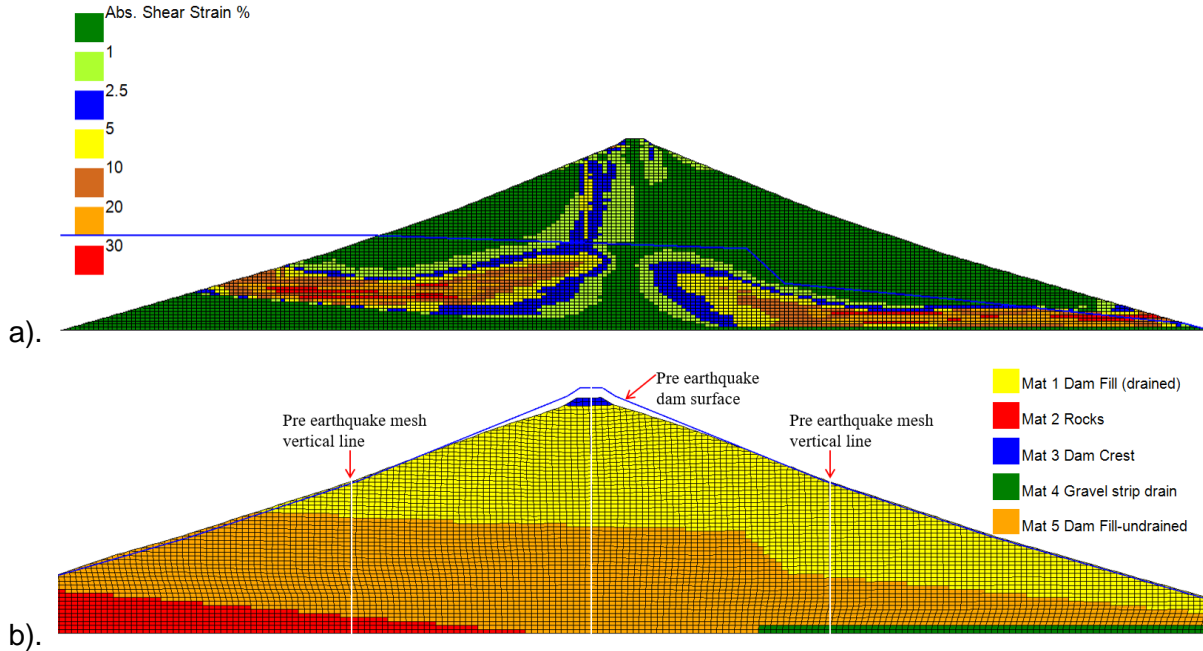


**Fig. 21** Post-earthquake Austrian dam calculated for Case 2b (see Table 3) using the total stress envelope  $c-\phi$  approach with the CLS-00° input accelerations: (a) contours of absolute shear strains (%); and (b) deformed dam configuration showing dam crest settlement of 2.4 m.

The dam crest displacements for the elastic base case (i.e., Case 3c reported in Table 3), computed using either the LEX-00 or the LEX-90 input velocities, are about the same as these computed using the respective input accelerations but applied to the rigid base (i.e., Case 3a in Table 3). It is not a surprise that the rigid base model and the elastic half space model have resulted in approximately the same dam crest displacements. The assumed shear modulus (calculated from  $V_{s30} = 1070$  m/s) of the bedrock is about 4.4 times that of the dam fills immediately above the model base. This large contrast of shear stiffness between the dam fills and its bedrock foundation has resulted in almost identical accelerations at the base of the finite element model, see Fig. 22(a). Using the LEX-00° input motions, the response accelerations at the dam crest in Fig. 22(b) from the two models are very similar in the duration of strong shaking (0-10 s) when the dam settlement occurs in Fig. 22(c); the computed PGAs at the dam crest are 0.55g and 0.63g for the elastic base model and for the rigid base model, respectively. If the foundation bedrock had been a lot softer than the assumed  $V_{s30}$  of 1070 m/s but had  $V_{s30}$  of 760 m/s, the

foundation bedrock of the dam would have some significant impact to the motion at the dam base and thus on dam response, most likely reducing the intensity of the input motion.

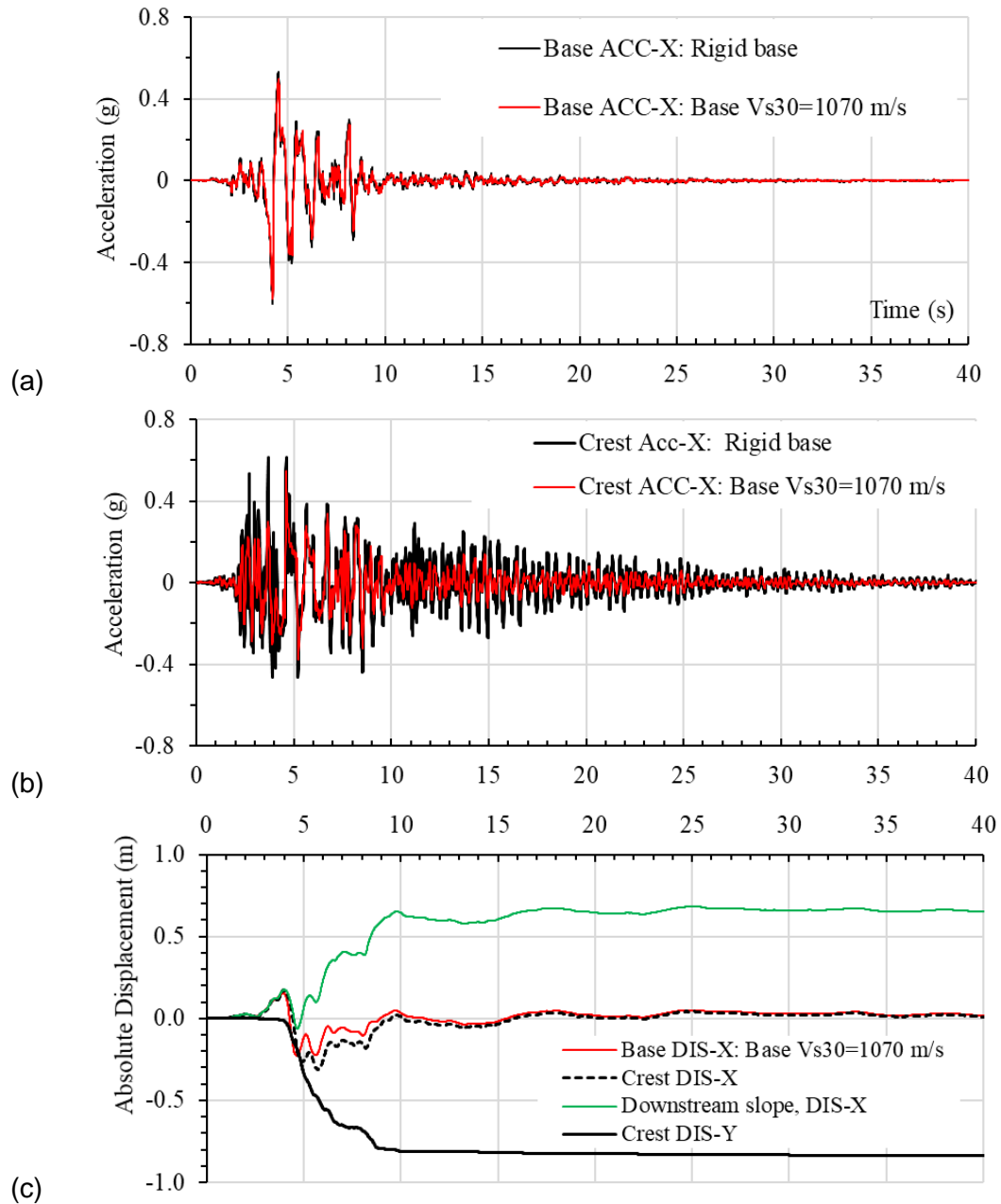


**Fig. 22** Response histories computed for Case 3c using the elastic base model with  $V_{s30} = 1070$  m/s and the LEX-00° input velocities: (a) accelerations at the base; (b) dam crest accelerations; and (c) total displacements at the dam crest.

## 6.7 Effect of Shear Wave Velocity of the Dam Fills on Response

In this sensitivity analysis on the shear wave velocity of the dam fills, reported as Case 3d in Table 3, the low-strain shear modulus constant  $K_{2max}$  is assigned a value of 98, i.e., a reduction of 20% from the base-case  $K_{2max}$  of 122. As a result, the dam crest settlements for Case 3d with  $K_{2max}$  of 98 increase about 9% to 0.79-0.92 m (for LEX 00°-90°) from the corresponding Case 3c with  $K_{2max}$  of 122. The increase of settlement is likely caused by the decrease in the fundamental frequency of the dam due to a less stiff dam that brings the frequency of the dam closer to the predominant frequency of the Lexington input motions [see Fig. 16(c) for their response spectra]; in this case, a less stiff dam results in increasing dam response similar to a resonant effect. On the contrary, a less stiff dam could have reduced dam crest settlements if it is subject to the Corralitos input motions (Boulanger 2019); this is because the Corralitos input motions had predominant frequencies higher than the dam, and a less stiff dam would drive the difference further apart thus reduce the dam response.

## 7.0 DISCUSSION

There are two noticeable uncertainties facing the current case history study of the Austrian dam: the uncertainty on input ground motions and the uncertainty on undrained shear strength characteristics of the saturated dam fill. Although it was considered more suitable to use the scaled Lexington ground motions as the input motions in the dynamic analyses, the actual ground motions experienced by the Austrian dam in 1989 can significantly differ from what were used in the analyses. One way to account for the effect of ground motion variability is to do dynamic analyses on a statistical basis by using hundreds or even thousands of input motions similarly to the approach taken by seismologists in development of GMPE. As automation of finite element dynamic analysis becomes available, the statistical based analysis would be a powerful tool for a practicing engineer to quantitatively assess the uncertainty related to input ground motions.

Uncertainty of the in-situ undrained shear strengths of the saturated dam fills, consisting of compacted clayey sands and clayey gravels, includes sampling disturbance, limited number of ICU triaxial tests conducted, and in particular lack of in-situ shear strength tests for characterization of the aleatory or statistical variability of soil strengths. The proposed  $S_u/\sigma'_m$  approach used in the case history study to characterize the

undrained strengths of the saturated dam fills is considered reasonable in engineering practices, but its suitability or applicability to cohesive soils are to be further verified with more laboratory and field shear strength test data. The results of the sensitivity analyses presented in foregoing sections by using the Lower and Middle strength representations provided some insight and illustrated the importance of shear strengths on the predicted seismic responses.

Other uncertainties would include the pre-earthquake static stress conditions of the dam that were related to the complexity on the loading histories of the dam fills, the actual phreatic surface on the downstream slope of the dam, and the extent of the unsaturated dam fills in the dam and their associated mechanical properties under earthquake loading. The epistemic or modelling uncertainties would include the applicability and tolerance of the adopted soil constitutive models (e.g., the earthquake loading or the PWP increasing rate effect on soil strength), representation of the soil strength in the finite element model (e.g., the total stress or effective stress analysis), and numerical modeling procedures (e.g., the 3D effect on dam response).

## **8.0 CONCLUSIONS**

Two-dimensional (2D) plane strain total stress dynamic analyses of the Austrian dam under the 1989 Loma Prieta earthquake were conducted using the finite element program VERSAT-2D (WGI 2019) and its built-in soil constitutive models, the VERSAT-CLAY model, for simulation of the undrained response of saturated dam fills with a total stress approach; the VERSAT-SAND model was adopted for modelling the unsaturated dam fills above the phreatic surface. The 55-m high compacted earthen dam consisted primarily of low plasticity clayey sands and clayey gravels; subjected to earthquake ground motions with estimated peak horizontal bedrock accelerations of 0.55-0.6g, the dam crest settled 0.76 m on average, developed extensive longitudinal cracks up to 300 mm wide on both the upstream and downstream faces of the dam. Noticeably, a piezometer tube (installed on the midway of the downstream slope) deformed significantly at a location about 8 m above the bedrock foundation; the shear displacement suggested that the dam had deep deformations related to lateral spreading of soils due to shear failure.

The ground motion recorded at the Lexington dam, located at about 9 km away from the Austrian dam, was linearly scaled up by 1.36 and applied as the input motion for the dynamic analyses. It was found that the scaled Lexington dam motion is more suitable

as the input ground motion for dynamic analyses of the Austrian dam than the Corralitos station motion; the judgement was made by the close similarity between the Austrian dam and the Lexington dam in earthquake source directivity and in foundation bedrock characteristics. The VERSAT-2D dynamic analyses showed that the proposed  $S_u/\sigma'_m$  approach for calculating the undrained strengths of the saturated dam fills provides reasonably conservative approach for engineering analysis and design; the calculated dam crest settlements ranged from 0.70 to 0.83 m (among the three assumptions on phreatic surface) are in good agreement with the measured average of 0.76 m. The computed distribution of shear strains indicated that the dam experienced deep deformations with lateral spreading type of shear failure; large shear strains greater than 20% were computed to occur in the region where significant deformation was observed in the piezometer tube. Parametric analyses demonstrated the significance of  $S_u$  on dam performance and revealed limitations in using the total stress envelope  $c-\phi$  approach for characterizing the undrained strengths of cohesive soils; it is suggested that the  $c-\phi$  approach be avoided whenever possible for dynamic analysis of dams and be excluded if the analysis involves large vertical input accelerations. Dynamic analysis of the effect of foundation bedrock stiffness on dam response found that the use of  $V_{s30} = 1070$  m/s for the elastic bedrock half space, instead of a rigid base model, has little effect on dam crest settlement because of the large contrast in stiffness between the bedrock and the dam fills above it.

## **ACKNOWLEDGMENTS 致谢**

Any opinions, findings, conclusions, or recommendations expressed herein are those of the author and do not represent the views of any other parties. The anonymous reviewers provided valuable comments and suggestions related to input ground motions and discussions on the undrained response of saturated clayey soils that significantly improved the paper. The author sincerely thanks them for their supports.

## **REFERENCE**

Boulanger, R. W. 2019. "Nonlinear dynamic analyses of Austrian Dam in the 1989 Loma Prieta earthquake." *J. Geotech. Geoenviron. Eng.* 145 (11). [https://doi.org/10.1061/\(ASCE\)GT.1943-5606.0002156](https://doi.org/10.1061/(ASCE)GT.1943-5606.0002156).

Bozorgnia, Y., et al. (32 authors) 2014. "NGA-West2 research project." *Earthquake Spectra* 30 (3): 973–987. <https://doi.org/10.1193/072113EQS209M>.

Bray, J. D., and J. Macedo. 2019. "Procedure for estimating shear-induced seismic slope displacement for shallow crustal earthquakes." *J. Geotech. Geoenviron. Eng.* 145 (12). [https://doi.org/10.1061/\(ASCE\)GT.1943-5606.0002143](https://doi.org/10.1061/(ASCE)GT.1943-5606.0002143).

Duncan, J. M., and S. G. Wright. 2005. *Soil strength and slope stability*. New York: Wiley.

Finn, W. D. L, M. Yogendrakumar, N., Yoshida, and H. Yoshida. 1986. *TARA-3: A program for nonlinear static and dynamic effective stress analysis*. Vancouver, BC, Canada: Department of Civil Engineering, University of British Columbia.

Finn W. D. L and G. Wu. 2013. "Dynamic analyses of an earthfill dam on over-consolidated silt with cyclic strain softening." In *Proc., 7th Int. Conf. on Case Histories in Geotechnical Engineering*, Keynote paper, edited by S. Prakash. Chicago, US,

Hadidi, R., Y. Moriwaki, J. Barneich, R. Kirby, and M. Mooers. 2014. "Seismic deformation evaluation of Lenihan Dam under 1989 Loma Prieta Earthquake." In *Proc. 10th US National Conf. on Earthquake Engineering, Frontiers of Earthquake Engineering*. Oakland, CA: Earthquake Engineering Research Institute.

Harder, L. F., Jr., J. D. Bray, R. L. Volpe, and K. V. Rodda. 1998. "Performance of earth dams during the Loma Prieta earthquake." In *US Geological Survey Professional Paper 1552-D*, edited by T. L. Holzer, 3–26. Washington, DC: US Government Printing Office, USGS.

Ladd, C. C., and R. Foote. 1974. "New design procedure for stability of soft clays." *J. Geotech. Eng.* 100 (7): 763-786. US: ASCE.

Ladd, C. C. and D. J. DeGroot. 2004 revised. "Recommended practice for soft ground site characterization: Arthur Casagrande Lecture." In *Proc. 12th Pan-American Conference on Soil Mechanics*. Cambridge: US

Lysmer, J., and R. L. Kuhlemeyer. 1969. "Finite dynamic model for infinite media." *J. Eng. Mechanics*. 95 (4): 859-877. US: ASCE.

PEER (Pacific Earthquake Engineering Research Center). *2021 PEER Ground Motion Database*. <https://ngawest2.berkeley.edu>. Berkeley, CA: PEER

Ryan, M.J., M. Mooers, F. I. Makdisi, J. Nelson, and C. Slack. 2013. "Seismic stability evaluation of Anderson Dam." In *Proc. 2013 Annual United States Society of Dams Conference*. Santa Clara County, California.

Seed, H.B., and I. M. Idriss. 1970. Soil moduli and damping factors for dynamic response analyses. *Report UCB/ERRC-70/10, Earthquake Engineering Research Center, Berkeley CA: University of California.*

Sherstobitoff, J., D. Siu, I. Stewart, and Q. Chen. 2004. "First Narrows and Port Mann water supply crossings seismic vulnerability assessment." In *Proc. 13th World Conference on Earthquake Engineering, Vancouver, Canada.*

Sun, J. I., R. Golesorkhi, and H. B. Seed. 1988. Dynamic moduli and damping ratios for cohesive soils. *Report UCB/ERRC-88/15, Earthquake Engineering Research Center, Berkeley CA: University of California.*

Sweeney, N. and L. Yan. 2014. "Dam safety upgrade of the Ruskin dam right abutment." In *Proc. 2014 Annual Conference.* Alberta, Canada: Canadian Dam Association.

USBR (US Bureau of Reclamation). 2019. *Best Practices in Dam and Levee Safety Risk Analysis - Chapter D-5 Embankment Slope Instability.* Washington, US: USBR

Wahler Associates. 1979. *Initial evaluation of seismic stability of Austrian Dam, December, 1979.* File No. 622-13, Item No. 8. Sacramento, CA: California Dept. of Water Resources, Division of Safety of Dams.

Wahler Associates. 1981. *Seismic safety evaluation of Austrian Dam for San Jose Water Works, August 1981.* File No. 622-13, Item No. 10. Sacramento, CA: California Dept. of Water Resources, Division of Safety of Dams.

Wahler Associates. 1990. *Austrian dam-investigation and remedial construction following the October 17, 1989 Loma Prieta Earthquake: Report prepared for the San Jose Water Company.* Palo Alto, CA: Wahler Associates.

Wu, G. 2001. "Earthquake induced deformation analyses of the Upper San Fernando dam under the 1971 San Fernando earthquake." *Can. Geotech. J.* 38 (1): 1-15. <https://doi.org/10.1139/t00-086>

Wu, G and S. Chan. 2002. "Design of the Russ Baker Way overpass on liquefiable sand - Vancouver Airport Connector - Sea Island, Richmond, B.C." In *Proc. 6th Int. Conf. on Short and Medium Span Bridges*, edited by P. Brett, N. Banthia, and P. G. Buckland, 579-586. Vancouver

Wu, G., T. Fitzell, and D. Lister. 2006. "Impacts of deep soft soils and lightweight fill approach embankments on the seismic design of the Hwy. 15 North Serpentine River



bridges, Surrey, B.C.” *Proc. 59th Canadian Geotechnical Conference*, 596-601. Vancouver: CGS (Canadian Geotechnical Society).

Wu, G. 2010. “Seismic soil pressures on rigid walls with sloped backfills.” *Proc., 5th Int. Conf. on Recent Advances in Geotechnical Earthquake Engineering and Soil Dynamics*, edited by S. Prakash, Paper No. 6.20a. San Diego, US

Wu, G. 2015. “Seismic design of dams.” In *Encyclopedia of Earthquake Engineering*, edited by M. Beer, I. A. Kougiumtzoglou, E. Patelli and I. S-K. Au. Berlin Heidelberg, Germany: Springer-Verlag

Wu, G. 2018. “Probabilistic approach to design of seismic upgrade to withstand both crustal and subduction earthquake sources.” In *Proc., 25th Annual Symposium on Ground Improvement*. Vancouver, BC, Canada: VGS (Vancouver Geotechnical Society)

Wu, G. 2021. “Reliability-based dynamic analyses for seismic design optimization in British Columbia.” In *Proc., 27th Annual Symposium on Risk and Liability*. Vancouver, BC, Canada: VGS (Vancouver Geotechnical Society)

WGI (Wutec Geotechnical International). 2019. *VERSAT-2D v.2019: A computer program for 2-dimensional static and dynamic finite element analysis of continua*. BC, Canada: WGI



**APPENDIX A      BACKGROUND INFORMATION**

# The Loma Prieta, California, Earthquake of October 17, 1989—Earth Structures and Engineering Characterization of Ground Motion

THOMAS L. HOLZER, *Editor*

PERFORMANCE OF THE BUILT ENVIRONMENT  
THOMAS L. HOLZER, *Coordinator*

---

**U.S. GEOLOGICAL SURVEY PROFESSIONAL PAPER 1552-D**

*Prepared in cooperation with the National Science Foundation*



## APPENDIX A Background Information

UNITED STATES GOVERNMENT PRINTING OFFICE, WASHINGTON : 1998

---

## AUSTRIAN DAM

Austrian Dam was the earth dam most heavily damaged by the Loma Prieta earthquake. This dam is located directly above the projected northern segment of the fault rupture and about 7 miles from the epicenter (fig. 2). Because of its proximity to the earthquake, it is also thought to have been the dam to have experienced the largest shaking with peak ground accelerations estimated to have been between 0.55 and 0.6 g.

Fortunately, at the time of the earthquake, the reservoir elevation was about 100 feet below the dam crest. In fact, the reservoir level had been depressed during a 3 to 4 year drought prior to the earthquake, and the upper embankment materials were not fully saturated. The damage sustained by the embankment included moderate settlement, downstream movement, and moderate longitudinal and transverse crack-

ing (fig. 3). The concrete spillway located on the right abutment was also heavily damaged. Details of the investigations and remedial construction are described in a report by Wahler Associates (1990). Previous summaries of damage were presented by Bureau and others (1989), Rodda and others (1990), and Seed and others (1990).

Austrian Dam is a 185-foot-high rolled earth fill dam and was completed in 1950. The dam site is situated between the San Andreas and the Sargent faults. The dam is about 4,000 feet southeast of the main intersection of these fault zones, with the trace of the 1906 movement on the San Andreas fault located only 1,700 feet south of the dam. The Sargent fault is located less than 700 feet north of the dam. The dam is founded on rocks typical of the Franciscan Complex, including highly fractured sandstone, graywacke, cobble conglomerate, shale, and serpentine.

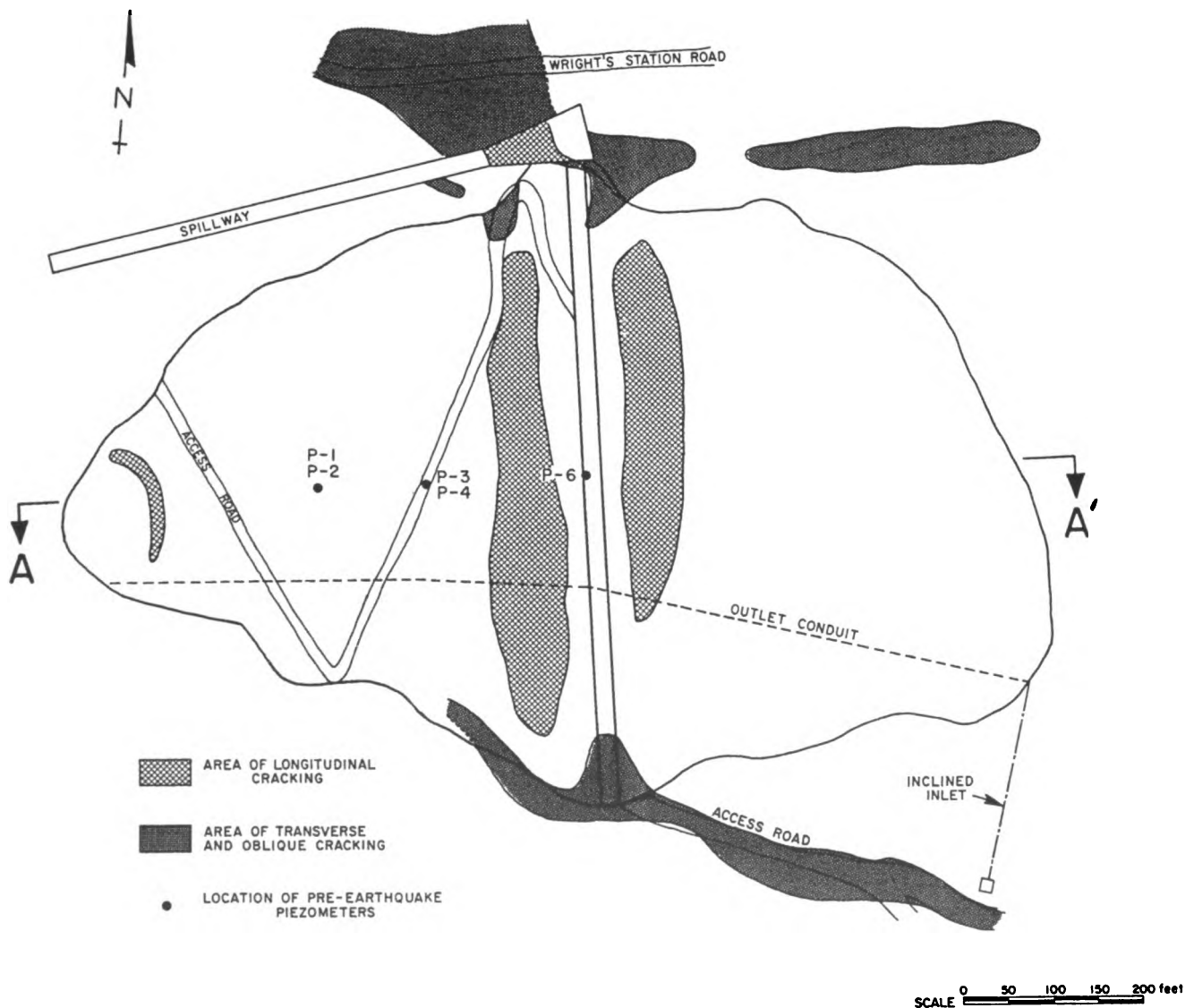


Figure 3.—Plan view of Austrian Dam locating cracks induced by the earthquake—section A-A' shown in figure 4 (adapted from Wahler Associates, 1990).

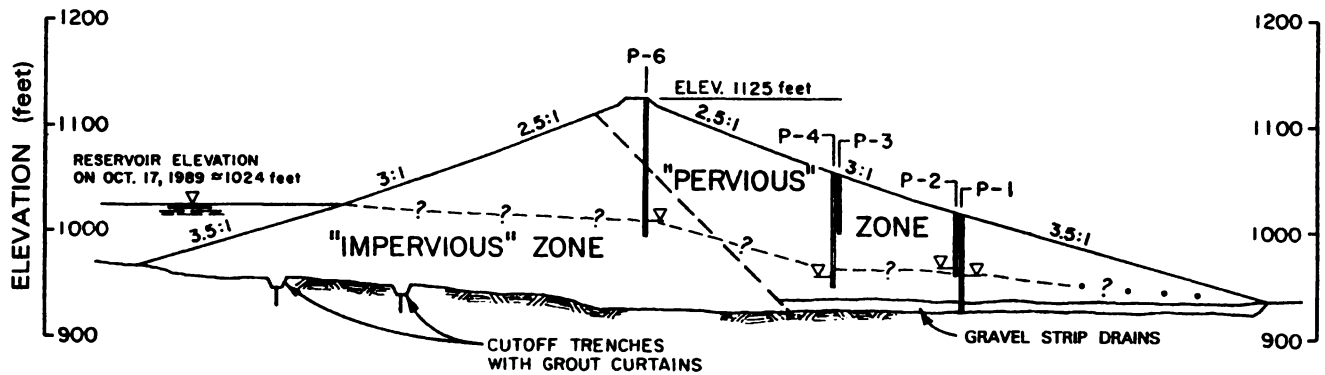


Figure 4.—Maximum cross section of Austrian Dam (section A-A' adapted from Wahler Associates, 1990).

The embankment was built by selective borrowing in an attempt to create a more impervious upstream zone in comparison to the downstream half of the embankment. Gravel strip drains were also placed beneath the downstream "pervious" zone. Figure 4 presents a view of the maximum cross section, together with the approximate reservoir and piezometer levels on the day of the earthquake.

Sampling of the embankment materials during earlier studies of the dam and the piezometer readings together indicate that there is not an appreciable difference between the upstream "impervious" and downstream "pervious" zones, and that the gravel drains are not completely effective in relieving downstream seepage pressures. Hence, the dam can be considered to be nearly homogeneous.

Selected embankment material properties are summarized in table 6. This table presents gradation, compacted density, and placement moisture content values from control tests performed during the original construction in 1950, together with dry density results measured in the dam following the earthquake. Table 6 also presents plasticity, shear strength, and  $K_{2max}$  values from laboratory tests performed on undisturbed tube samples taken in 1979. During the remedial construction in 1989, the average relative compaction measured in the preexisting upstream shell of the dam (based on a compactive effort of 20,000 ft.-lb/ft<sup>3</sup>) was 93 percent. As shown in table 6, the in-situ dry densities of the fill materials in those tests were generally in the upper half of the range of dry densities determined during the 1950 construction control tests.

Significant ground movement in the vicinity of the dam was observed on the downstream right abutment above the spillway chute, on the upstream left abutment between the dam crest and the inclined inlet, and along the right side of the reservoir upstream of the dam (fig. 3).

On the right abutment, a nearly continuous arcuate scarp was observed, extending up to about 200 feet above the dam crest and about 1,000 feet downstream, with maximum vertical and horizontal displacements of about 3 feet. The cracking and movements observed in this area were coincident with topographic features associated with landsliding. Observations in exploration trenches indicated that these cracks

split bedrock materials and that the fissures existed prior to the earthquake.

On the left abutment, nearly continuous cracking was observed about 400 feet along an access road from the dam crest to the upstream inlet structure. The cracking generally paralleled the slope, with vertical scarps up to 14 inches in height, and was subsequently determined by exploratory trenching to be the expression of a shallow landslide in loose material overlying graywacke and shale bedrock that had experienced previous, lesser movements. This landslide did not threaten the inclined inlet.

In addition to several small slumps and landslides around the rim of the reservoir, a set of aligned fissures was observed after the earthquake on the right side of the reservoir. These fissures developed along a topographic bench for a distance of about 1,500 feet upstream of the dam (fig. 3). In general, the fissures appeared to correspond to slumping of the ground toward the reservoir, with vertical scarps up to 3 feet being measured. The dam owner's geotechnical consultant excavated borrow and exploration trenches in this area and concluded that the aligned cracking resulted from shaking-

Table 6.—Characterization of Austrian Dam fill materials

Engineering property	Range	Mean
USCS Classification	SC, GC, CL	
Gradation: > No. 4 (%)	26.0 - 71.5	46.3
Gradation: < No. 200 (%)	16.0 - 43.7	31.8
Specific Gravity, $G_s$	2.60 - 2.78	2.70
Liquid Limit	28 - 32	31
Plasticity Index	11 - 15	13
$W_c$ (as compacted ~1950, %)	9.5 - 19.5	14.5
$\gamma_d$ (as compacted ~1950, pcf)	107.5 - 132.0	121.1
$\gamma_d$ (in situ-1989, pcf)	121.3 - 131.6	126.6
$C'$ (psf)		0
$\phi'$ (degrees)		44
$C$ (psf)		290
$\phi$ (degrees)		21
$K_{2max}$	106 - 128	122

induced settlement of loose, clayey fill overlying a steep bedrock surface and that the linear orientation of the fissures was most likely a result of excavation and/or shaping of the ground during the initial dam construction (Wahler Associates, 1990).

There remains, however, some disagreement as to the cause of the aligned fissures. In a study by Aydin and others (1992), another set of cracks, located approximately 500 feet upslope of the aligned fissures, was mapped. These higher cracks had offsets commonly between 2 and 8 inches, and the study concluded that they were associated with sympathetic tectonic movements on the primary strand of the Sargent fault during the earthquake. That study went on to suggest that the aligned fissures on the bench along the reservoir might be associated with movements along another strand of the Sargent fault.

Figure 5 presents horizontal and vertical movements for crest monuments measured just prior and after the earthquake. These measurements indicated that the dam crest settled over 2.5 feet along most of its length. In addition, the right end of the dam appeared to move downstream horizontally 1.5 feet relative to the left end. Since the survey monuments were not tied into a stationary benchmark, absolute displacement vectors cannot be calculated. Movements and damage near the toe of the dam suggest that the dam moved primarily downstream.

The strong shaking and ground movements produced extensive cracking in the crest of the dam near both abutments. Near the left end of the crest, predominantly transverse cracks in the embankment were up to about 8 inches in width and 10 feet in depth. However, the most pronounced cracking near the left end of the dam occurred along the embankment-foundation contact, where vertical scarps up to 16 inches were observed at the surface. Subsequent explorations traced open cracks varying from 1/8 inch to as much as 1 1/2 feet in width along this contact to depths of up to about 27 feet. The explorations suggested that the cracks were within old landslide deposits that had been left in place on the upper part of the abutment. The possibility that some undisclosed separations might have occurred at even greater depths led to a subsequent remedial grouting program to further examine the contact at greater depths.

Particularly severe cracking occurred where the right end of the dam abuts onto the concrete spillway. This area of the spillway includes an entrance section from the unlined approach channel, the weir, and a transition section which converges to the chute section. The entrance section includes a wing wall extending upstream along the left side of the approach channel, and a "return" wall coming back in a downstream direction, presumably intended to prevent scour around the upstream end of the wing wall. The two walls thus form a "U" pointing downstream, with the right end of the dam abutting on the outside of the return wall and also backfilling the space between the two walls. Up to 9-inch-

wide diagonal cracks occurred in the embankment between the walls. Separations up to 10 inches also developed between the inner faces of the walls and the enclosed embankment. A separation along the outside face of the return wall extended to a depth of about 23 feet (nearly the base of the wall). This would have been particularly dangerous had the reservoir been full, as the normal amount of freeboard was only about 15 feet.

Immediately downstream of the spillway entrance, where the dam abuts the left wall of the transition section, several cutoff collars on the outer (embankment) side of the wall were sheared-off due to upstream-downstream movement of the adjoining embankment relative to the wall.

Extensive damage also occurred in the transition and chute sections of the spillway walls. Up to 3/4-inch-wide tension cracks were observed in the walls and slab of both sections. The cracking in the slab of the chute section was somewhat regularly spaced at about 2 to 4 feet, normal to the axis of the spillway. The 80 feet of chute and transition section farthest upstream was found to have elongated a total of about 7 inches. In the transition section, tension cracks generally paralleled the trend of cracking which occurred in the natural slope above the spillway. Up to 1-inch-wide separations were observed between the bottom of the slab and its highly weathered bedrock foundation along the left wall of the transition section. Subsequent grouting through the slab indicated that these voids developed existed primarily beneath the walls, but not beneath the central part of the slab. This suggested that the spillway walls had been subjected to some sort of rocking action. At the downstream end of the chute, the concrete wingwall on the left side was rotated and torn away from the left wall, while the right wing wall could not be found.

In addition to the damage to the crest and spillway, a series of roughly parallel longitudinal cracks formed in the upstream and downstream faces of the dam. The initial widths of the cracks were relatively small, but ultimately widened within a few weeks to as much as a foot in places. These time-dependent movements may have resulted from major aftershocks, rainfall during this period, soil creep, and/or pore-pressure dissipation and consolidation. Seven days after the main shock, the four longitudinal cracks which formed in the upper 50 feet of the upstream face were approximately 5 to 15 feet deep and 1 to 4 inches wide. A number of longitudinal cracks which were 3 to 8 feet deep and 2 to 6 inches wide formed in the downstream face. The majority of the longitudinal cracks in the downstream face were located near the crest, although some limited cracking also occurred near the toe of the dam. In addition, there was some minor bulging of the downstream toe. Exploration trenches indicated that the longitudinal cracks generally dipped steeply toward the dam crest on both embankment slopes. Hence, the cracks did not appear to result from slope instability, but rather from settlement and rearrangement of the earth embankment.

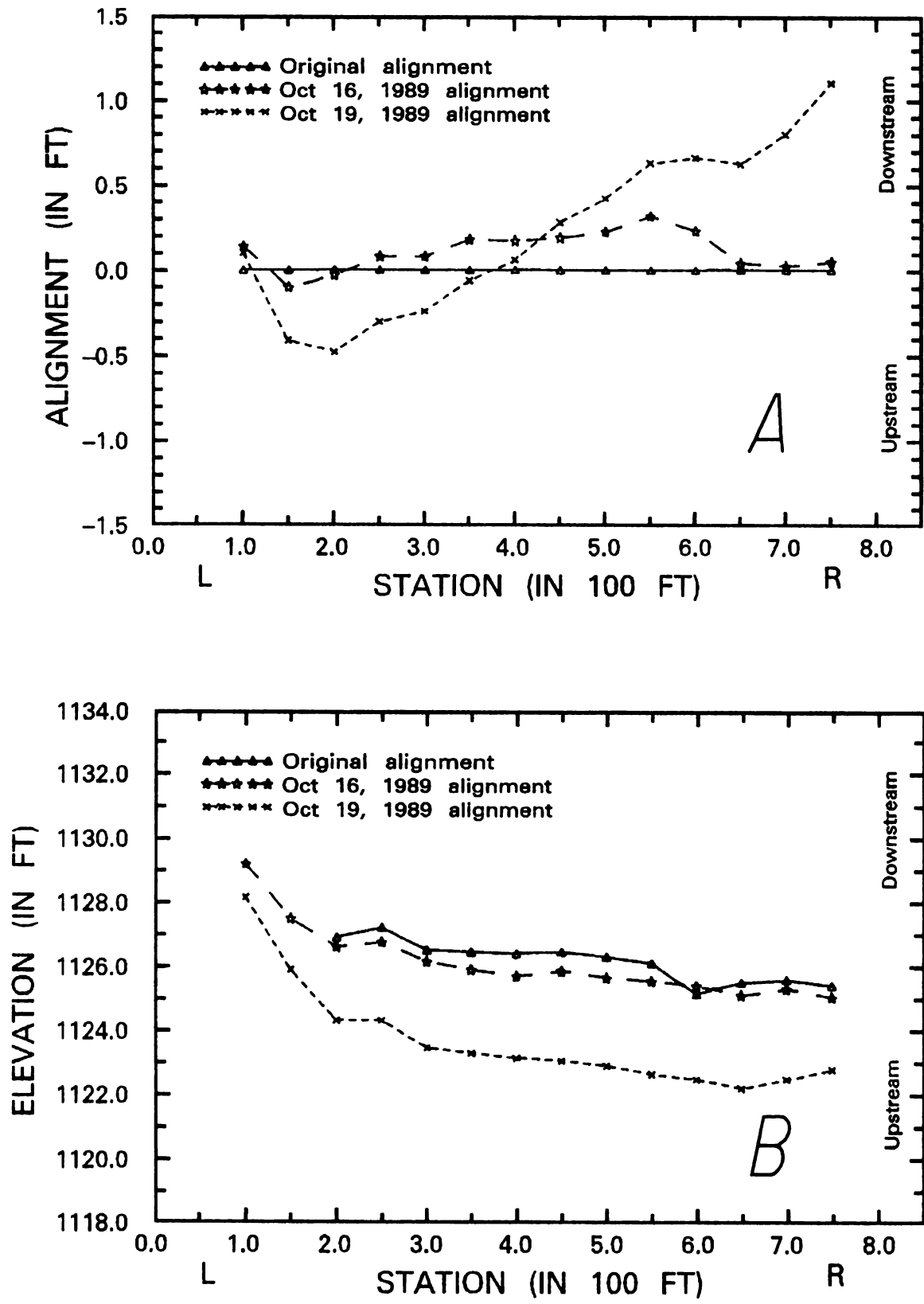


Figure 5.—Horizontal (A) and vertical (B) movements of crest monuments at Austrian Dam (from Seed and others, 1990).



The movements of the embankment were concluded to be due to general settlement and spreading of the fill during the strong earthquake shaking, followed by subsequent downslope creep. Figure 6 presents piezometer measurements made for 5 standpipe piezometers installed prior to the earthquake. These instruments recorded pore-pressure increases between 12 and 54 feet of water. Possibly related to the pore-pressure increases is the fact that some of the trenches excavated across the longitudinal cracks near the crest encountered free water at elevations considerably higher than reservoir levels at the time of the investigation (Wahler Associates, 1990).

The largest pore-pressure increase, 54 feet of water, occurred in piezometer P-1, with its tip located within the downstream "pervious" zone near the bedrock contact. The standpipe for this instrument was found to be significantly deformed between elevations 955 and 960 (about 25 to 30 feet above the bedrock contact). The standpipe for piezometer P-6, which measured an increase in hydraulic head of about 49 feet of water, was also found to be deformed be-

tween elevations 1,017 and 1,041 feet (about mid-height of the embankment). These deformations were suggestive of earthquake-induced internal movements corresponding to lateral spreading of the embankment.

The repair of the earthquake damage consisted of (1) excavating and recompacting the fill in the areas of extensive cracking, (2) placing a zoned fill with chimney and blanket drains in the crest fill at both embankment ends, (3) excavating and recompacting the upstream face of the fill to create an impervious blanket, (4) epoxy grouting the cracking in the spillway and cement grouting voids beneath the spillway slabs, and (5) grouting of the rock at the left abutment contact with the fill.

This repair successfully remediated the earthquake-induced damage to the embankment and was accomplished within 8 weeks following the earthquake. Details of the repair can be found in Wahler Associates (1990). Due to the severity of damage to the concrete spillway and concern about potential future landslides in the right abutment, a new spillway was later constructed on the left abutment of the dam in 1993-1994.

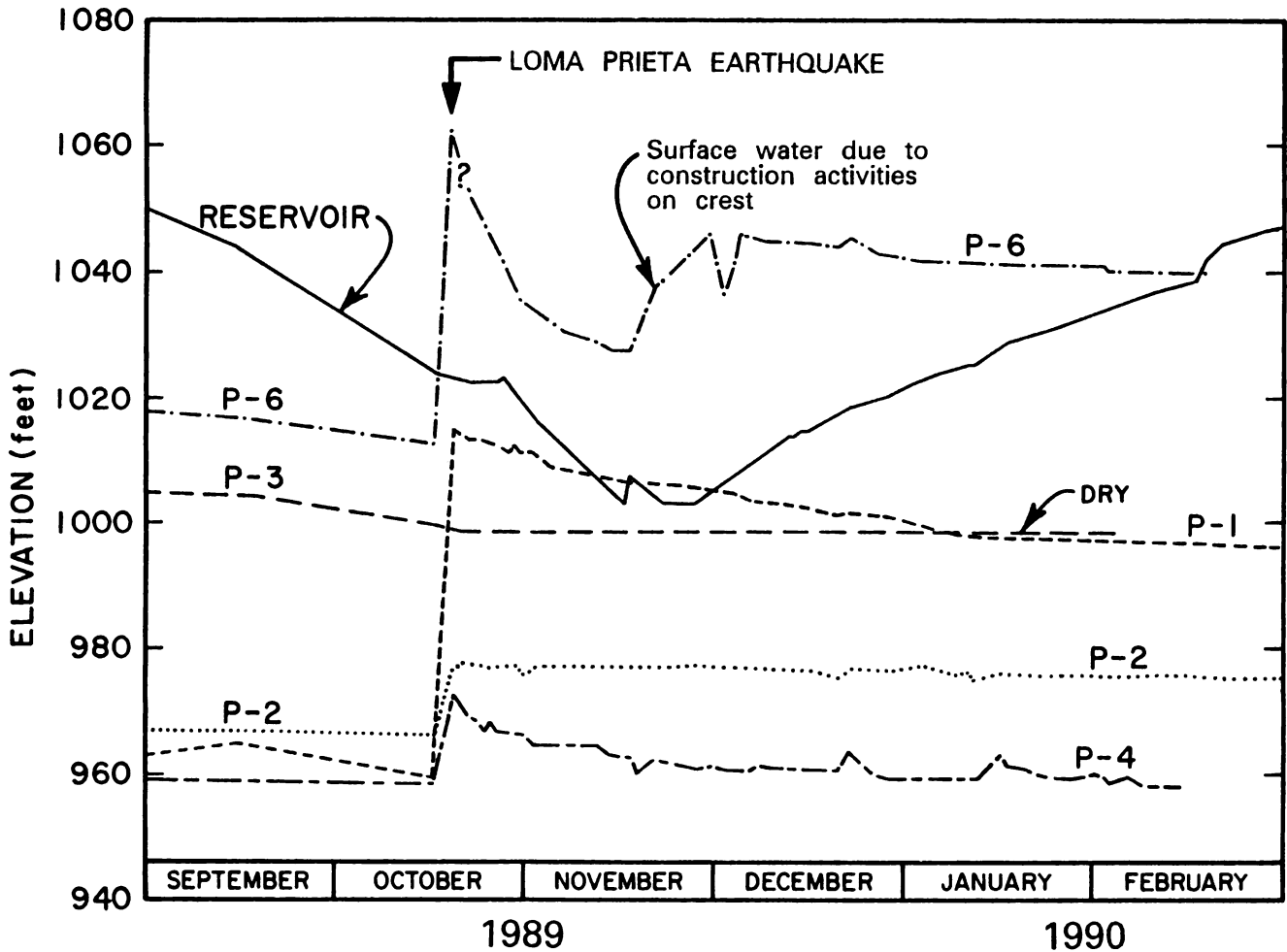


Figure 6.—Piezometer measurements for preearthquake piezometers at Austrian Dam (from Wahler Associates, 1990).

### LEXINGTON DAM (now the LENIHAN DAM)

Lexington Dam is a 205-foot-high dam located about 6 miles downstream of Austrian Dam and about 2 miles from the fault rupture associated with the earthquake (fig. 2). The dam was completed in 1953 as a zoned earth structure having a relatively thick sandy and gravelly clay core that is supported by upstream and downstream random shell zones of clayey sands and gravels. The dam also has relatively flat upstream (5.5:1) and downstream (3:1) slopes. A plan view and cross section are shown in figure 7. The embankment material properties are summarized in table 7. At the time of the earthquake, the reservoir was about 100 feet below the crest of the dam. Previous summaries of damage were presented by Bureau and others (1989), Seed and others (1990), and in the studies by R. L. Volpe & Associates (1990a).

Lexington Dam was instrumented with strong-motion instruments on the left abutment, left crest, and right crest. These accelerographs recorded transverse peak accelerations of 0.45, 0.39, and 0.45  $g$ , respectively. This shaking was composed of about 6 to 7 s of relatively strong long-period motion. The left abutment or "bedrock" peak acceleration is within the range predicted by appropriate strong-motion attenuation relationships for a site approximately 2 miles from the nearest point on the fault rupture surface for a  $M_s = 7.1$  event, but is a bit lower than the mean or expected value based on such relationships. In addition, there appears to be some spectral acceleration amplification at lower frequencies (0.9 to 1.2 Hz). This low frequency amplification may indicate that the recorded "bedrock" motion may have been affected by local topographic or geologic conditions.

The strong ground shaking produced transverse cracking on both the upstream and downstream sides of both abutments, oblique cracking on the crest about 150 feet in from the left abutment, longitudinal cracking on both the upstream and downstream slopes of the dam, and cracking of an access road on the right abutment upstream of the dam. The cracks, which were fairly isolated, were commonly less than 3/4 of an inch wide, and trenching indicated that they only extended to depths generally between 2 and 7 feet (R. L. Volpe & Associates, 1990a). The maximum earthquake-induced crest deformations were approximately 0.85 feet of vertical settlement, and 0.25 feet of lateral displacement in the downstream direction (R. L. Volpe & Associates, 1990a). An old slope indicator casing was found to have raised from beneath the crest to over 3 inches above the crest due to the embankment settling around it. The earthquake shaking and ground movements produced extensive cracking in the bridge abutment at the left abutment and ruptured a buried water line near the crest of the dam.

About 6 weeks after the earthquake, a relatively large seepage area developed high up on the downstream face of the dam. The seepage area was about 170 feet long and 35 feet wide and oriented at an oblique angle with the axis of the dam. This seepage area was really more of a wet or damp

area and never really flowed water. Although the cause of the seepage area is not definitively known, one explanation that has been offered is the fact that old exploration holes extending into the rock foundation lie within the area and that these old borings could have been acting as relief wells for earthquake-induced pore pressures within the lower portions of the embankment and bedrock (R. L. Volpe & Associates, 1990a). Another possible explanation is that the fill is relatively impervious at this elevation and that any surface water that infiltrates the dam becomes perched at this level.

The repairs made to the dam consisted of trenching the cracked areas to depths ranging between 3 and 7 feet and compacting the excavated soil back into the trenches (R. L. Volpe & Associates, 1990b).

### GUADALUPE DAM

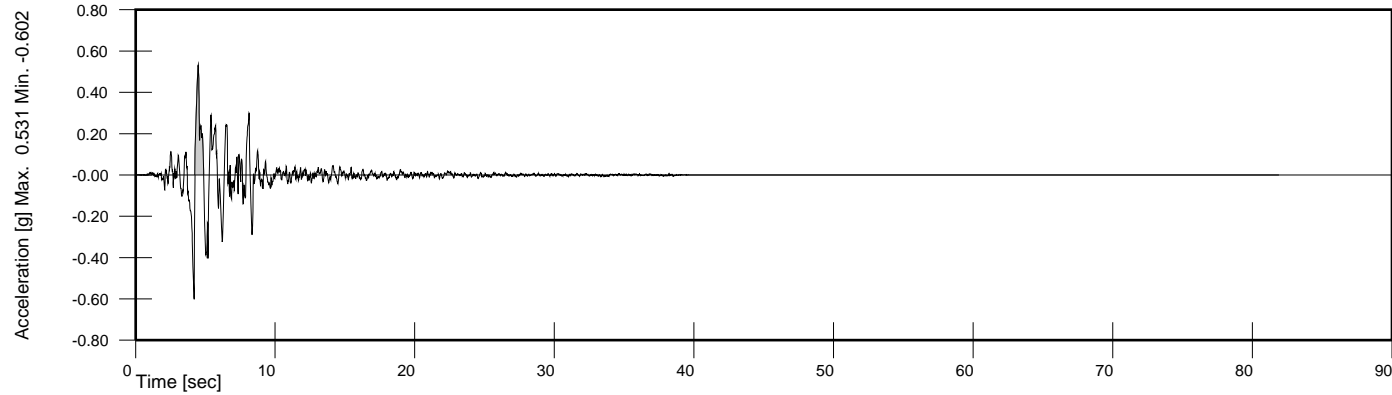
Guadalupe Dam is a 142-foot-high dam located about 6 miles from the Loma Prieta fault-rupture zone, and it probably experienced peak ground accelerations between 0.4 and 0.45  $g$  (fig. 2). The dam was completed in 1935 as a rolled earth structure with an upstream facing of concrete panels for erosion protection. In a manner similar to that described for Austrian Dam, the embankment is apparently nearly homogeneous, as the selective borrowing to create upstream "impervious" and downstream "pervious" zones did not appear to be completely successful in creating distinctly different zones. In 1972, an upstream buttress was added to the dam to improve drawdown stability. A plan view and cross section are shown in figure 8. At the time of the earthquake, the reservoir was about 78 feet below the crest of the dam; however, the reservoir had been full up to about 3 months before the earthquake, and it is assumed that the upstream shell materials were nearly saturated at the time of the earthquake. Previous summaries of damage were presented by Bureau and others (1989), Seed and others (1990), and in the studies by R. L. Volpe & Associates (1990a).

The earthquake induced up to 0.64 feet of settlement and 0.15 feet of lateral displacement in the upstream direction as measured on the crest. Minor transverse cracking developed at the crest at both abutment contacts along with minor longitudinal cracking on the crest. The principal damage was to the upstream slope, where the upper portion of the buttress fill developed longitudinal cracking. Shortly after the earthquake, these cracks were observed to have a maximum width of less than 1 inch and extended across the entire face of the dam. About 5 weeks later, the cracks had widened to about 4 inches and extended to a depth of about 5 feet (R. L. Volpe & Associates, 1990a).

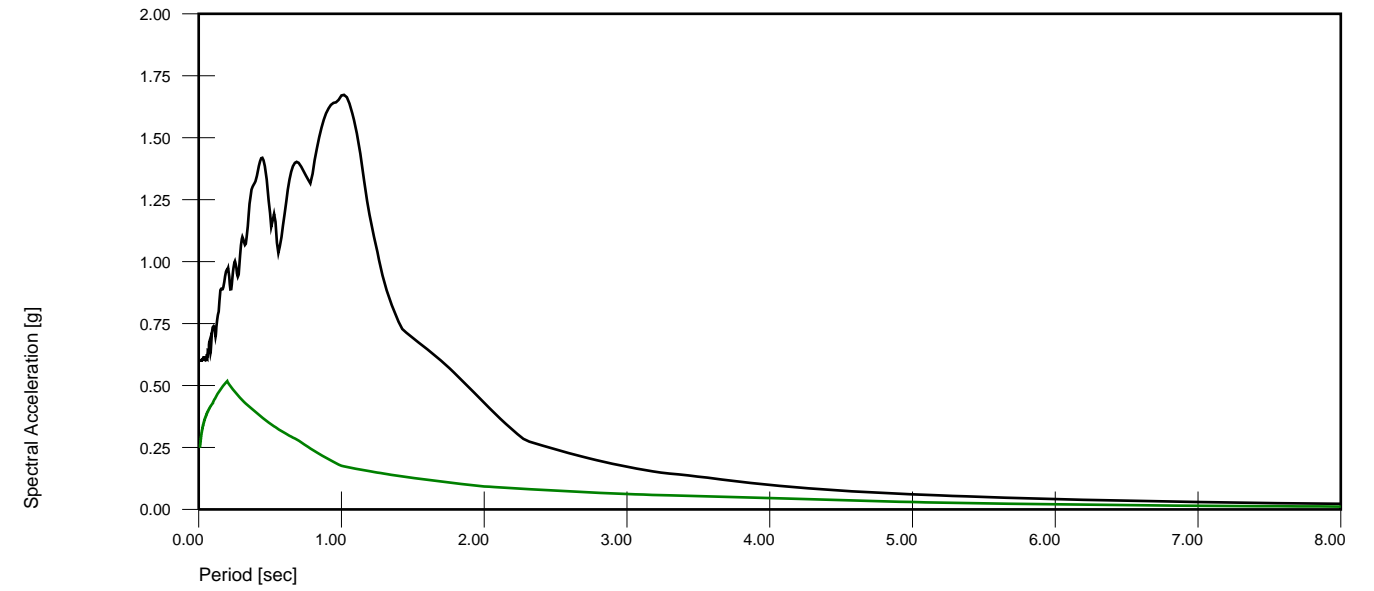
These cracks may have been caused by concentrations of dynamic stresses induced by the change in slope geometry. Alternatively, they may have resulted from possible past settlements caused by the placement of the berm. These past settlements may have created preexisting cracks which surfaced only after the development of strong ground motion.

**APPENDIX B      INPUT EARTHQUAKE RECORDS: LEX & CLS**

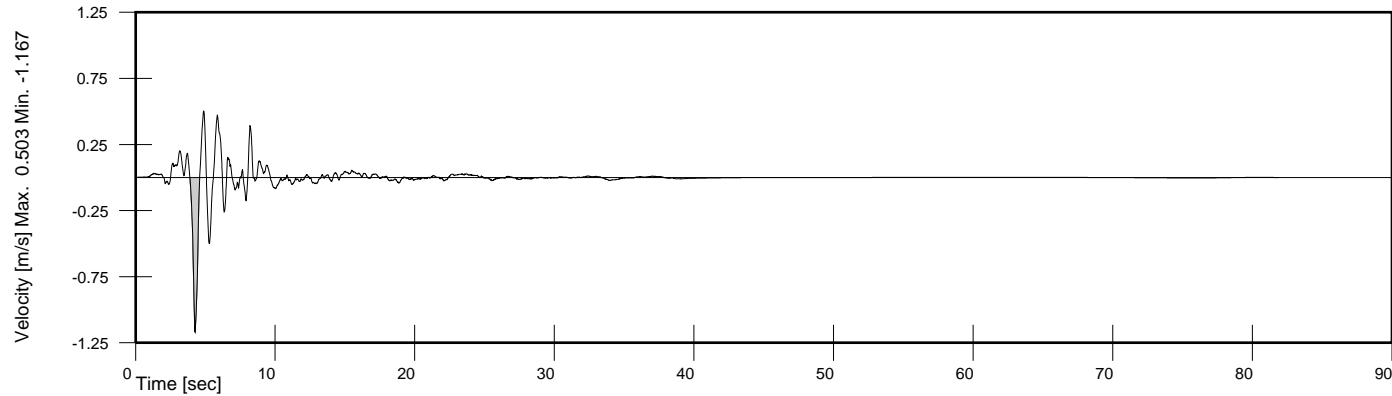
### Acceleration Time History



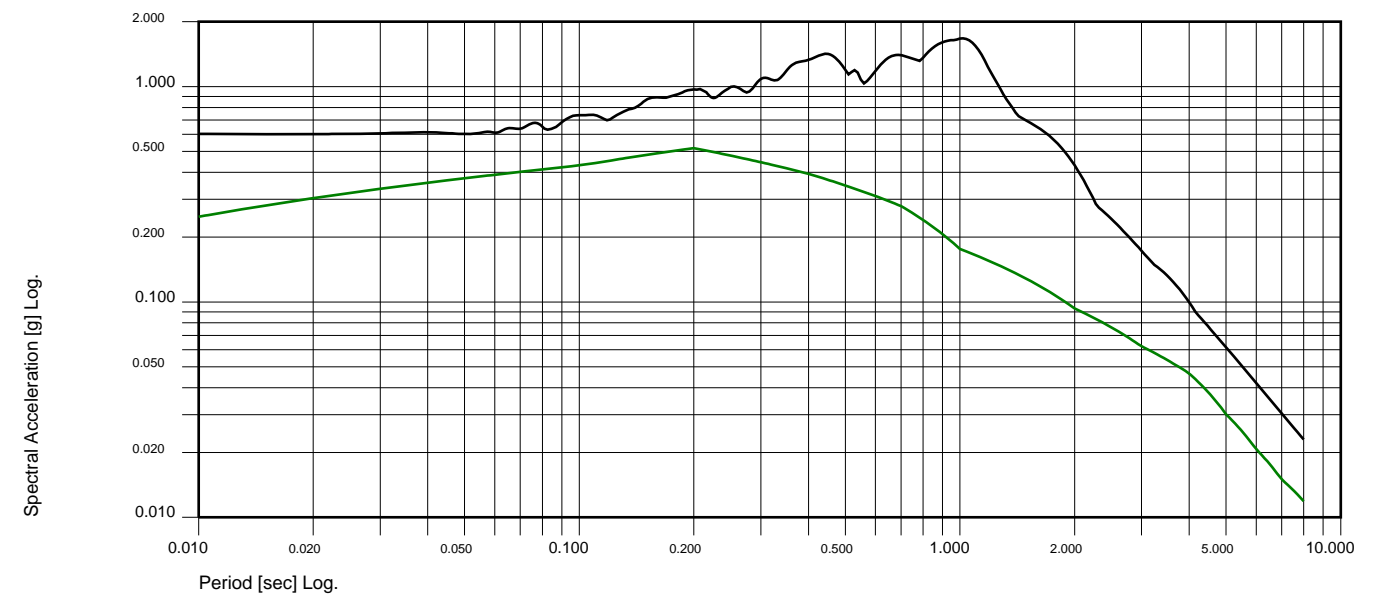
### Acceleration Spectrum



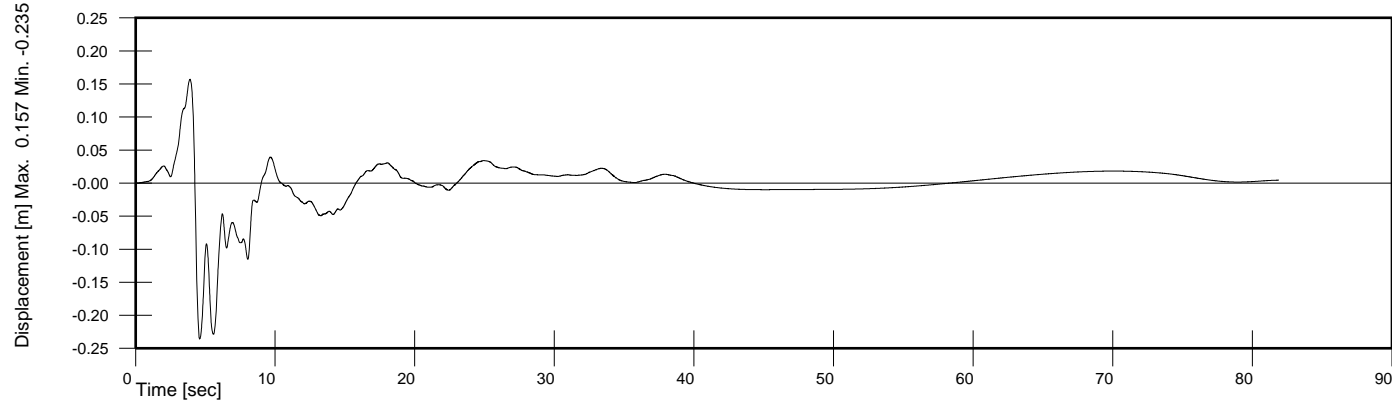
### Velocity Time History



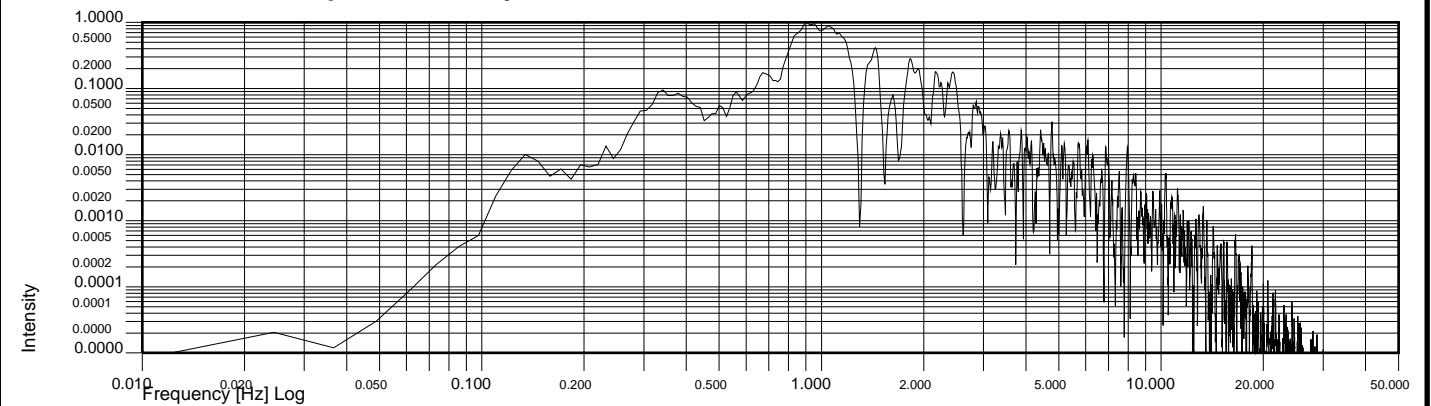
### Acceleration Spectrum



### Displacement Time History



### Normalized Power Spectral Density



Arias Intensity 3.443982 [m/s]  
 0.05, 4.000 [sec]  
 0.25, 4.290 [sec]  
 0.75, 6.110 [sec]  
 0.95, 8.330 [sec]  
 5% to 95% Duration 4.330 [sec]  
 25% to 75% Duration 1.820 [sec]  
 Strong Part Ratio 42.03%

Set:001, Dir:X, File: C:\2021\THS\RSN3548\_LOMAP\_LEX000.AT2.txt

Desc.: Loma Prieta, 10/18/1989, Los Gatos - Lexington Dam, 0

Incremental Velocity 1.668 [m/s], Incremental Displacement 0.392 [m]  
 PGA Ratio 0.412, Area Ratio 0.353 [ 1.000 Hz to 10.000 Hz], MSE 0.245343

USACE Long-norm

Wutec

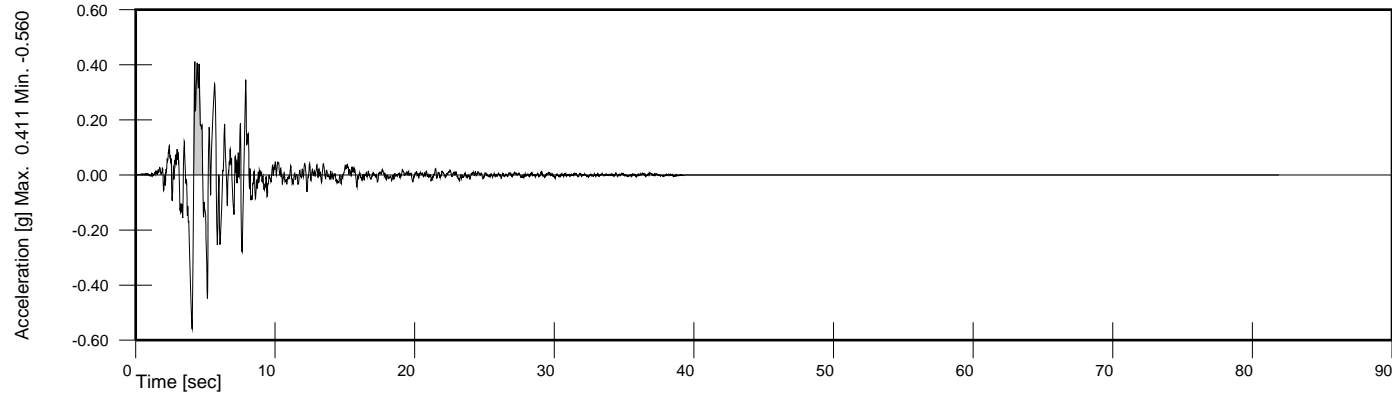
Sa for scaled LEX-00,90,UP

THS by A. Felber, Program Version 0.01, 2010 June 15  
 Date: 2022, February, 25

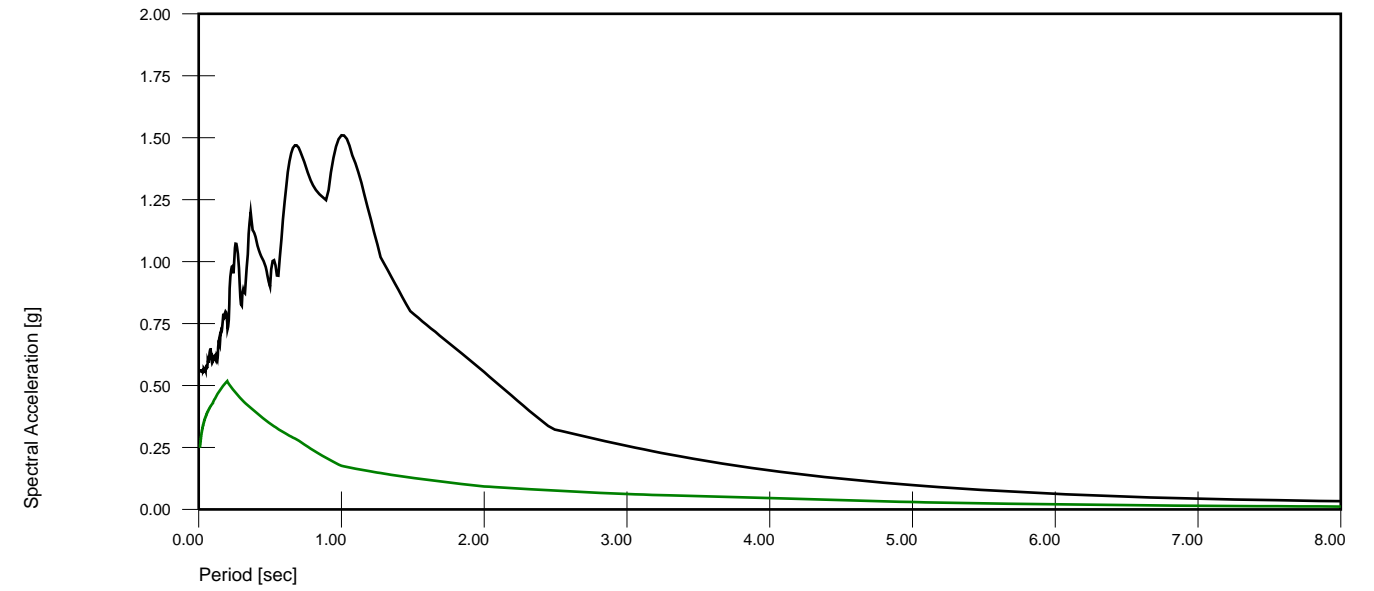
Time: 17:05:13

Page 7 of 9

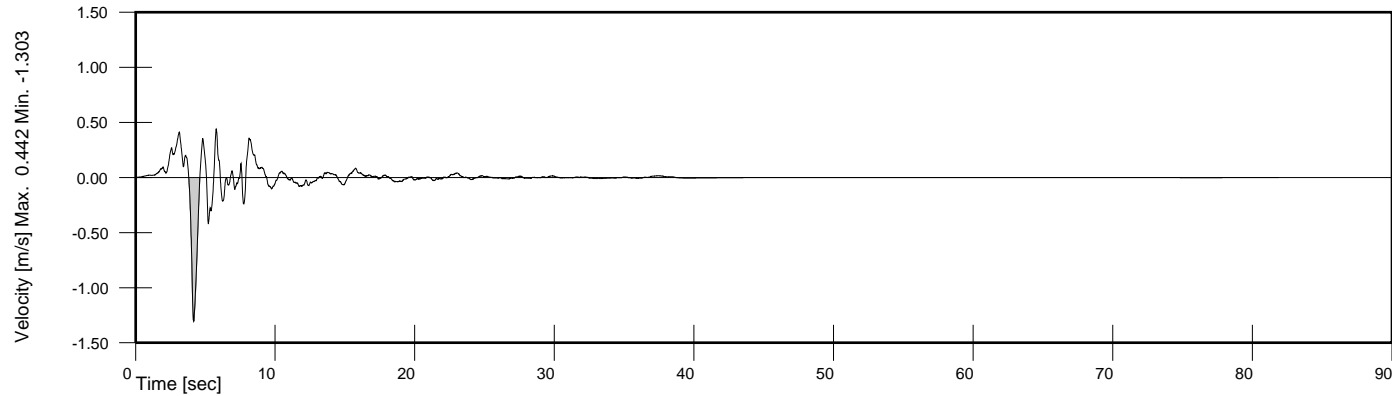
### Acceleration Time History



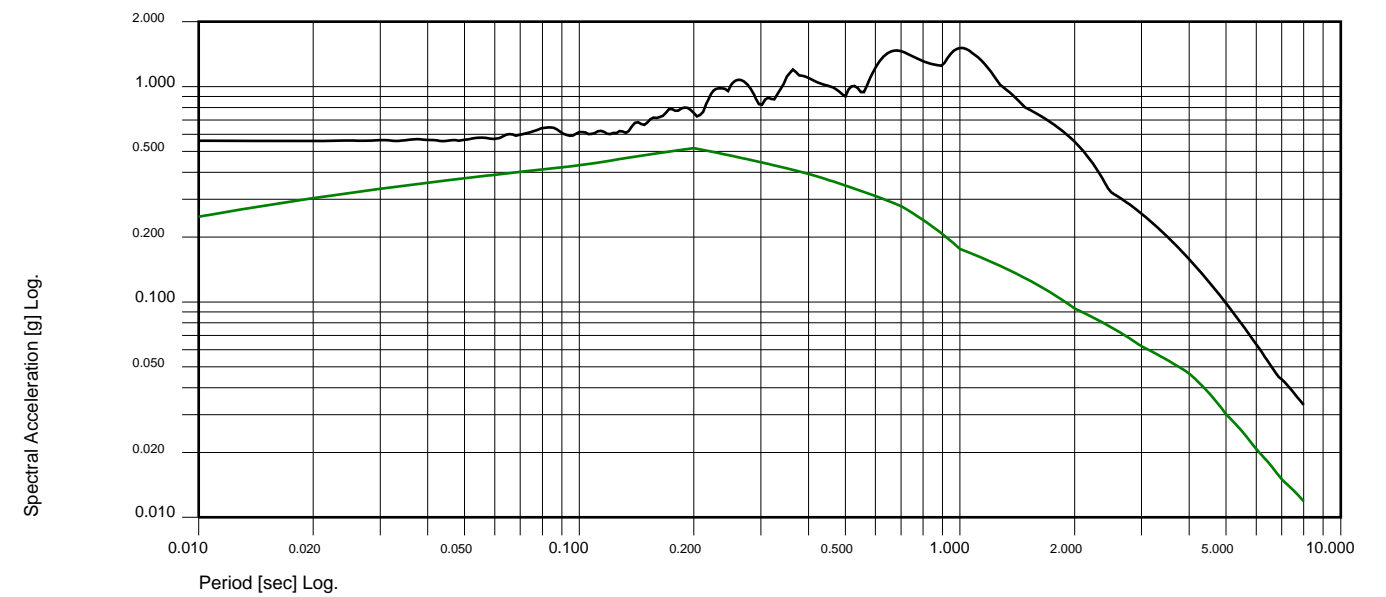
### Acceleration Spectrum



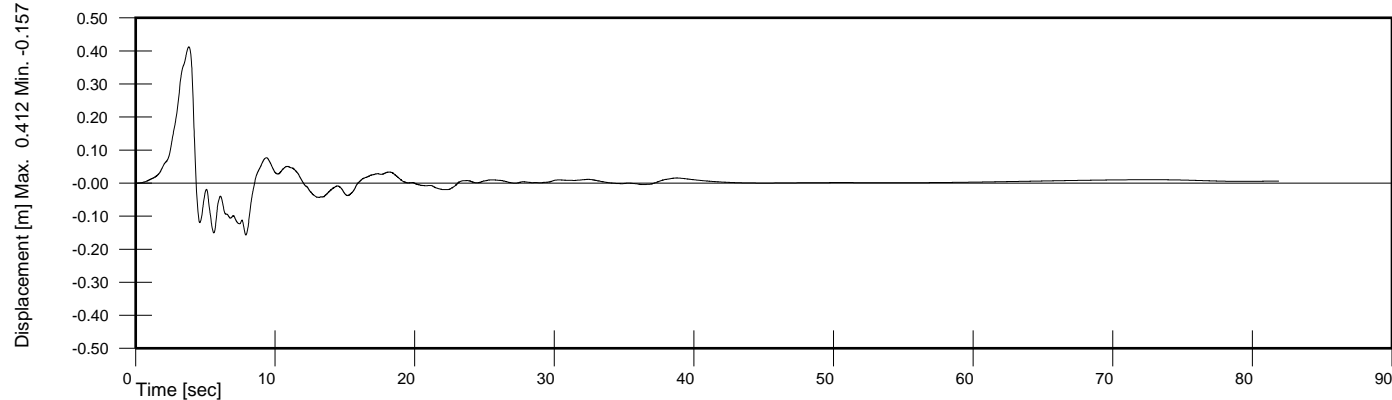
### Velocity Time History



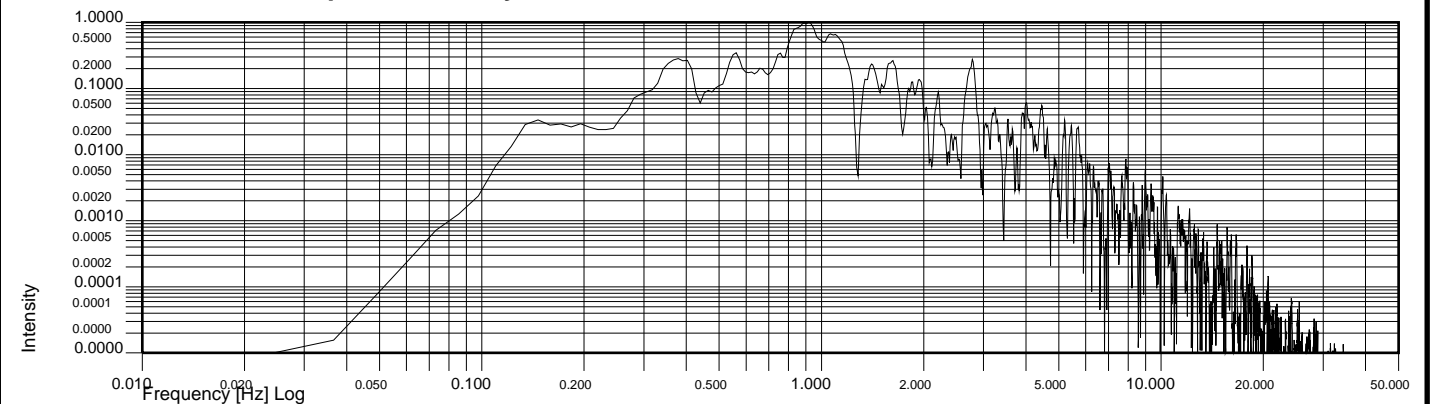
### Acceleration Spectrum



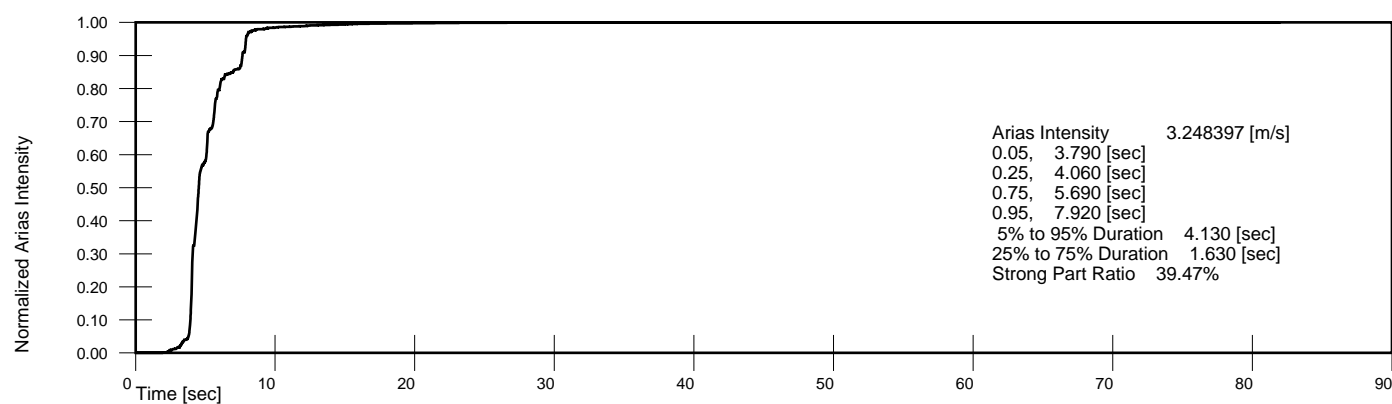
### Displacement Time History



### Normalized Power Spectral Density



### Husid Plot



Set:001, Dir:X, File: C:\2021\THS\RSN3548\_LOMAP\_LEX090.AT2.txt

Desc.: Loma Prieta, 10/18/1989, Los Gatos - Lexington Dam, 90

Incremental Velocity 1.657 [m/s], Incremental Displacement 0.531 [m]  
 PGA Ratio 0.444, Area Ratio 0.401 [ 1.000 Hz to 10.000 Hz], MSE 0.274115

USACE Long-norm

Wutec

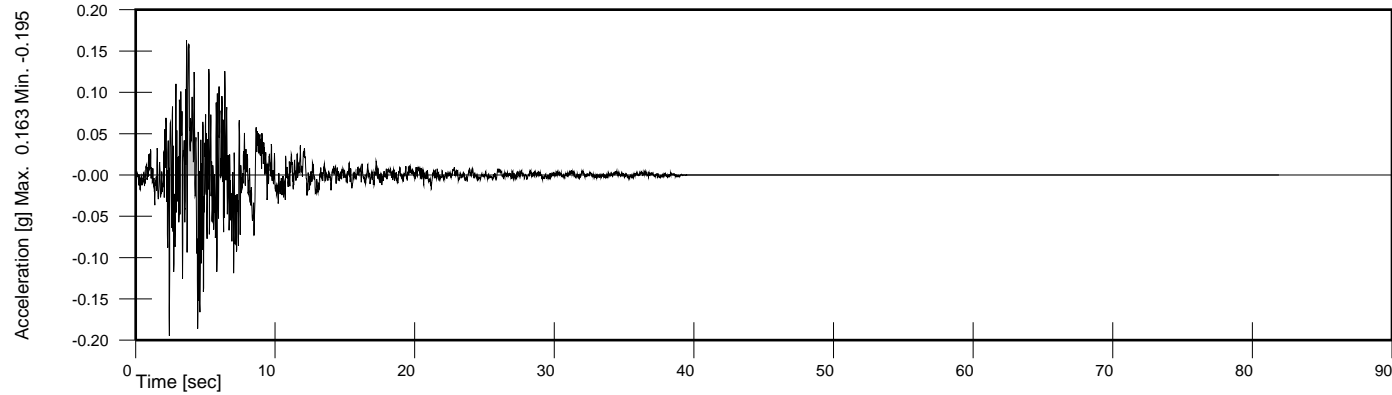
Sa for scaled LEX-00,90,UP

THS by A. Felber, Program Version 0.01, 2010 June 15  
 Date: 2022, February, 25

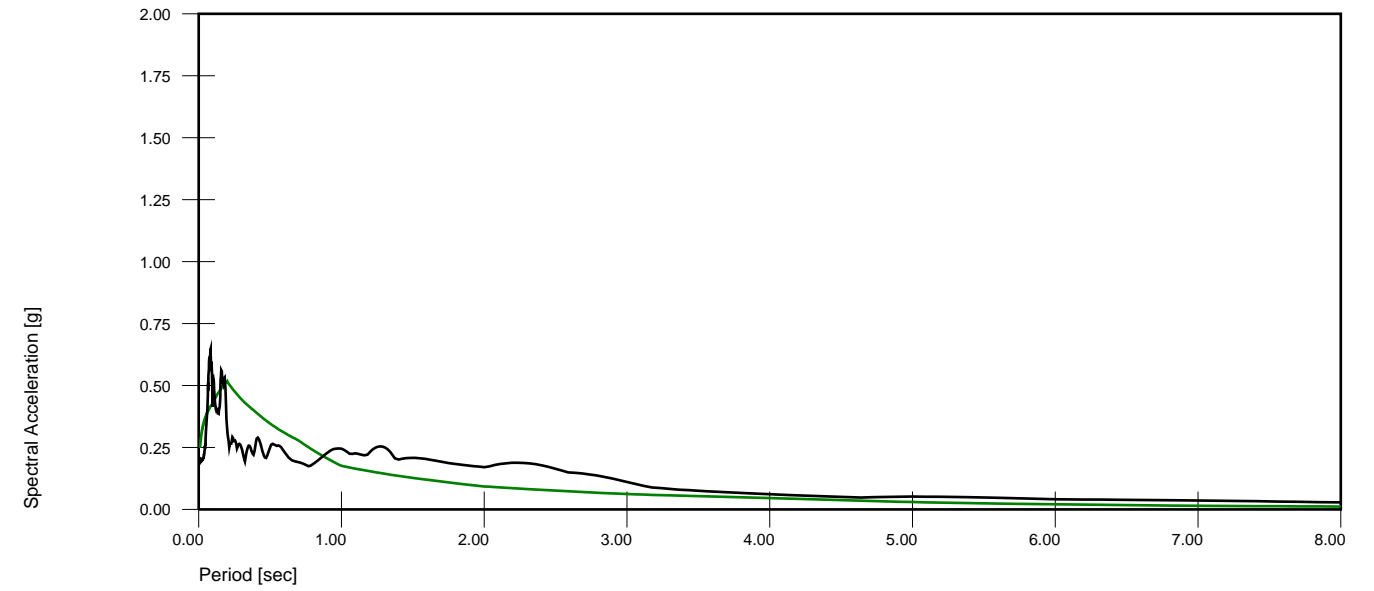
Time: 17:05:13

Page 8 of 9

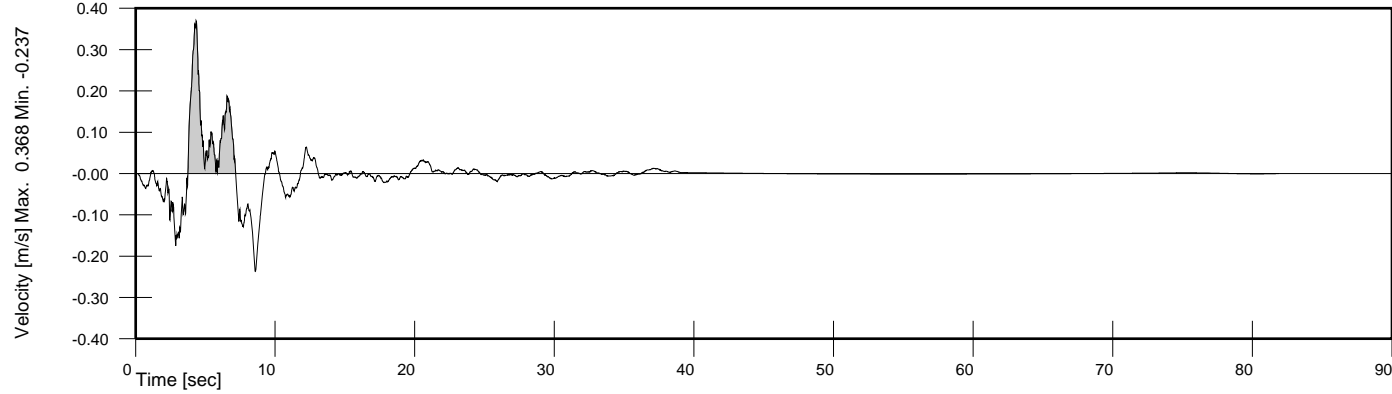
**Acceleration Time History**



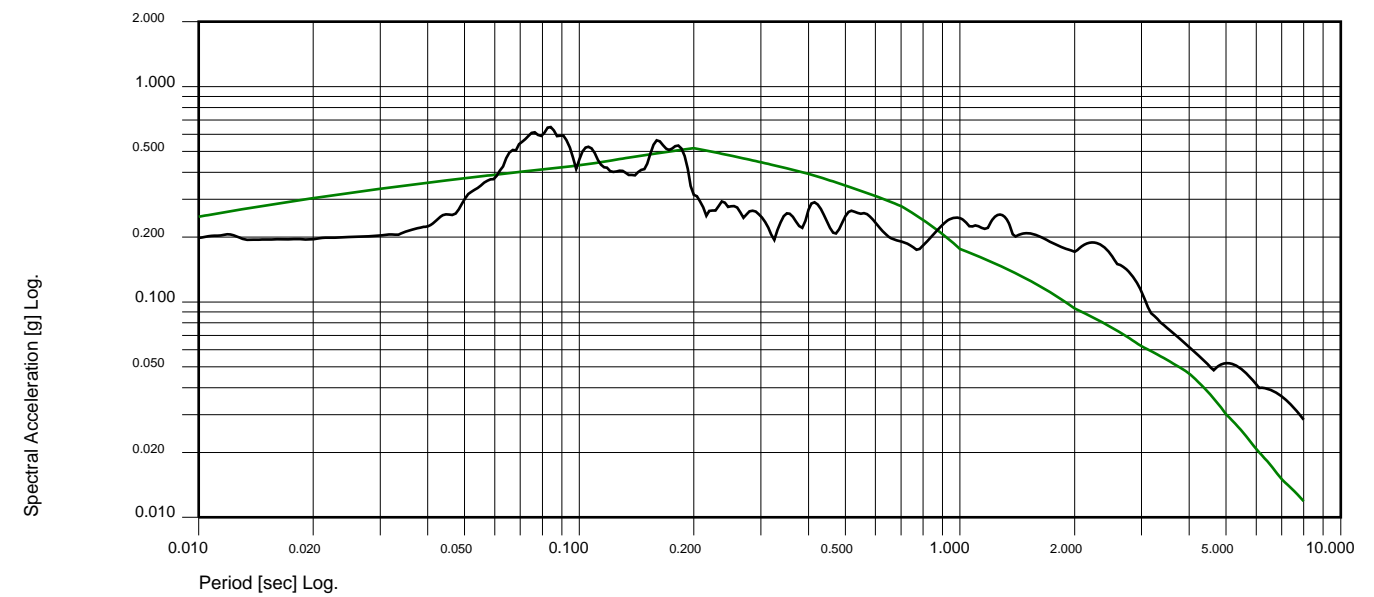
**Acceleration Spectrum**



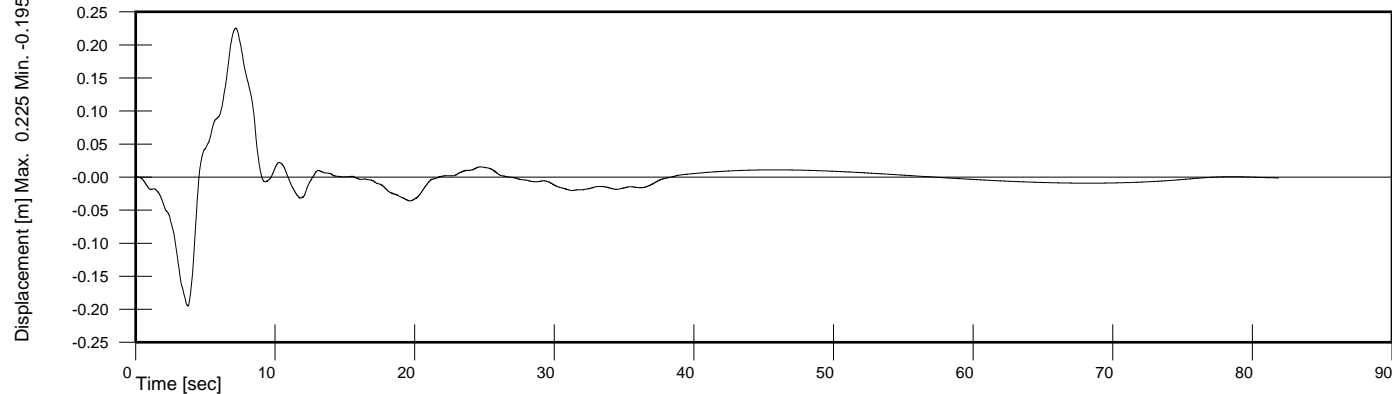
**Velocity Time History**



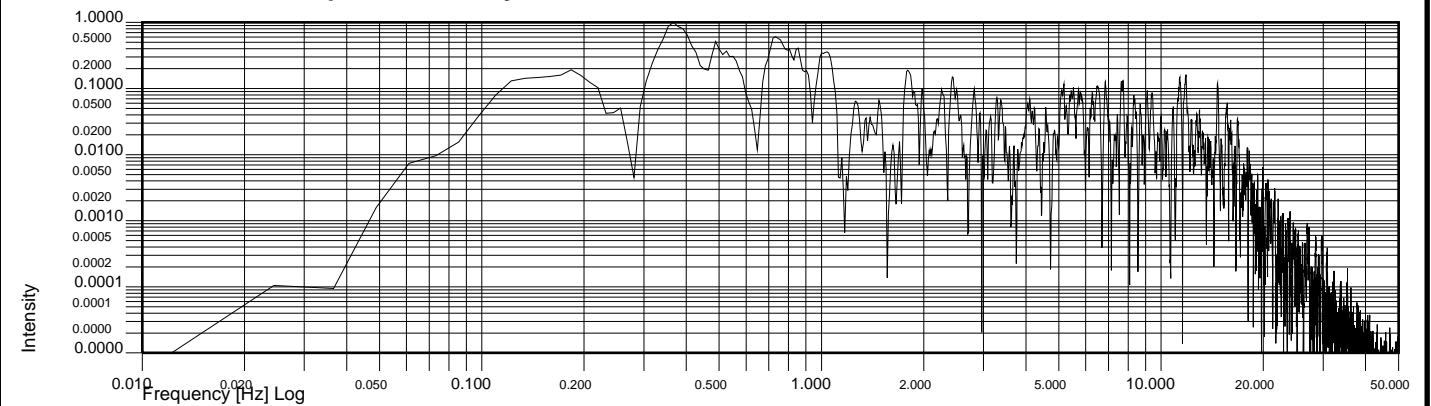
**Acceleration Spectrum**



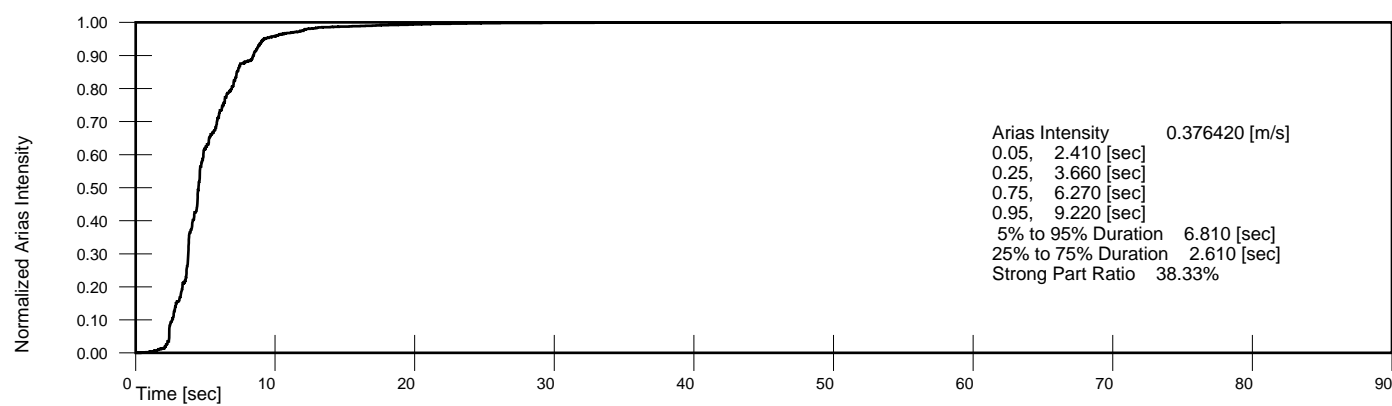
**Displacement Time History**



**Normalized Power Spectral Density**



**Husid Plot**



Set:001, Dir:X, File: C:\2021\THS\RSN3548\_LOMAP\_LEX-UP.AT2.txt

Desc.: Loma Prieta, 10/18/1989, Los Gatos - Lexington Dam, UP

Incremental Velocity 0.393 [m/s], Incremental Displacement 0.420 [m]  
 PGA Ratio 1.253, Area Ratio 1.333 [ 1.000 Hz to 10.000 Hz], MSE 0.069957

USACE Long-norm

Wutec

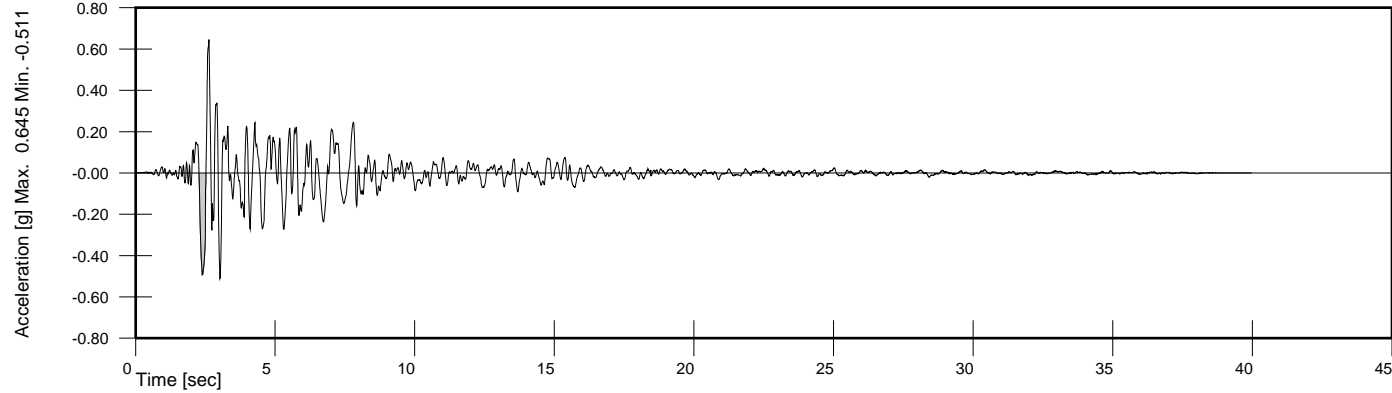
Sa for scaled LEX-00,90,UP

THS by A. Felber, Program Version 0.01, 2010 June 15  
 Date: 2022, February, 25

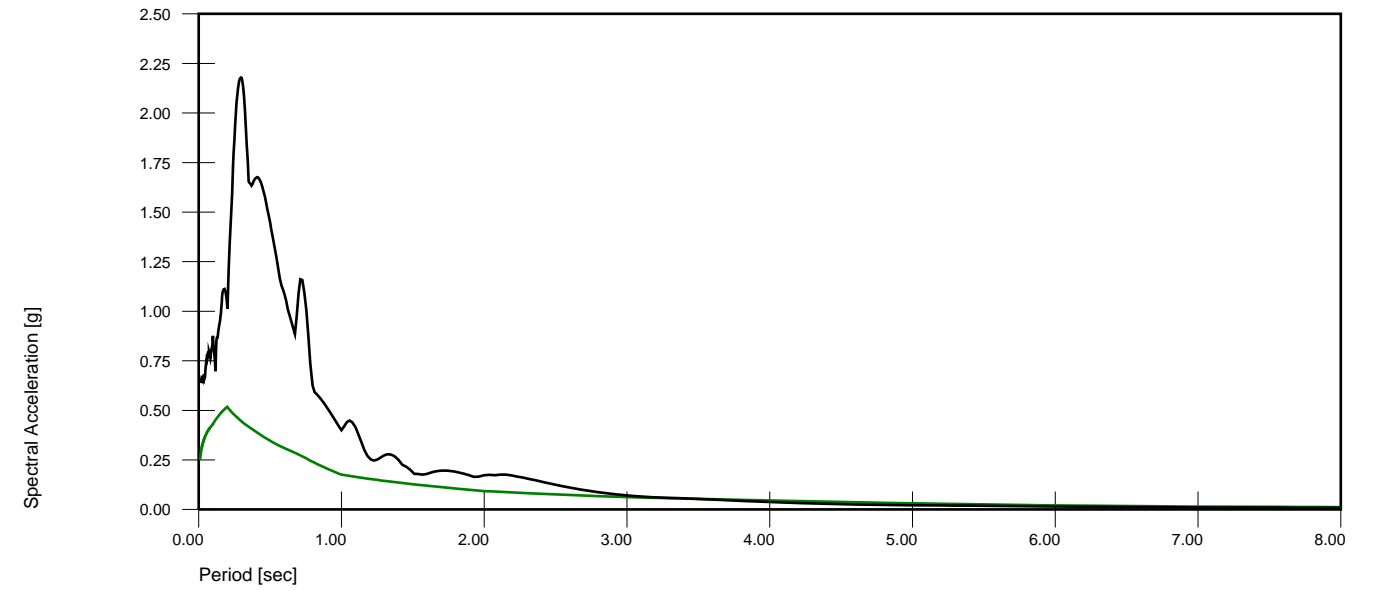
Time: 17:05:14

Page 9 of 9

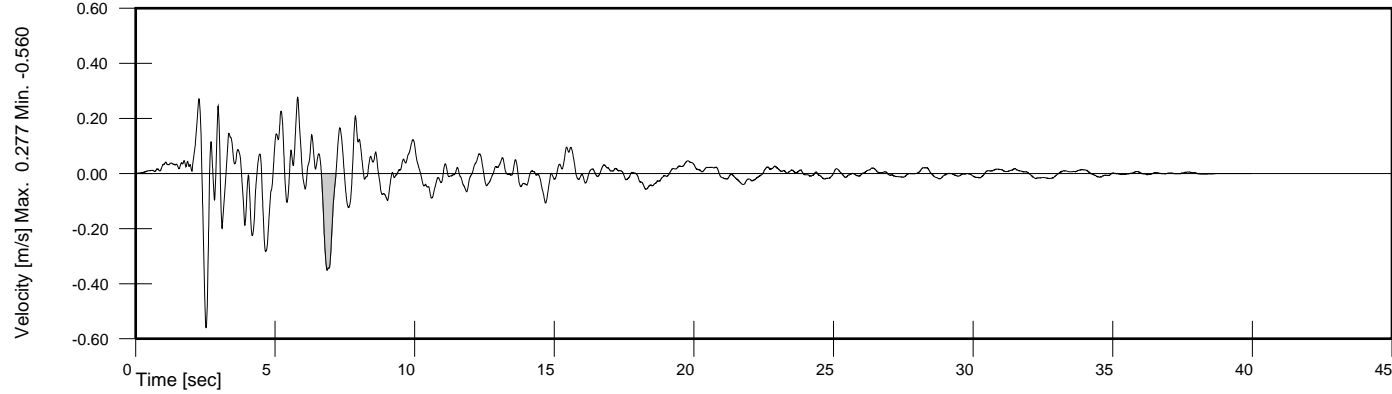
### Acceleration Time History



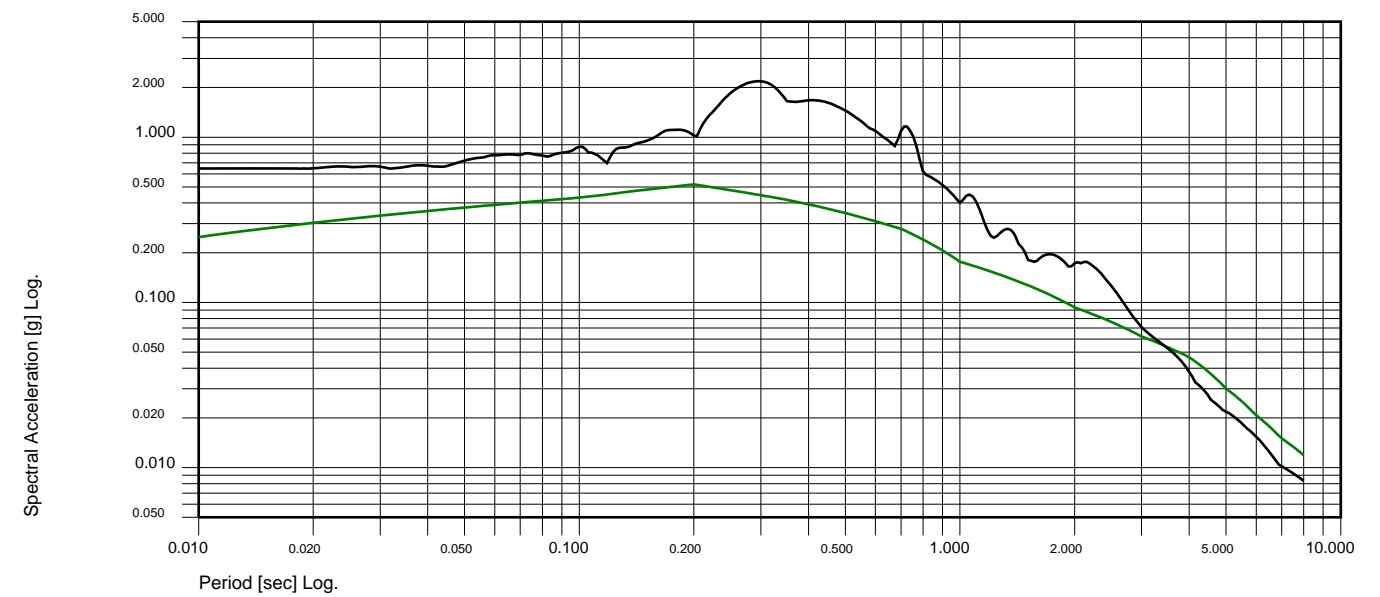
### Acceleration Spectrum



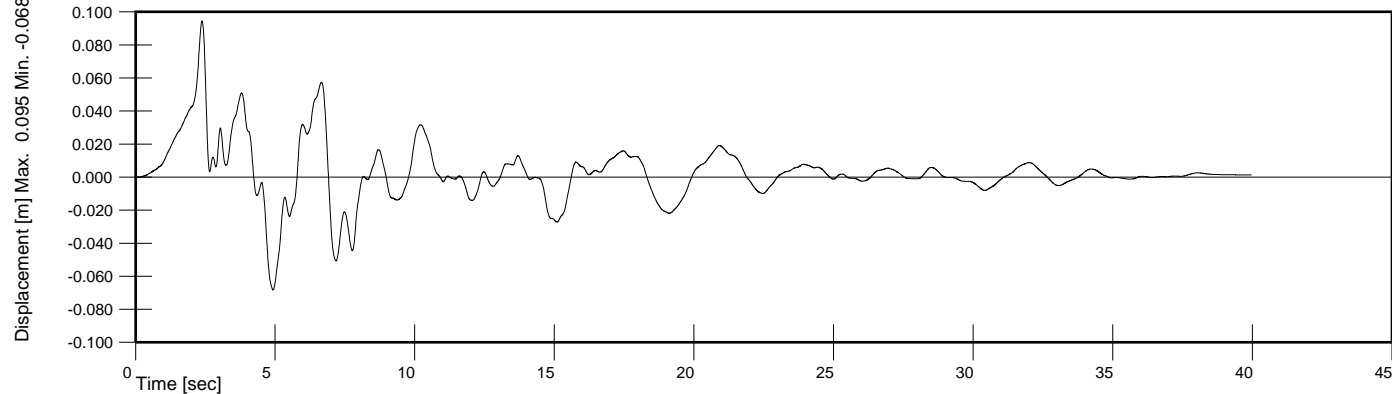
### Velocity Time History



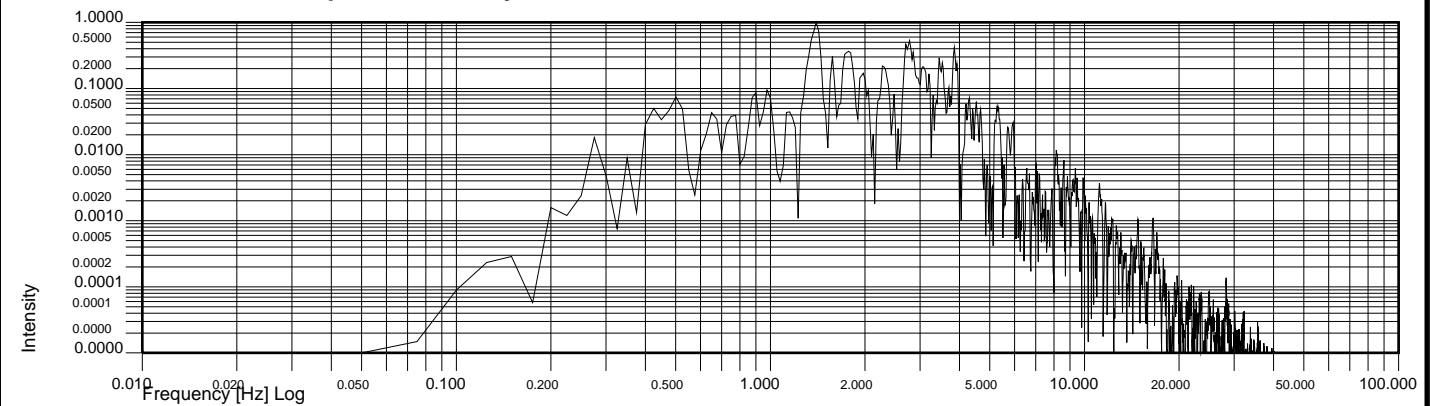
### Acceleration Spectrum



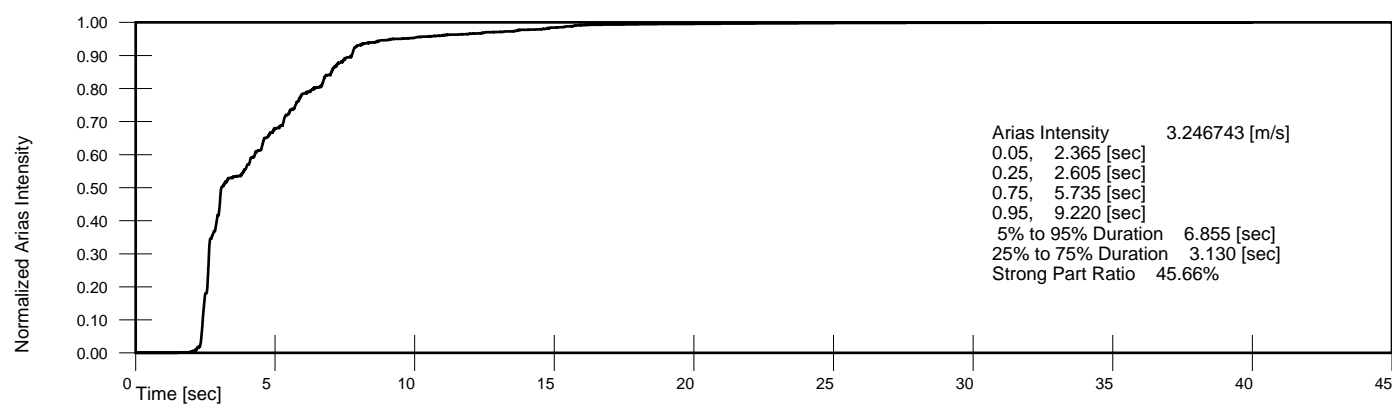
### Displacement Time History



### Normalized Power Spectral Density



### Husid Plot



Set:001, Dir:X, File: C:\2021\THS\RSN753\_LOMAP\_CLS000.AT2.txt

Desc.: Loma Prieta, 10/18/1989, Corralitos, 0

Incremental Velocity 0.830 [m/s], Incremental Displacement 0.108 [m]  
 PGA Ratio 0.385, Area Ratio 0.333 [ 1.000 Hz to 10.000 Hz], MSE 0.120910

USACE Long-norm

Wutec

Sa for recorded CLS-00,90,UP

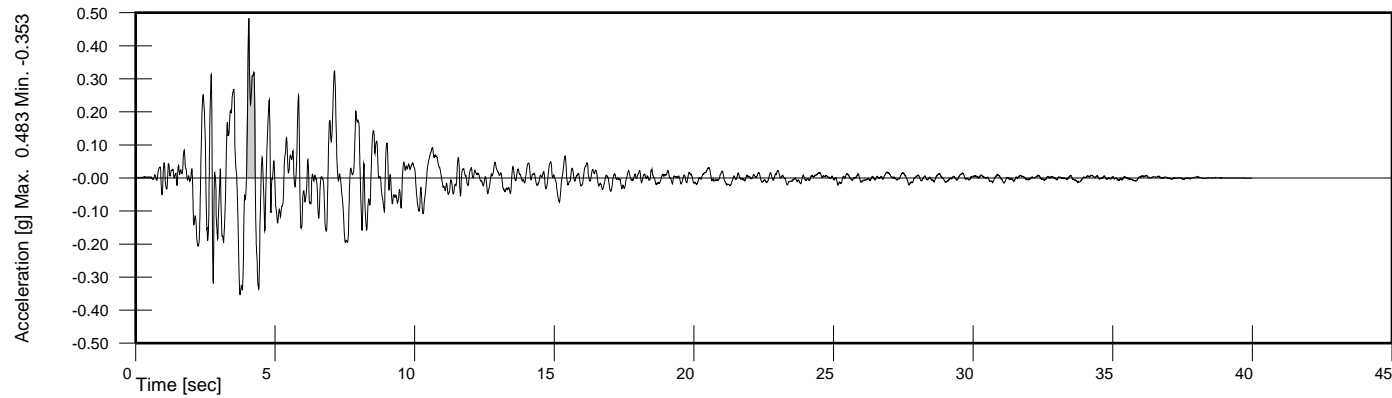
THS by A. Felber, Program Version 0.01, 2010 June 15  
 Date: 2022, February, 25

Time: 17:25:05

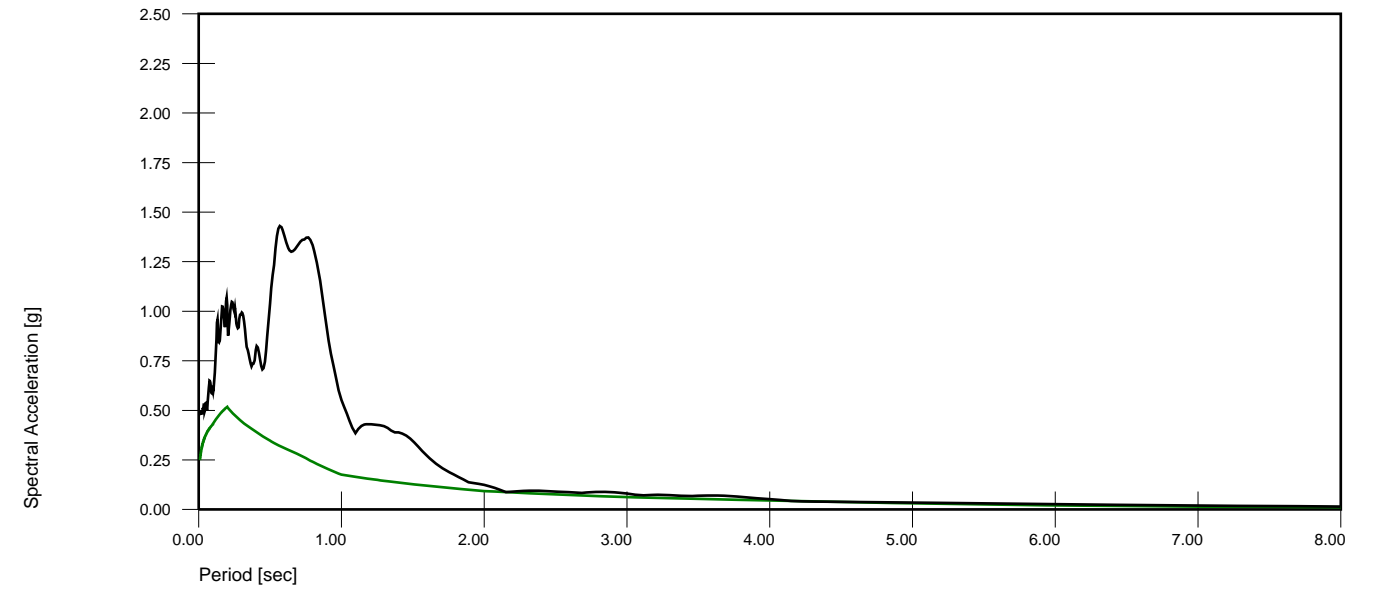
Page 7 of 9



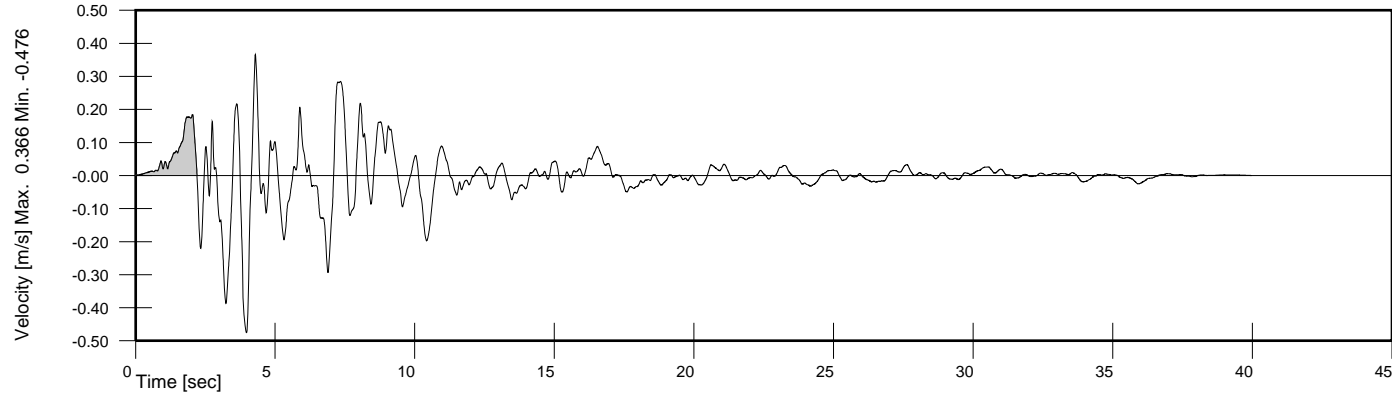
### Acceleration Time History



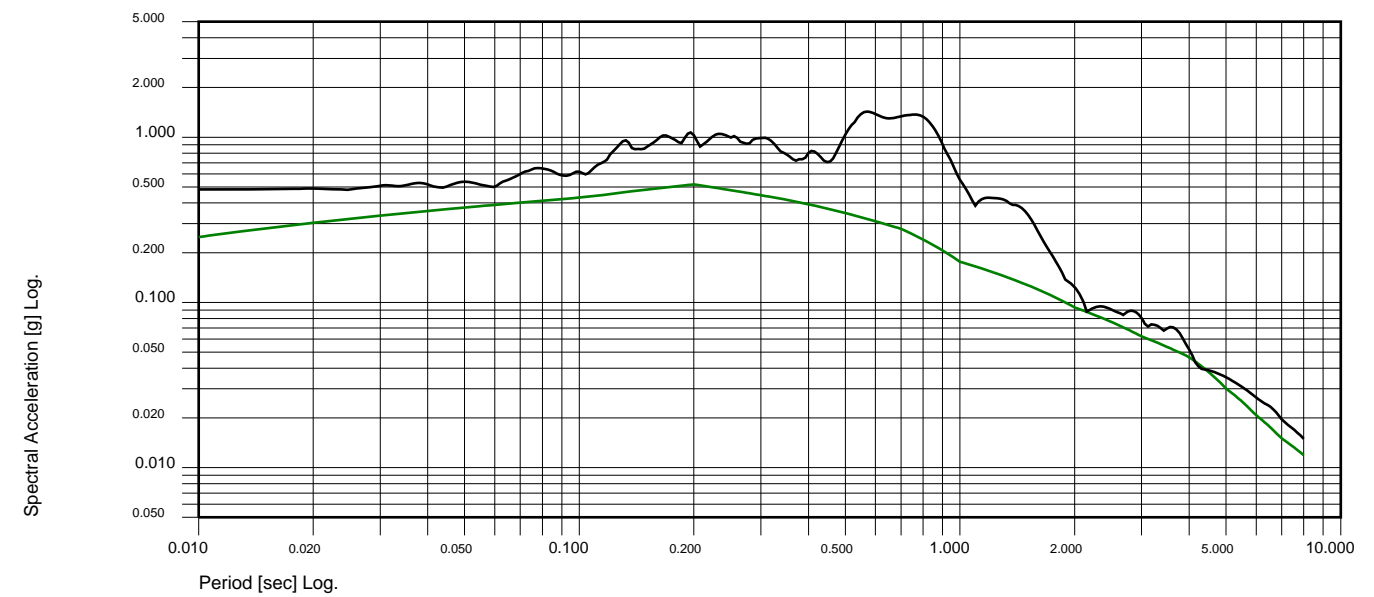
### Acceleration Spectrum



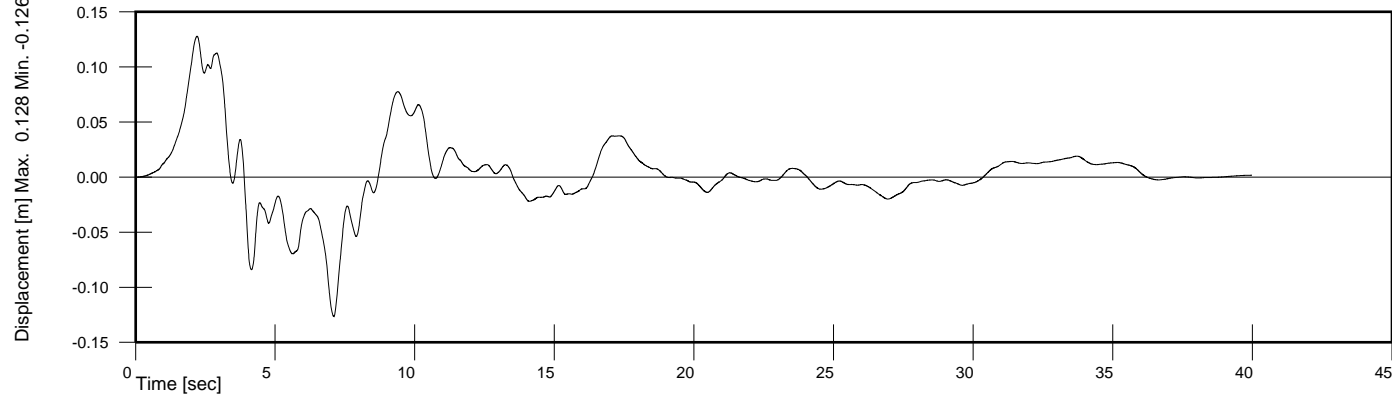
### Velocity Time History



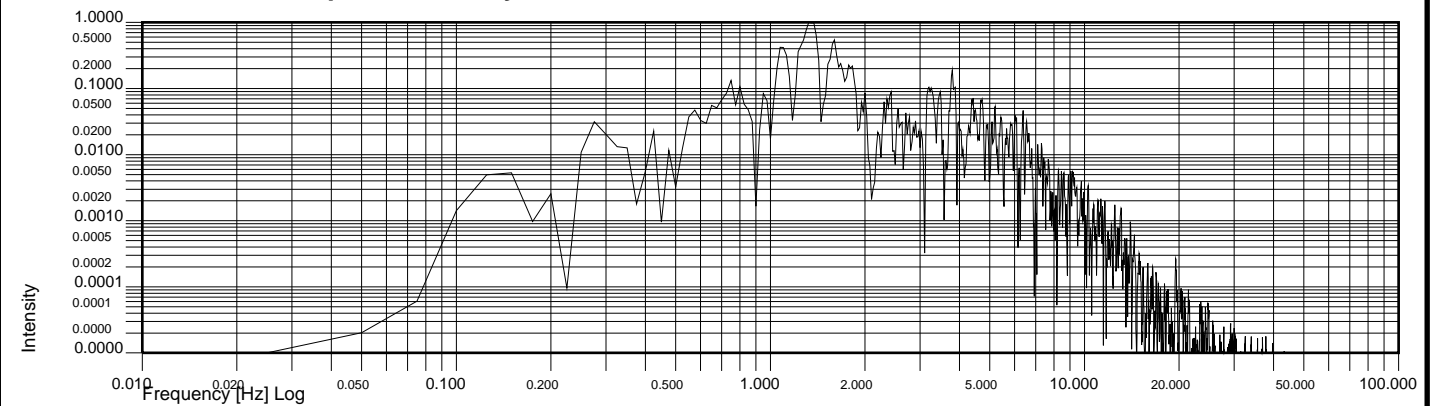
### Acceleration Spectrum



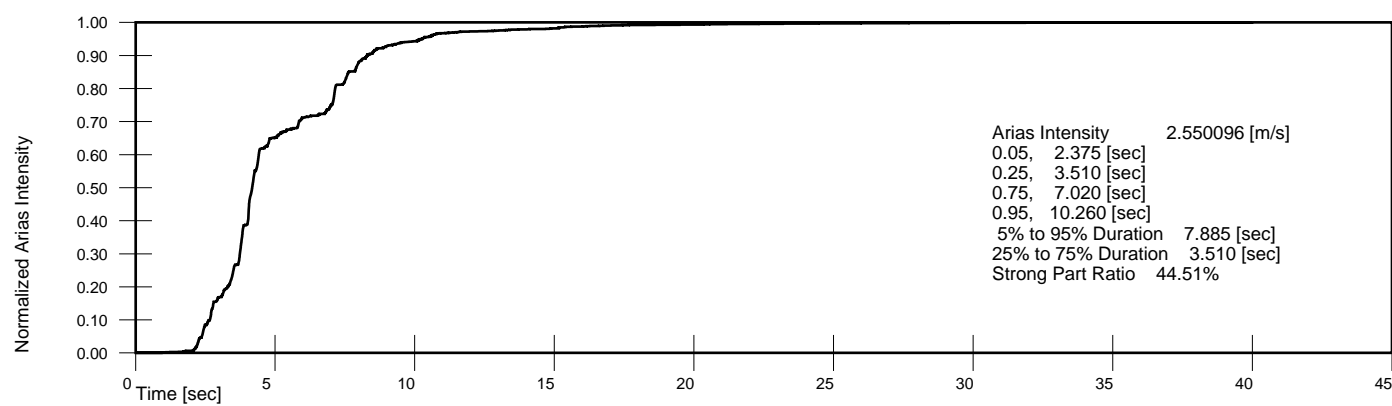
### Displacement Time History



### Normalized Power Spectral Density



### Husid Plot



Set:001, Dir:X, File: C:\2021\THS\RSN753\_LOMAP\_CLS090.AT2.txt

Desc.: Loma Prieta, 10/18/1989, Corralitos, 90

Incremental Velocity 0.841 [m/s], Incremental Displacement 0.128 [m]  
 PGA Ratio 0.515, Area Ratio 0.400 [ 1.000 Hz to 10.000 Hz], MSE 0.162557

USACE Long-norm

Wutec

Sa for recorded CLS-00,90,UP

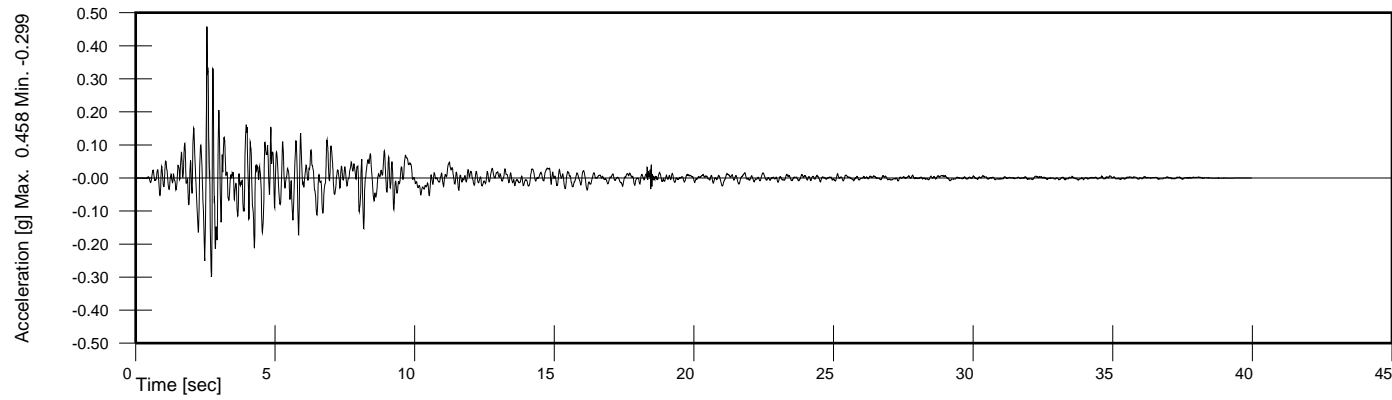
THS by A. Felber, Program Version 0.01, 2010 June 15  
 Date: 2022, February, 25

Time: 17:25:06

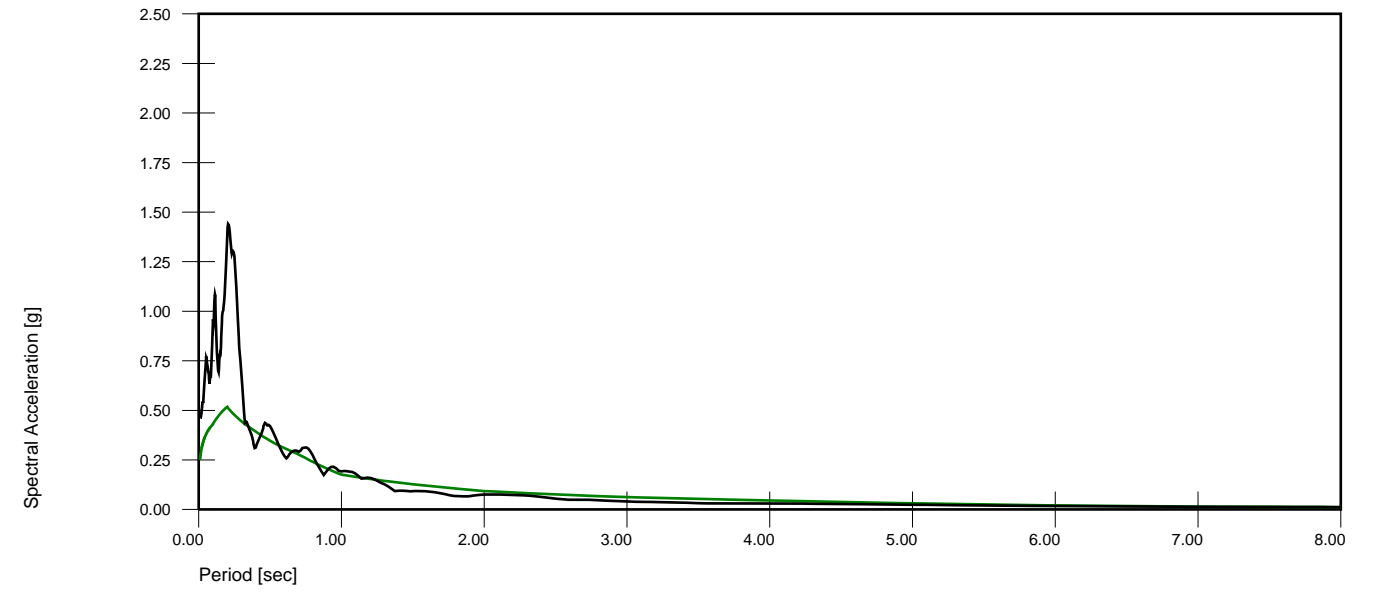
Page 8 of 9



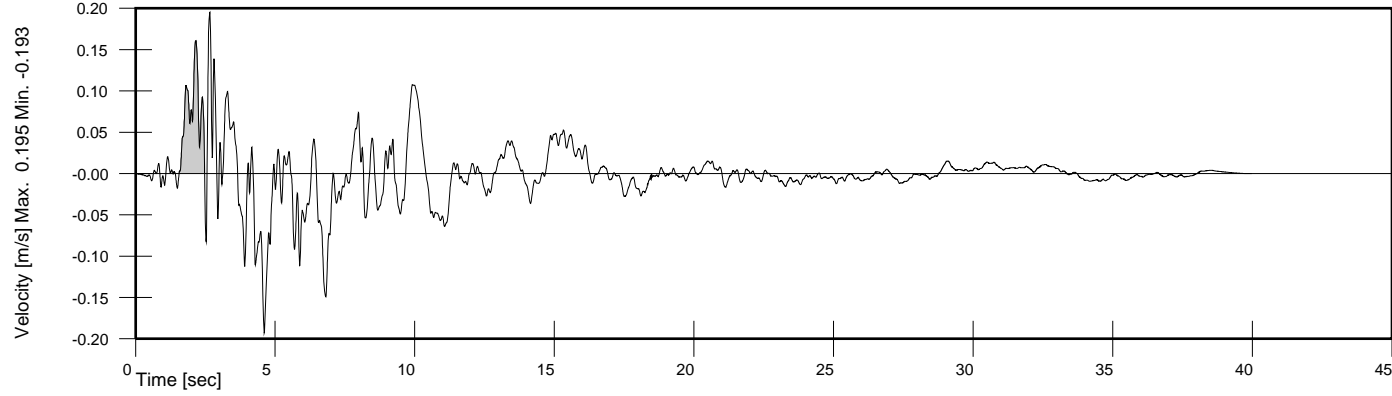
### Acceleration Time History



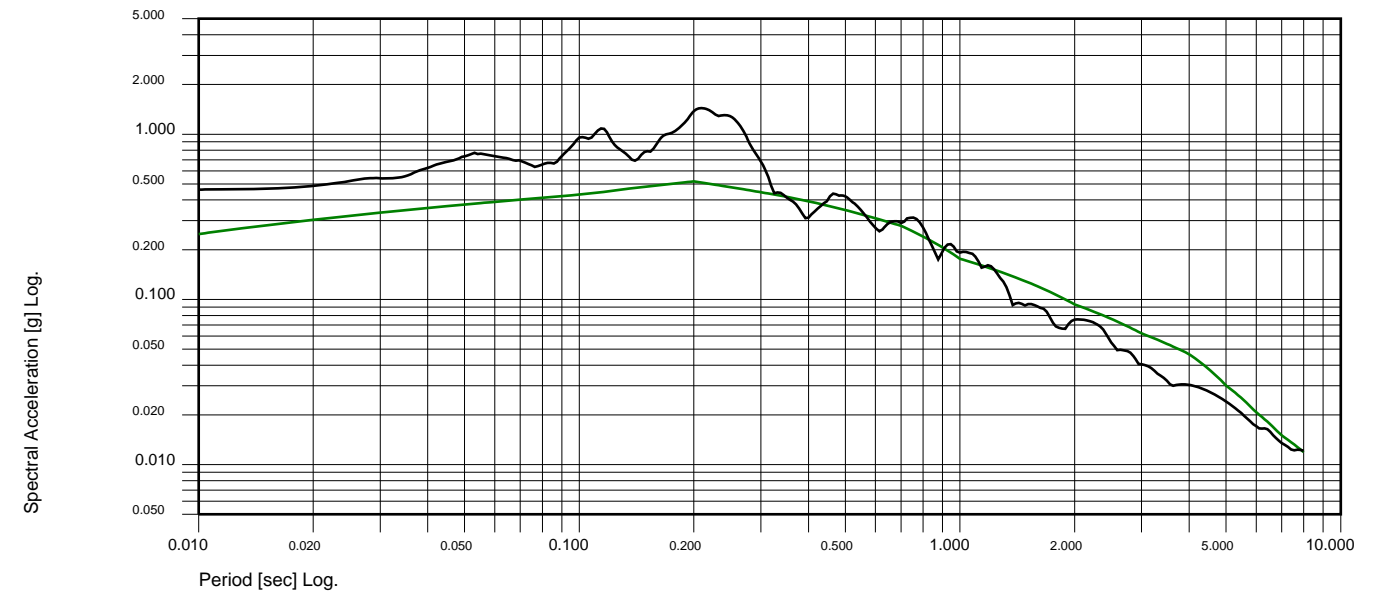
### Acceleration Spectrum



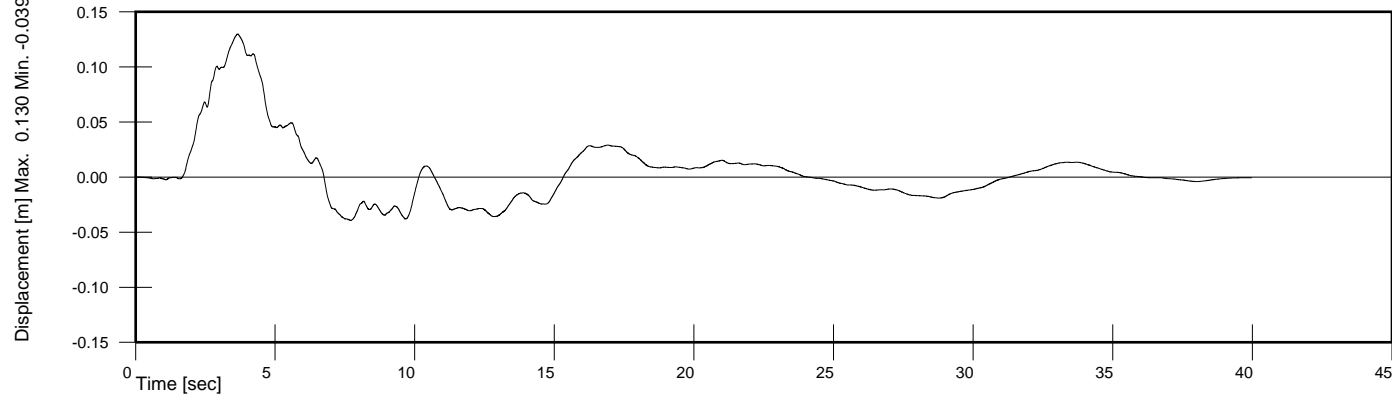
### Velocity Time History



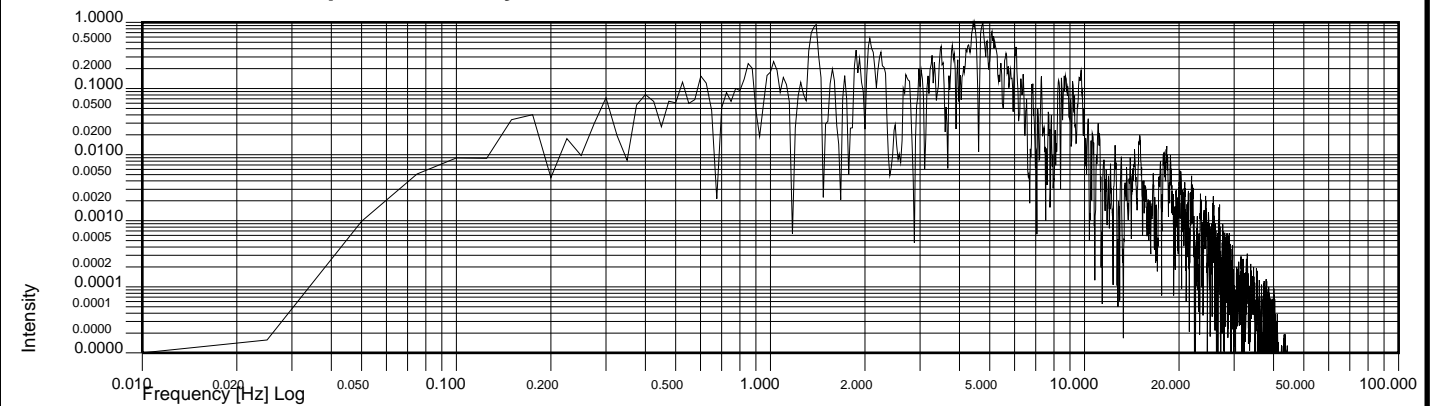
### Acceleration Spectrum



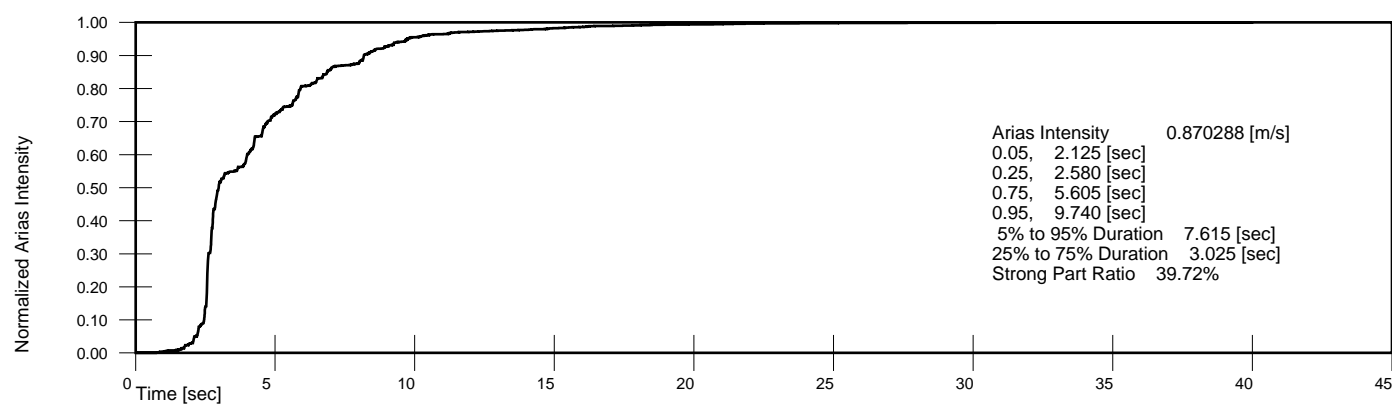
### Displacement Time History



### Normalized Power Spectral Density



### Husid Plot



Set:001, Dir:X, File: C:\2021\THS\RSN753\_LOMAP\_CLS-UP.AT2.txt

Desc.: Loma Prieta, 10/18/1989, Corralitos, UP

Incremental Velocity 0.277 [m/s], Incremental Displacement 0.070 [m]  
 PGA Ratio 0.538, Area Ratio 0.692 [ 1.000 Hz to 10.000 Hz], MSE 0.156037

USACE Long-norm

Wutec

Sa for recorded CLS-00,90,UP

THS by A. Felber, Program Version 0.01, 2010 June 15  
 Date: 2022, February, 25

Time: 17:25:06

Page 9 of 9

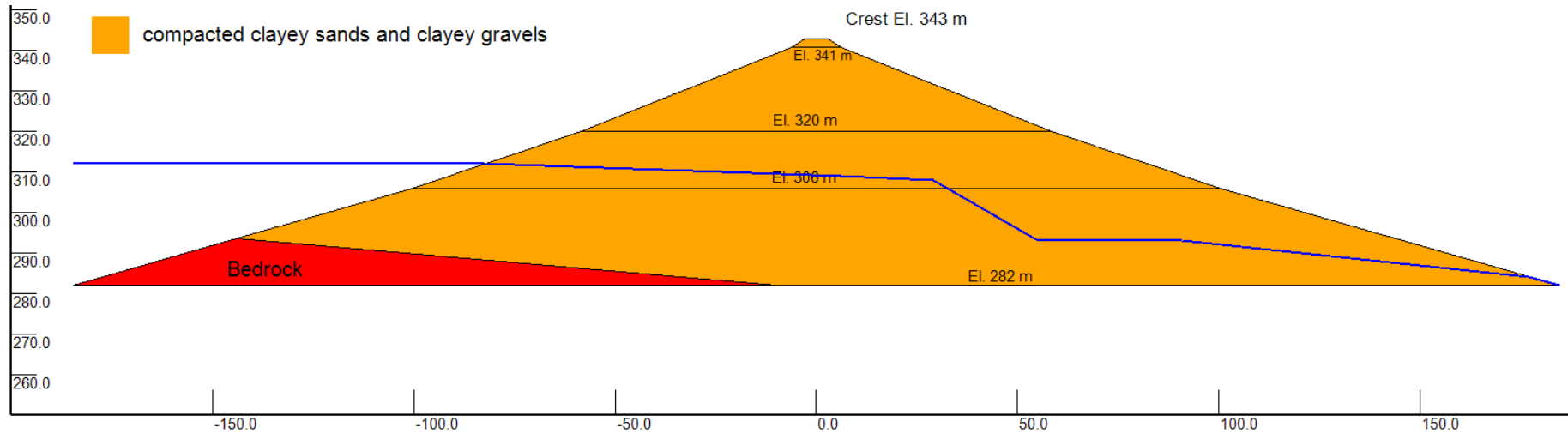


**APPENDIX C      SECTION A-A' GEOMETRY AND PHREATIC SURFACES**

Report No. WGI-220224  
February 24, 2022

## Austrian Dam - maximum cross-section (A-A') showing

- soil and rock zones, and
- phreatic surface from piezometers, i.e., Case 1 in Austrn-4

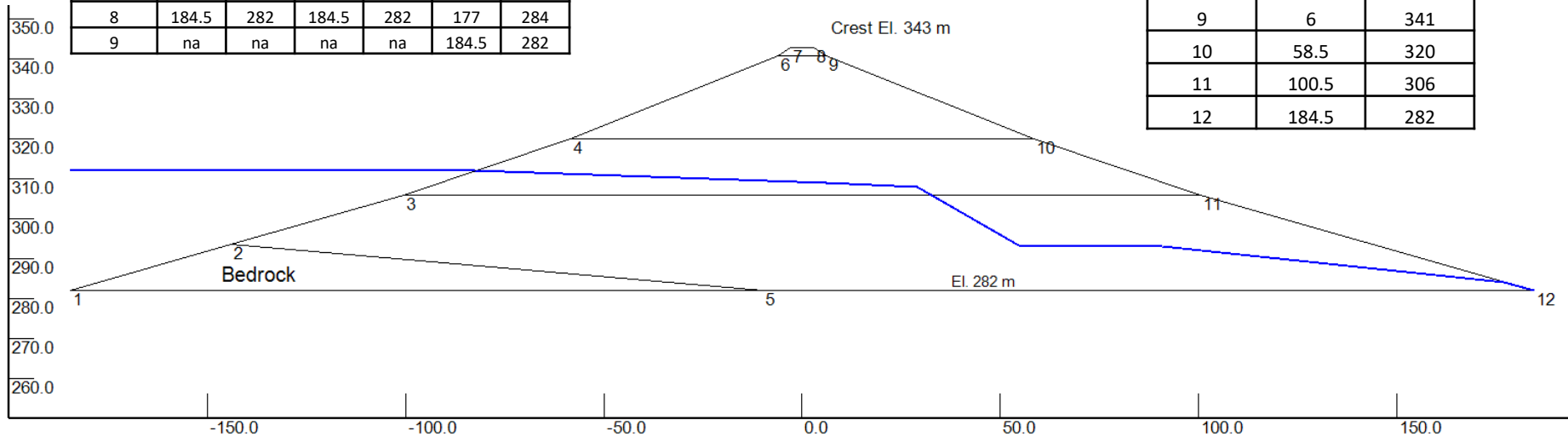


# Austrian Dam - maximum cross-section (A-A')

- Showing X and Y for phreatic surfaces (w. table)
- Showing X and Y for control points of the section

w.table	Case 1 (Austn-4)		CASE 2: (Austn-2)		CASE 3 (Austn-3)	
point #	X (m)	Y (m)	X (m)	Y (m)	X (m)	Y (m)
1	-184.5	312	-184.5	312	-184.5	312
2	-82.5	312	-82.5	312	-82.5	312
3	6	309	6	309	6	309
4	29	308	36	308	33	308
5	55	293	48	297	39	306
6	91	293	100.5	292	48	301
7	177	284	177	284	100.5	294
8	184.5	282	184.5	282	177	284
9	na	na	na	na	184.5	282

pt	X (m)	Y (m)
1	-184.5	282
2	-144	293.5
3	-100.5	306
4	-58.5	320
5	-10	282
6	-6	341
7	-3	343
8	3	343
9	6	341
10	58.5	320
11	100.5	306
12	184.5	282





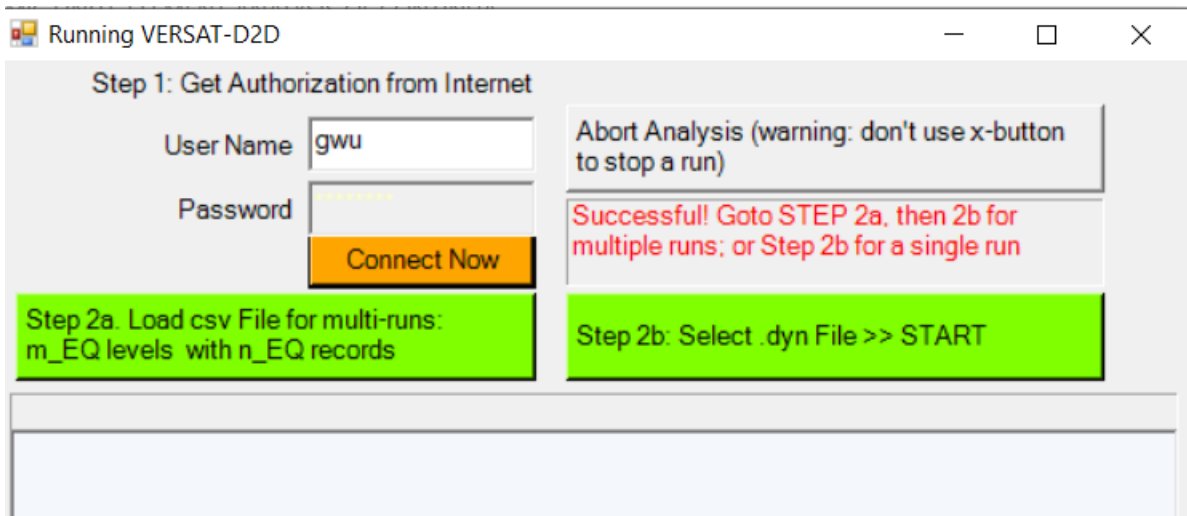
## APPENDIX D VERSAT-2D INPUT AND OUTPUT FILES

### Notes:

- All input files are in text format so they are convenient for import/export. See VERSAT-2D Technical and User Manuals for details.
- The node and element information (or data) are essentially the same for Input File 1, Input File 2 and Input File 4. However, when needed for modelling of special problems, the MAT data and the PWP data for each element can change in various stages of modelling.

### Steps:

1. Run 'VERSAT-S2D' using Input File 1: Case 1 phi=44.sta
2. Rename the stress output "Case 1 phi=44.pr4" as "Case 1 Reservoir\_and\_wt.prx"
3. Run 'VERSAT-S2D' using Input File 2: Case 1 Reservoir\_and\_wt.sta
4. Rename the stress output "Case 1 Reservoir\_and\_wt.pr4" as "Case 1a.prx"
5. Run "VERSAT-D2D" (see below interactive window)
  - a. Click Step 2a and load Input File 3: Case 1a.PSPA.csv; then
  - b. Click Step 2b and load Input File 4: Case 1a.dyn
6. Output of Step 5 above are saved in folder: ".\output" that will contain the following files
  - a. "Case 1a\_LomaPrietaEQ.LX\_dam\_0b.oud": main output with captions for quantities
  - b. "Case 1a\_LomaPrietaEQ.LX\_dam\_0b.csv": time histories at selected node/element
  - c. "Case 1a\_LomaPrietaEQ.LX\_dam\_0b.o21": modal frequencies with time
  - d. "Case 1a\_LomaPrietaEQ.LX\_dam\_0b.dis": displacement and acceleration for plotting
  - e. "Case 1a\_LomaPrietaEQ.LX\_dam\_0b.sig": stresses and strains output for plotting



## Input File 1 Build the Dam in Dry

File name: Case 1 phi=44.sta

```
1      Austrian Dam California US - Build Dry phi=44
2      0,9.81,9.81,101.3,1
3      7258,7072,4,0
4      15,0.5,0
5      NMAT=,5
6      1,1
7      2650,0.5,530,0.5,21,0
8      0,44,0,0,3,0
9      2,3
10     18720,9360,25.5,0,0,0
11     0,0,0,0,0,0
12     3,1
13     2650,0.5,530,0.5,21,0
14     0,44,0,0,3,0
15     4,1
16     2650,0.5,530,0.5,22.4,0
17     0,44,0,0,3,0
18     5,1
19     2650,0.5,530,0.5,22.4,0
20     0,44,0,0,3,0
21     NLAY=,6
22     1182,861,787,712,785,671,0,0,0,0
23     SOLVE,***** RUN 1 *****
24     NLAY=,7
25     570,470,374,290,206,124,40,0,0,0
26     SOLVE,***** RUN 2 *****
27     END,****
28     1,2,-184.50,282.00,0,0,0
29     2,2,-183.00,282.00,0,0,0
30     ... node information continues
31     7257,2,183.00,282.43,1,0,1
32     7258,2,184.50,282.00,0,0,0
33     1,5,4,0.00,7258,7257,7256,7256
34     2,5,2,0.00,1,2,3,3
35     ..... element information continues
36     7071,5,3,0.00,3717,3779,3780,3718
37     7072,5,3,0.00,3780,3779,3841,3780
**End of File: Case 1 phi=44.sta"
```



## Input File 2 Add Reservoir Water

File Name: Case 1 Reservoir\_and\_wt.sta

1	Austrian Dam California US - Add reservoir (lstep=lwstep=5)
2	0,9.81,9.81,101.3,1
3	7258,7072,4,7072
4	20,0.5,0
5	NMAT=,5
6	1,1
7	2650,0.5,530,0.5,21,0
8	0,44,0,0,3,0
9	2,3
10	18720,9360,25.5,0,0,0
11	0,0,0,0,0,0
12	3,1
13	2650,0.5,530,0.5,21,0
14	0,44,0,0,3,0
15	4,1
16	2650,0.5,530,0.5,22.4,0
17	0,44,0,0,3,0
18	5,1
19	2650,0.5,530,0.5,22.4,0
20	0,44,0,0,3,0
21	NLOD=,69
22	9,312.00,0.00
23	1,63.1351,0.0000,-220.2389
24	3,125.3588,0.0000,-437.2982
25	5,123.5359,0.0000,-430.9391
26	7,120.3186,0.0000,-424.6170
27	10,118.5169,0.0000,-418.3318
28	13,118.1094,0.0000,-412.0097
29	17,116.2865,0.0000,-405.6506
30	21,114.4636,0.0000,-399.2915
31	26,112.6406,0.0000,-392.9324
32	31,110.8177,0.0000,-386.5734
33	36,107.7483,0.0000,-380.2512
34	42,105.9466,0.0000,-373.9661
35	48,105.3913,0.0000,-367.6440
36	55,103.5683,0.0000,-361.2849
37	62,101.7454,0.0000,-354.9258
38	70,99.9225,0.0000,-348.5667
39	78,98.0995,0.0000,-342.2076
40	86,95.1780,0.0000,-335.8855
41	95,93.3763,0.0000,-329.6004
42	104,92.6731,0.0000,-323.2782
43	114,90.8502,0.0000,-316.9192

44	124,89.0272,0.0000,-310.5601
45	135,87.2043,0.0000,-304.2010
46	146,85.3813,0.0000,-297.8419
47	157,82.6077,0.0000,-291.5198
48	169,80.8060,0.0000,-285.2346
49	181,79.9549,0.0000,-278.9125
50	194,78.1320,0.0000,-272.5534
51	207,76.3090,0.0000,-266.1944
52	221,74.4861,0.0000,-259.8353
53	235,72.6632,0.0000,-253.4762
54	249,70.0375,0.0000,-247.1541
55	264,68.2357,0.0000,-240.8689
56	279,67.2367,0.0000,-234.5468
57	295,65.4138,0.0000,-228.1877
58	311,63.5909,0.0000,-221.8286
59	328,61.7679,0.0000,-215.4695
60	345,59.9450,0.0000,-209.1105
61	362,57.4672,0.0000,-202.7883
62	380,55.6654,0.0000,-196.5032
63	398,54.5186,0.0000,-190.1811
64	417,52.6956,0.0000,-183.8220
65	436,50.8727,0.0000,-177.4629
66	456,49.0498,0.0000,-171.1038
67	476,47.2268,0.0000,-164.7447
68	496,44.8969,0.0000,-158.4226
69	517,43.0951,0.0000,-152.1375
70	538,41.8004,0.0000,-145.8153
71	560,39.9775,0.0000,-139.4563
72	582,38.1545,0.0000,-133.0972
73	605,36.3316,0.0000,-126.7381
74	628,34.5086,0.0000,-120.3790
75	651,32.3266,0.0000,-114.0569
76	675,30.5249,0.0000,-107.7717
77	699,29.0822,0.0000,-101.4496
78	724,27.2593,0.0000,-95.0905
79	749,27.3463,0.0000,-88.4726
80	775,27.1124,0.0000,-81.3372
81	801,24.6476,0.0000,-73.9429
82	828,22.1829,0.0000,-66.5486
83	855,19.7181,0.0000,-59.1543
84	883,17.2533,0.0000,-51.7600
85	911,14.7886,0.0000,-44.3657
86	940,12.3238,0.0000,-36.9714
87	969,9.8591,0.0000,-29.5772
88	999,7.3943,0.0000,-22.1829
89	1029,4.9295,0.0000,-14.7886
90	1060,2.4648,0.0000,-7.3943
91	1091,0.6162,0.0000,-1.8486

92 NWAT=,8  
93 9  
94 1,-184.5,312  
95 2,-82.5,312  
96 3,6,309  
97 4,29,308  
98 5,55,293  
99 6,91,293  
100 7,177,284  
101 8,184.5,282  
102 SOLVE,\*\*\*\*\* RUN 1 \*\*\*\*\*  
103 END,\*\*\*\*  
104 1,2,-184.50,282.00,0,0,0  
105 2,2,-183.00,282.00,0,0,0  
106 ... node information continues  
107 7257,2,183.00,282.43,1,0,1  
108 7258,2,184.50,282.00,0,0,0  
109 1,5,4,0.00,7258,7257,7256,7256  
110 2,5,2,0.00,1,2,3,3  
111 ... element information continues  
112 7071,5,3,0.00,3717,3779,3780,3718  
113 7072,5,3,0.00,3780,3779,3841,3780

End of File: Case 1 Reservoir\_and\_wt.sta

## Output from Input File 2

File Name: Case 1 Reservoir\_and\_wt.out

```
1          *****
2          |
3          |
4          | versat-s2d: static 2-dimensional
5          |       finite element analysis of continua
6          |
7          |       Versions 1998/2001/2005/2008/2009/2011
8          |       2012/2013/2021.11.18
9          |
10         |       copyright (c) 1998-2021 Dr. G. Wu
11         |       copyright (c) 1998-2021 w.g.i.
12         |       wutec geotechnical international
13         |
14         |       input: *.sta; *.prx(optional)
15         |       output: *.out; .pr4; .oug; .dis; .sig
16         |
17         |
18         | *****
19
20         compiled v.2022.01.15; 130 MB; max size of [K], variables= 25600000 50400
21
22         Austrian Dam California US - Add reservoir (lstep=lwstep=5)
23
24         *****
25         gravity is on (0=yes; 1=no)      0
26         gravity acceleration=           9.81
27         unit weight of water=           9.81
28         atmospheric pressure=            101.30
29         ichang=1: elastic non-linear analysis
30
31         total number of nodes            7258
32         total number of elements         7072
33         maximum number of nodes in an element4
34         number of elements having stresses 7072
35
36         maximum number of iterations =   20
37         residual (unbalanced) force allowed 0.50
38         imsh=0: small strain application
39
40
41         total number of materials 5
42         =====
43         ky      area  i  Unit. W  rr      (beam)
44         kb      k-sh  Unit. W      (elas)
45         SOIL   kb  n  kg  m  Unit. W  c  phi/-k  Soil Model
46         =====
47         SAND 1 2650.00 0.50 530.00 0.50 21.00 0.00 44.00 SAND Model - Mohr-Coulomb
48         ELAS 2 18720.00 9360.00 25.50
```

Report No. WGI-220224  
February 24, 2022

```

49 SAND 3 2650.00 0.50 530.00 0.50 21.00 0.00 44.00 SAND Model - Mohr-Coulomb
50 SAND 4 2650.00 0.50 530.00 0.50 22.40 0.00 44.00 SAND Model - Mohr-Coulomb
51 SAND 5 2650.00 0.50 530.00 0.50 22.40 0.00 44.00 SAND Model - Mohr-Coulomb
52 =====
53
54 nl=69, lstep=9; ywt0(>0 to increase RESERVOIR level gradually)=312.000
55 node nodal load: fx, mxy fy
56 1 63.1351 0.0000 -220.2389
57 3 125.3588 0.0000 -437.2982
58 5 123.5359 0.0000 -430.9391
59 7 120.3186 0.0000 -424.6170
60 10 118.5169 0.0000 -418.3318
61 13 118.1094 0.0000 -412.0097
62 17 116.2865 0.0000 -405.6506
63 21 114.4636 0.0000 -399.2915
64 26 112.6406 0.0000 -392.9324
65 31 110.8177 0.0000 -386.5734
66 36 107.7483 0.0000 -380.2512
67 42 105.9466 0.0000 -373.9661
68 48 105.3913 0.0000 -367.6440
69 55 103.5683 0.0000 -361.2849
70 62 101.7454 0.0000 -354.9258
71 70 99.9225 0.0000 -348.5667
72 78 98.0995 0.0000 -342.2076
73 86 95.1780 0.0000 -335.8855
74 95 93.3763 0.0000 -329.6004
75 104 92.6731 0.0000 -323.2782
76 114 90.8502 0.0000 -316.9192
77 124 89.0272 0.0000 -310.5601
78 135 87.2043 0.0000 -304.2010
79 146 85.3813 0.0000 -297.8419
80 157 82.6077 0.0000 -291.5198
81 169 80.8060 0.0000 -285.2346
82 181 79.9549 0.0000 -278.9125
83 194 78.1320 0.0000 -272.5534
84 207 76.3090 0.0000 -266.1944
85 221 74.4861 0.0000 -259.8353
86 235 72.6632 0.0000 -253.4762
87 249 70.0375 0.0000 -247.1541
88 264 68.2357 0.0000 -240.8689
89 279 67.2367 0.0000 -234.5468
90 295 65.4138 0.0000 -228.1877
91 311 63.5909 0.0000 -221.8286
92 328 61.7679 0.0000 -215.4695
93 345 59.9450 0.0000 -209.1105
94 362 57.4672 0.0000 -202.7883
95 380 55.6654 0.0000 -196.5032
96 398 54.5186 0.0000 -190.1811
97 417 52.6956 0.0000 -183.8220
98 436 50.8727 0.0000 -177.4629
99 456 49.0498 0.0000 -171.1038
100 476 47.2268 0.0000 -164.7447
101 496 44.8969 0.0000 -158.4226
102 517 43.0951 0.0000 -152.1375
103 538 41.8004 0.0000 -145.8153

```

```

104      560  39.9775 0.0000 -139.4563
105      582  38.1545 0.0000 -133.0972
106      605  36.3316 0.0000 -126.7381
107      628  34.5086 0.0000 -120.3790
108      651  32.3266 0.0000 -114.0569
109      675  30.5249 0.0000 -107.7717
110      699  29.0822 0.0000 -101.4496
111      724  27.2593 0.0000 -95.0905
112      749  27.3463 0.0000 -88.4726
113      775  27.1124 0.0000 -81.3372
114      801  24.6476 0.0000 -73.9429
115      828  22.1829 0.0000 -66.5486
116      855  19.7181 0.0000 -59.1543
117      883  17.2533 0.0000 -51.7600
118      911  14.7886 0.0000 -44.3657
119      940  12.3238 0.0000 -36.9714
120      969  9.8591 0.0000 -29.5772
121      999  7.3943 0.0000 -22.1829
122     1029  4.9295 0.0000 -14.7886
123     1060  2.4648 0.0000 -7.3943
124     1091  0.6162 0.0000 -1.8486
125
126      nwat=8, lwstep=9
127      point x-coor; y-coor of water table
128      1 -184.50 312.00
129      2 -82.50 312.00
130      3 6.00 309.00
131      4 29.00 308.00
132      5 55.00 293.00
133      6 91.00 293.00
134      7 177.00 284.00
135      8 184.50 282.00
136      ***** end of data for RUN 1 *****
137
138      .... Output for increments 1 to 8 (deleted to save space here)
139      -----
140      results after load increment ..9
141      -----
142      net degrees of freedom= 14022 bandwidth=126
143      lband*(nnet-1)+1= 1766647 < ak dimension 25600000
144      ***runs[i_run - 1].nwatbl0=2
145      Water table pt#1 x= -184.500 y= 282.000
146      Water table pt#2 x= 184.500 y= 282.000
147
148      Reservoir level at ywt0= 312.00 for increment# 9 to 312.00
149      Water table pt#1 x= -184.500 y= 312.000
150      Water table pt#2 x= -82.500 y= 312.000
151      Water table pt#3 x= 6.000 y= 309.000
152      Water table pt#4 x= 29.000 y= 308.000
153      Water table pt#5 x= 55.000 y= 293.000
154      Water table pt#6 x= 91.000 y= 293.000
155      Water table pt#7 x= 177.000 y= 284.000
156      Water table pt#8 x= 184.500 y= 282.000
157

```

```

158      *CHECK Node#,fx,fy = 1  0.0, 0.0,
159      *CHECK Node#,fx,fy = 3 125.357,-437.298,
160      ...*CEHCK continues ...
161      *CHECK Node#,fx,fy = 1091  0.614,-1.843,
162      Iteration 1 Unbalanced force(UF)= 6086.688, UF ratio=2.4731e-002
163      Iteration 2 Unbalanced force(UF)= 46.924, UF ratio=1.9066e-004
164      Iteration 3 Unbalanced force(UF)= 31.701, UF ratio=1.2880e-004
165      Iteration 4 Unbalanced force(UF)= 28.567, UF ratio=1.1607e-004
166      Iteration 5 Unbalanced force(UF)= 23.926, UF ratio=9.7211e-005
167      Iteration 6 Unbalanced force(UF)= 13.584, UF ratio=5.5192e-005
168      Iteration 7 Unbalanced force(UF)= 10.677, UF ratio=4.3383e-005
169      Iteration 8 Unbalanced force(UF)= 8.524, UF ratio=3.4634e-005
170      Iteration 9 Unbalanced force(UF)= 6.757, UF ratio=2.7453e-005
171      Iteration 10 Unbalanced force(UF)= 5.506, UF ratio=2.2371e-005
172      Iteration 11 Unbalanced force(UF)= 4.469, UF ratio=1.8160e-005
173      Iteration 12 Unbalanced force(UF)= 3.605, UF ratio=1.4647e-005
174      Iteration 13 Unbalanced force(UF)= 2.916, UF ratio=1.1849e-005
175      Iteration 14 Unbalanced force(UF)= 2.319, UF ratio=9.4224e-006
176      Iteration 15 Unbalanced force(UF)= 1.946, UF ratio=7.9077e-006
177      Iteration 16 Unbalanced force(UF)= 1.559, UF ratio=6.3329e-006
178      Iteration 17 Unbalanced force(UF)= 1.254, UF ratio=5.0946e-006
179      Iteration 18 Unbalanced force(UF)= 0.991, UF ratio=4.0274e-006
180      Iteration 19 Unbalanced force(UF)= 0.777, UF ratio=3.1559e-006
181      Iteration 20 Unbalanced force(UF)= 0.663, UF ratio=2.6954e-006
182      -----
183      node disp-x rot. disp-y elem sig-x(mx0) sig-y(ta) tau-xy(sh.) gamm_xy%(mi) pp su fos sig-m
184      -----
185      1 0.0000 0.0000 1 -1.66 -2.02 1.27 0.004 1.89 1.28 1.00 -1.72
186      2 0.0000 0.0000 2 -1.99 -4.82 -0.60 0.000 292.19 0.00 0.00 -2.92
187      3 0.0000 0.0000 3 -3.28 -7.14 -1.21 0.000 291.14 0.00 0.00 -4.47
188      4 0.0000 0.0000 4 -4.62 -5.59 3.40 0.002 2.72 3.55 1.03 -4.79
189      5 0.0000 0.0000 5 -9.02 -10.44 5.14 0.001 5.74 6.76 1.30 -9.12
190      ... output continues
191      7254 0.0000 0.0000
192      7255 0.0000 0.0000
193      7256 0.0000 0.0000
194      7257 0.0000 0.0000
195      7258 0.0000 0.0000

```

End of File: Case 1 Reservoir\_and\_wt.out

## Input Files 3 and 4 for Earthquake Loading

Input File 3 Name: Case 1a.**PSPA.csv**

	A	B	C	D	E	F
1	1 case history performance - Austrian dam in 1989					
2	Prob.Level	SF_x	SF_y			
3	LomaPrietaEQ	<b>1</b>	<b>1</b>			
4	1	N-points	dt			
5	LX_dam_0b	5000	0.01	Scaled by 1.36 for H0.6g, V0.19g		
6	0	0				
7	0					

The format for the Acceleration Input File Names (Line 5 in Input File 3): LX\_dam\_0b.ACX & LX\_dam\_0b.ACY

```

1 Loma Prieta, 10/18/1989, Los Gatos - Lexington Dam, 0 ACCELERATION in G (0.01 sec 2800pts) scaled 1.36
2 5000,0.01,13.34,9
3 1639,5
4 8.08113E-04,8.23073E-04,8.02505E-04,8.18394E-04,8.02370E-04
5 8.20005E-04,8.03703E-04,8.19427E-04,7.92800E-04,8.03090E-04
6 7.85301E-04,8.05999E-04,7.80552E-04,7.93134E-04,7.81818E-04
7 8.21790E-04,8.20319E-04,7.87454E-04,7.41411E-04,7.86812E-04
8 ....

```



Input File 4 Name: Case 1a.dyn

1 Austrian Dam California US: Austn-4 Lower\_Su=14+\*tan(22); using VERSAT-2D\_v.2021.10.23  
2 0,9.81,9.81,101.3,1  
3 7258,7072,4,7072  
4 3,0,0,1  
5 999,1,999,10  
6 7,2  
7 1,3,1,6,3656,1,3656,3,3656,4  
8 3656,6,5630,1,0,0,0,0,0,0  
9 5  
10 1,1  
11 7942,0.5,2647,0.5,21,500  
12 0,44,0,0,3,0  
13 0,0,0,0,0,0,0,0,0,0,0  
14 2,3  
15 18720,9360,25.5,0,0,0  
16 1,1.51,0.0011,0,0,0  
17 3,1  
18 7942,0.5,2647,0.5,21,500  
19 0,44,0,0,3,0  
20 0,0,0,0,0,0,0,0,0,0,0  
21 4,2  
22 20500,0,2647,0.5,22.4,500  
23 14,-0.404,-1,0,2,0  
24 5,2  
25 20500,0,2647,0.5,22.4,500  
26 14,-0.404,-1,0,2,0  
27 70, 312.00, 0.00  
28 1,63.1351,0.0000,-220.2389  
29 3,125.3588,0.0000,-437.2982  
30 5,123.5359,0.0000,-430.9391  
31 7,120.3186,0.0000,-424.6170  
32 10,118.5169,0.0000,-418.3318  
33 13,118.1094,0.0000,-412.0097  
34 17,116.2865,0.0000,-405.6506  
35 21,114.4636,0.0000,-399.2915  
36 26,112.6406,0.0000,-392.9324  
37 31,110.8177,0.0000,-386.5734  
38 36,107.7483,0.0000,-380.2512  
39 42,105.9466,0.0000,-373.9661  
40 48,105.3913,0.0000,-367.6440  
41 55,103.5683,0.0000,-361.2849  
42 62,101.7454,0.0000,-354.9258  
43 70,99.9225,0.0000,-348.5667  
44 78,98.0995,0.0000,-342.2076  
45 86,95.1780,0.0000,-335.8855  
46 95,93.3763,0.0000,-329.6004

47 104,92.6731,0.0000,-323.2782  
48 114,90.8502,0.0000,-316.9192  
49 124,89.0272,0.0000,-310.5601  
50 135,87.2043,0.0000,-304.2010  
51 146,85.3813,0.0000,-297.8419  
52 157,82.6077,0.0000,-291.5198  
53 169,80.8060,0.0000,-285.2346  
54 181,79.9549,0.0000,-278.9125  
55 194,78.1320,0.0000,-272.5534  
56 207,76.3090,0.0000,-266.1944  
57 221,74.4861,0.0000,-259.8353  
58 235,72.6632,0.0000,-253.4762  
59 249,70.0375,0.0000,-247.1541  
60 264,68.2357,0.0000,-240.8689  
61 279,67.2367,0.0000,-234.5468  
62 295,65.4138,0.0000,-228.1877  
63 311,63.5909,0.0000,-221.8286  
64 328,61.7679,0.0000,-215.4695  
65 345,59.9450,0.0000,-209.1105  
66 362,57.4672,0.0000,-202.7883  
67 380,55.6654,0.0000,-196.5032  
68 398,54.5186,0.0000,-190.1811  
69 417,52.6956,0.0000,-183.8220  
70 436,50.8727,0.0000,-177.4629  
71 456,49.0498,0.0000,-171.1038  
72 476,47.2268,0.0000,-164.7447  
73 496,44.8969,0.0000,-158.4226  
74 517,43.0951,0.0000,-152.1375  
75 538,41.8004,0.0000,-145.8153  
76 560,39.9775,0.0000,-139.4563  
77 582,38.1545,0.0000,-133.0972  
78 605,36.3316,0.0000,-126.7381  
79 628,34.5086,0.0000,-120.3790  
80 651,32.3266,0.0000,-114.0569  
81 675,30.5249,0.0000,-107.7717  
82 699,29.0822,0.0000,-101.4496  
83 724,27.2593,0.0000,-95.0905  
84 749,27.3463,0.0000,-88.4726  
85 775,27.1124,0.0000,-81.3372  
86 801,24.6476,0.0000,-73.9429  
87 828,22.1829,0.0000,-66.5486  
88 855,19.7181,0.0000,-59.1543  
89 883,17.2533,0.0000,-51.7600  
90 911,14.7886,0.0000,-44.3657  
91 940,12.3238,0.0000,-36.9714  
92 969,9.8591,0.0000,-29.5772  
93 999,7.3943,0.0000,-22.1829  
94 1029,4.9295,0.0000,-14.7886

95 1060,2.4648,0.0000,-7.3943  
96 1091,0.6162,0.0000,-1.8486  
97 1123,0.0000,0.0000,0.0000  
98 8  
99 1,-184.5,312  
100 2,-82.5,312  
101 3,6,309  
102 4,29,308  
103 5,55,293  
104 6,91,293  
105 7,177,284  
106 8,184.5,282  
107 1,2,-184.50,282.00,0,0,0  
108 2,2,-183.00,282.00,0,0,0  
109 ... node information continues  
110 7257,2,183.00,282.43,1,0,1  
111 7258,2,184.50,282.00,0,0,0  
112 1,5,4,0.00,7258,7257,7256,7256  
113 2,5,2,0.00,1,2,3,3  
114 ... element information continues  
115 7071,5,3,0.00,3717,3779,3780,3718  
116 7072,5,3,0.00,3780,3779,3841,3780

End of File: Case 1a.dyn

## Output File from Input File 4 for Earthquake Loading

File Name: Case 1a\_LomaPrietaEQ.LX\_dam\_0b.oud

```
1          *****
2          |
3          |
4          | versat-d2d: dynamic 2-dimensional
5          |       finite element analysis of continua
6          |
7          |       versions 1998 - 2013; 2016
8          |       2018.05 (PSPA)- 2021.06-sv
9          |
10         |       copyright (c) 1998-2021 Dr. G. Wu
11         |       copyright (c) 1998-2021 WGI
12         |       Wutec Geotechnical International
13         |
14         |       input: *.dyn; *.prx; *.ACX; (*.ACY;*.FXY;*.SIN)
15         |       output: *.oud; *.csv; *.oug; *.dis; *.sig
16         |       *.o21; *.o23; *.soil-strength.csv
17         |
18         | *****
19
20         compiled 2021.06.09; 670 MB; max size of [K], variables= 25600000  50400
21
22         Austrian Dam California US: Austn-4 Lower_Su=14+*tan(22); using VERSAT-2D_v.2021.10.23
23
24         *****
25         gravity is on (0=yes; 1=no)      0
26         gravity acceleration=           9.81
27         unit weight of water=           9.81
28         atmospheric pressure=            101.30
29         ichang=1: elastic non-linear analysis
30
31         number of nodes                  7258
32         number of elements                7072
33         number of nodes in an element(nnodel)4
34         number of elements having stresses 7072
35
36         INPUT BASE ACCELERATIONS(2=hor;3=hor&vert)=3
37         viscous damping (%) mass & stiffnes =0 1
38
39         time interval(s) for node/element response =999
40         time interval(s) for updating viscous damping=1
41         PWP not generated afte this time (sec) =999
42         static iterations at end of dynamic loads =10
43
44         total no. of time history output  7
45         List of node & element number for time history output
46         1  3
47         1  6
48         3656  1
49         3656  3
50         3656  4
```

Report No. WGI-220224  
February 24, 2022

51 3656 6  
52 5630 1  
53  
54  
55 total number of materials 5  
56 =====  
57 ky area i unit. w rr [C]\_a [C]\_b (beam)  
58 kb k-sh unit. w [C]\_a [C]\_b (elas)  
59 SOIL kb n kg m unit. w c phi/-k Rf Soil Shear Strength (ss): Mohr-Coulomb  
60 -----  
61 SAND 1 7942.00 0.50 2647.00 0.50 21.00 0.00 44.00 500.00 SAND Model: ss=f(current stresses, c, phi)  
62 ELAS 2 18720.00 9360.00 25.50 1.510 0.001100  
63 SAND 3 7942.00 0.50 2647.00 0.50 21.00 0.00 44.00 500.00 SAND Model: ss=f(current stresses, c, phi)  
64 CLAY 4 20500.00 0.00 2647.00 0.50 22.40 14.00 -0.40 500.00 CLAY Model: ss=f(pre-existing stresses, c,  
65 phi/k)  
66 CLAY 5 20500.00 0.00 2647.00 0.50 22.40 14.00 -0.40 500.00 CLAY Model: ss=f(pre-existing stresses, c,  
67 phi/k)  
68  
69  
70 \*\*\*\*\* PWP parameters \*\*\*\*\*  
71 (SAND) No. , 1  
72 PWP Model Type: Wu model ,M=0  
73 No PWP: Soil Dry, 0  
74 Vol. strn constant C1 =, 0  
75 Vol. strn constant C2 =, 3  
76  
77 (SAND) No. , 3  
78 PWP Model Type: Wu model ,M=0  
79 No PWP: Soil Dry, 0  
80 Vol. strn constant C1 =, 0  
81 Vol. strn constant C2 =, 3  
82  
83 \*\*\*\*\*  
84  
85 Loma Prieta, 10/18/1989, Los Gatos - Lexington Dam, 0 ACCELERATION in G (0.01 sec 2800pts) scaled 1.36  
86 number of time increments used in analysis=5000  
87 maximum allowed time increment (nmaxeq) =100000  
88 time increment (sec) =0.01  
89 number of sub time step(0,1,2,3,4) nrsub =9  
90 input data are multiplied; & sf\_EQ =13.34 1  
91 number of lines in the input data(\*.ACX) =1639  
92 numbers per line =5  
93  
94 Loma Prieta, 10/18/1989 Los Gatos - Lexington Dam UP ACCELERATION in G NPTS= 8192 DT= .0100 SEC scale  
95 factor 1.36  
96 input data for vertical scaled by & sf\_EQ =13.34 1  
97 note: time increment of vert. motion is treated as the same as for hori. motion  
98 number of lines in the input data (vert.) =1639  
99 numbers per line =5  
100 peak scaled acceleration in record (hori. & vert.) =5.906 1.910  
101 peak accelerations used in analysis (hori.&vert.) = 0.602g 0.195g  
102  
103  
104 number of nodes having loads (nl)=70 & ywt0(>0 to update water loads)=312  
105 node nodal load: fx, mxy fy

```

106      1  63.1351 0.0000 -220.2389
107      3 125.3588 0.0000 -437.2982
108      .... Echo of input data continues....
109      1060  2.4648 0.0000 -7.3943
110      1091  0.6162 0.0000 -1.8486
111      1123  0.0000 0.0000 0.0000
112
113      number of points defining a water table (nwat)= 8
114      point  x-coor; y-coor of water table
115      1  -184.50  312.00
116      2  -82.50  312.00
117      3   6.00  309.00
118      4   29.00  308.00
119      5   55.00  293.00
120      6   91.00  293.00
121      7  177.00  284.00
122      8  184.50  282.00
123
124      net degrees of freedom= 14022 bandwidth=126
125      lband*(nnet-1)+1= 1766647 < ak dimension 25600000
126      **ichang=1: pwp computed but not used in the analysis
127
128      number of nodes with free field stress boundary=0
129
130      =====
131      state at the end of earthquake, except PEAKgamm_max, including static @ time=49.9910 sec
132      =====
133      -----
134      node disp-x disp-y acc-x(g) acc-y(g) elem sig-x(mx0) sig-y(ta) tauxy(sh.) gamm_xy%(mj) PEAKgamm_max(%) vol(%)
135      ppr(FSlig)
136      -----
137      1  0.0000 0.0000 0.0000 0.0000    1 11.96 11.84 14.11 5.951 5.969 0.00 0.00 ppr
138      2  0.0000 0.0000 0.0000 0.0000    2 -0.71 -4.71 -0.24 0.000 0.000 0.00 0.00 ppr
139      3  0.0000 0.0000 0.0000 0.0000    3 -2.00 -7.03 -0.85 0.000 0.000 0.00 0.00 ppr
140      4  0.0000 0.0000 0.0000 0.0000    4 -17.36 -9.55 11.00 7.921 8.169 0.00 0.00 ppr
141      5  0.0000 0.0000 0.0000 0.0000    5 -31.45 -18.56 11.97 11.453 11.852 0.00 0.00 ppr
142
143      ... output continues..
144      3656 -0.1951 -0.7699 0.0000 0.0000    3656 -483.53 -518.61 176.85 0.626 0.935 0.00 0.00 ppr
145      ... output continues..
146      7257 0.0257 0.0019 0.0000 0.0000
147      7258 0.0000 0.0000 0.0000 0.0000
148
149      =====
150      peak dynamic response between 0.0 to 49.9910 sec
151      =====
152      -----
153      node disp-x disp-y acc-x(g) acc-y(g) elem sig-x(mx0) sig-y(ta) tauxy(sh.) gamm_xy%(mj) DynStressRatio vol(%)
154      ppr(FSlig)
155      -----
156      1  0.0000 0.0000 0.6021 0.1947    1 14.75 14.75 14.75 5.953 -6.767 0.00 0.00 ppr
157

```

158 2 0.0000 0.0000 0.6021 0.1947 2 -1.08 -5.64 -3.44 0.000 -0.747 0.00 0.00 ppr  
159 3 0.0000 0.0000 -0.6021 -0.1947 3 -7.90 -11.73 -9.22 0.001 -1.308 0.00 0.00 pp  
160 .... Output continues ....  
161 7249 0.1687 0.0112 0.5349 -0.2577  
162 7250 0.2331 0.0299 0.5390 -0.3107  
163 7251 0.0000 0.0000 0.6021 0.1947  
164 7252 0.1107 0.0146 -0.5428 -0.2709  
165 7253 0.1584 0.0277 0.5344 -0.3132  
166 7254 0.0000 0.0000 0.6021 0.1947  
167 7255 0.0806 0.0156 -0.5502 -0.3736  
168 7256 0.0000 0.0000 0.6021 0.1947  
169 7257 0.0257 0.0019 -0.5774 -0.3609  
170 7258 0.0000 0.0000 0.6021 0.1947  
171

End of File: Case 1a\_LomaPrietaEQ.LX\_dam\_0b.oud





**APPENDIX E      FULL SIZE FIGURES**

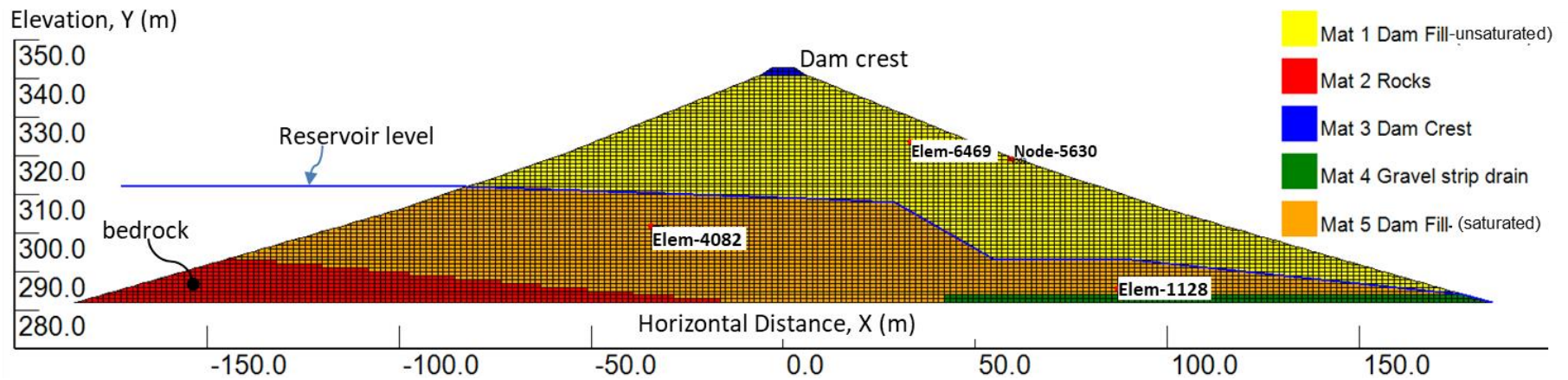


Fig. 6 VERSAT finite element model

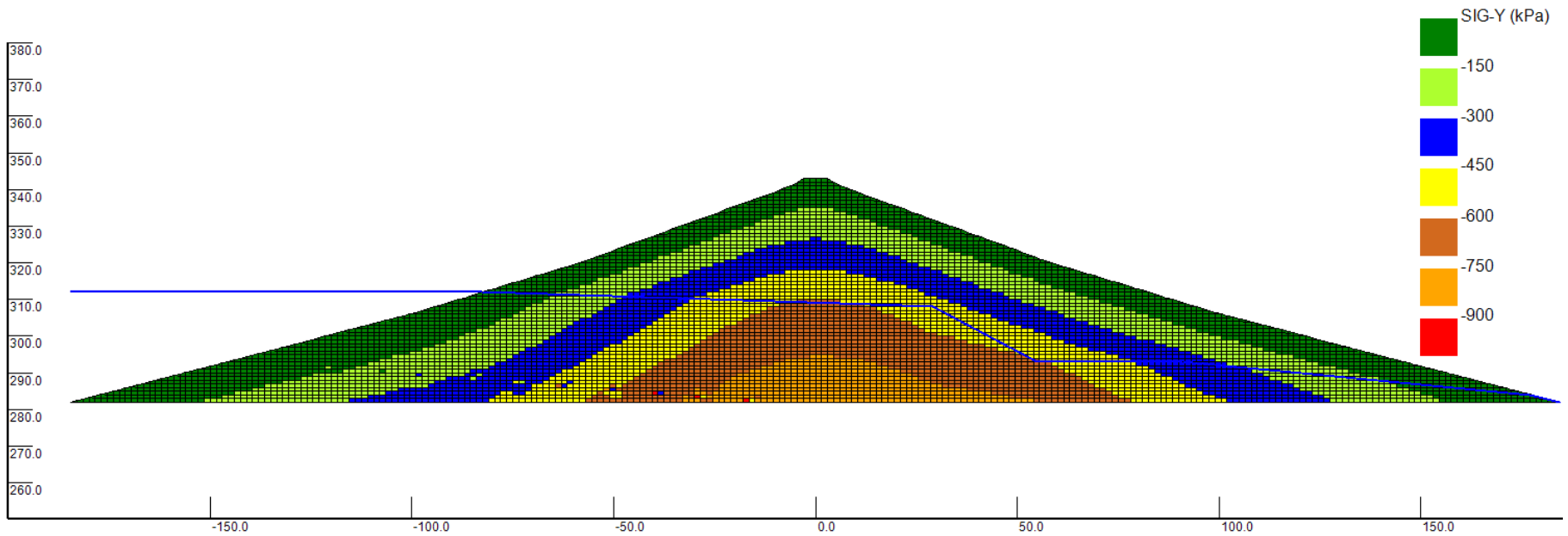


Fig. 7(a) Static effective vertical stresses, SIG-Y

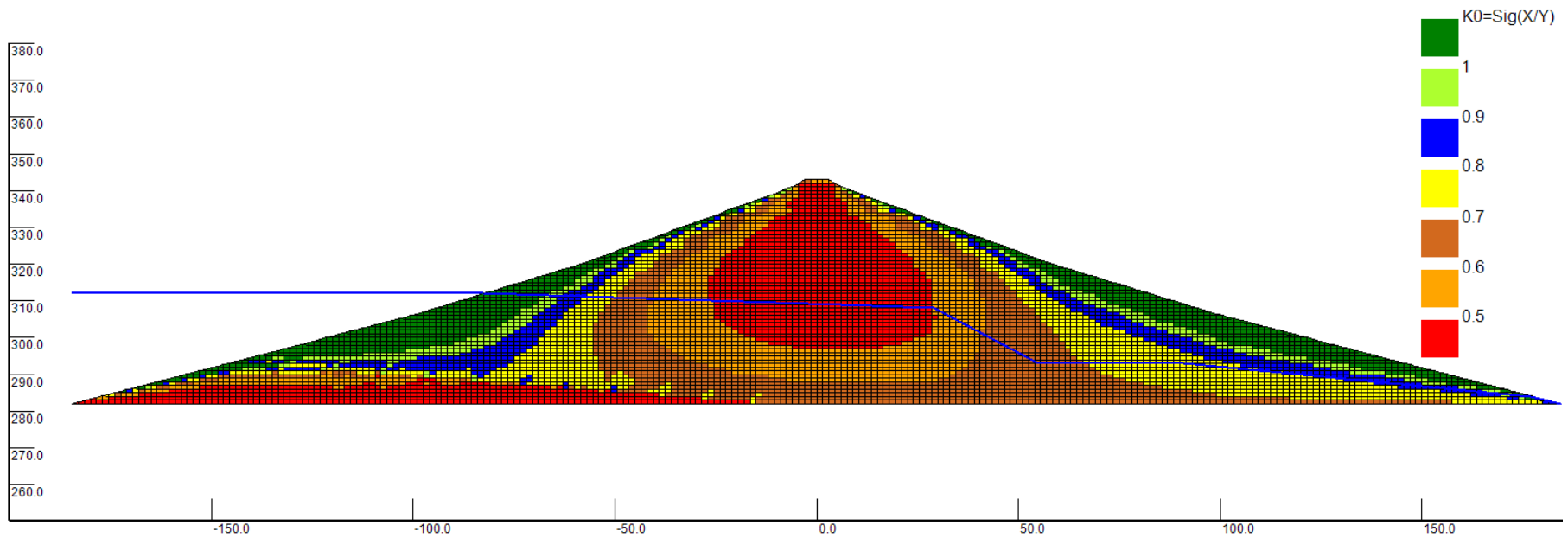


Fig. 7(b) ) Static effective horizontal stress coefficient, SIG-X / SIG-Y

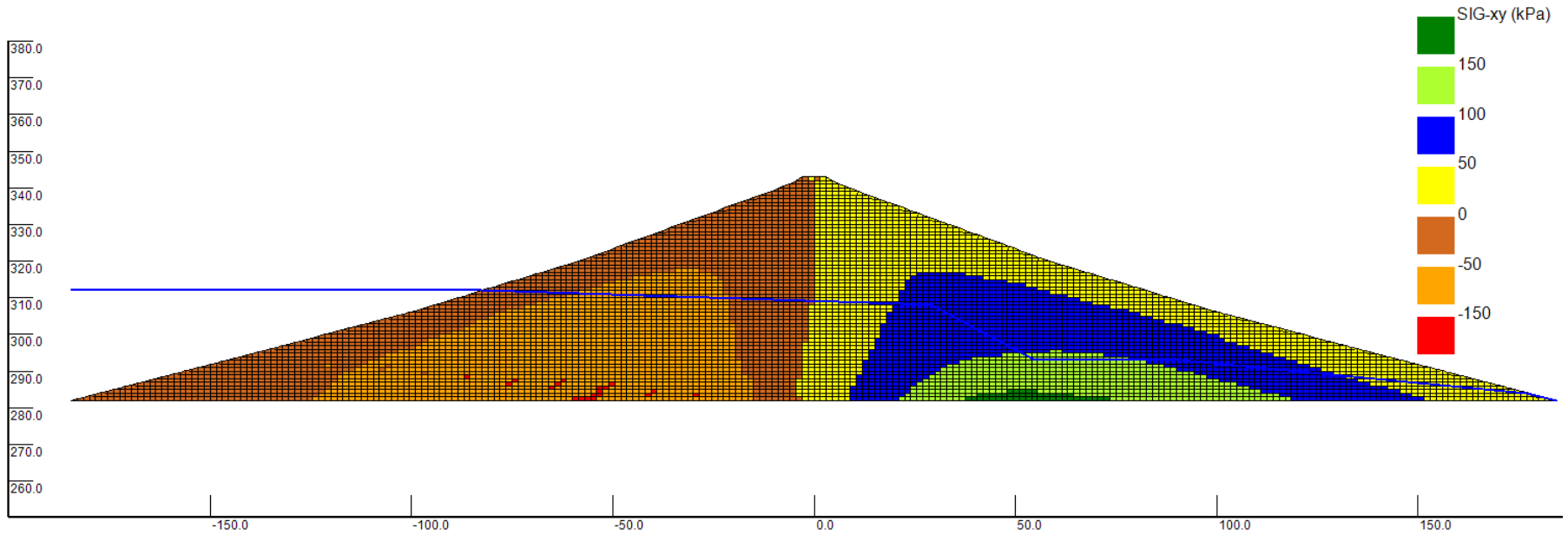


Fig. 7(c) static shear stresses

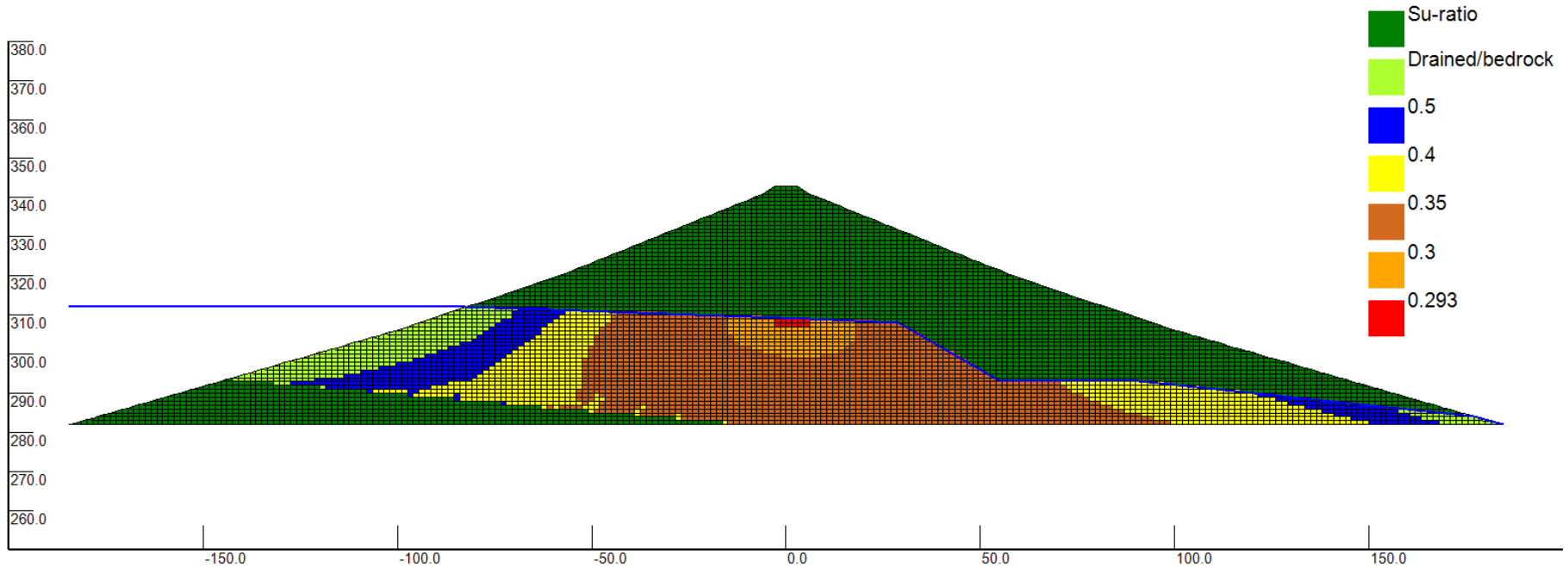


Fig. 8 Undrained shear stress ratio,  $S_u/SIG-Y$

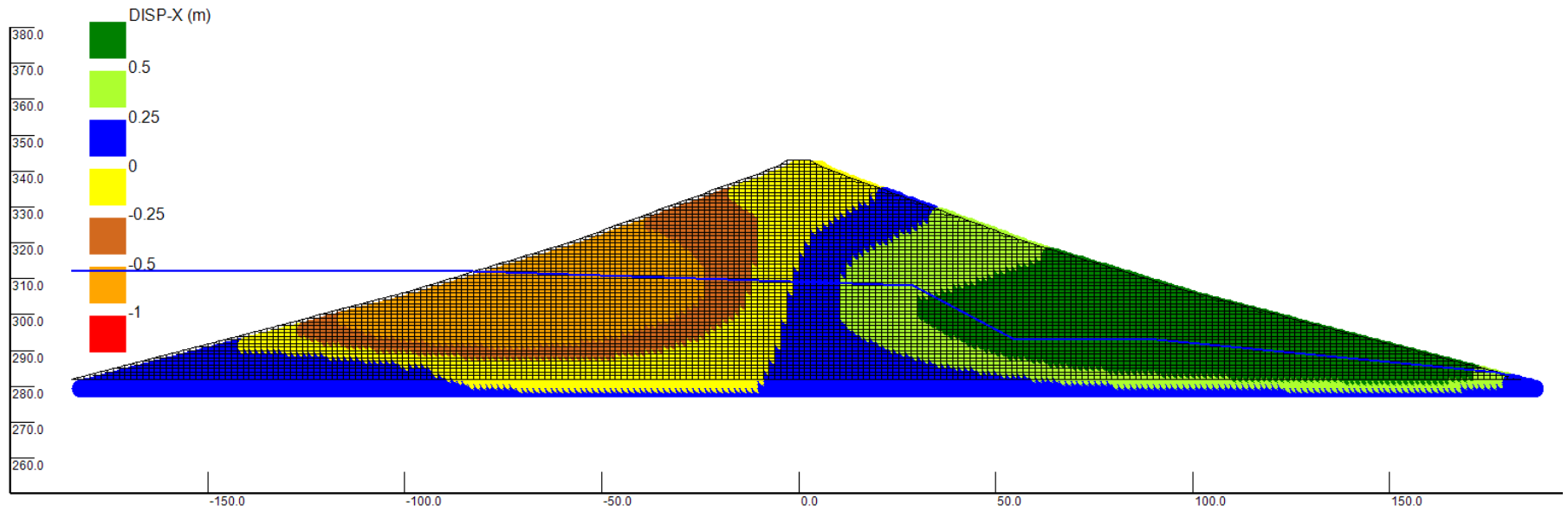


Fig. 12(a) Displacement X for Case 1a

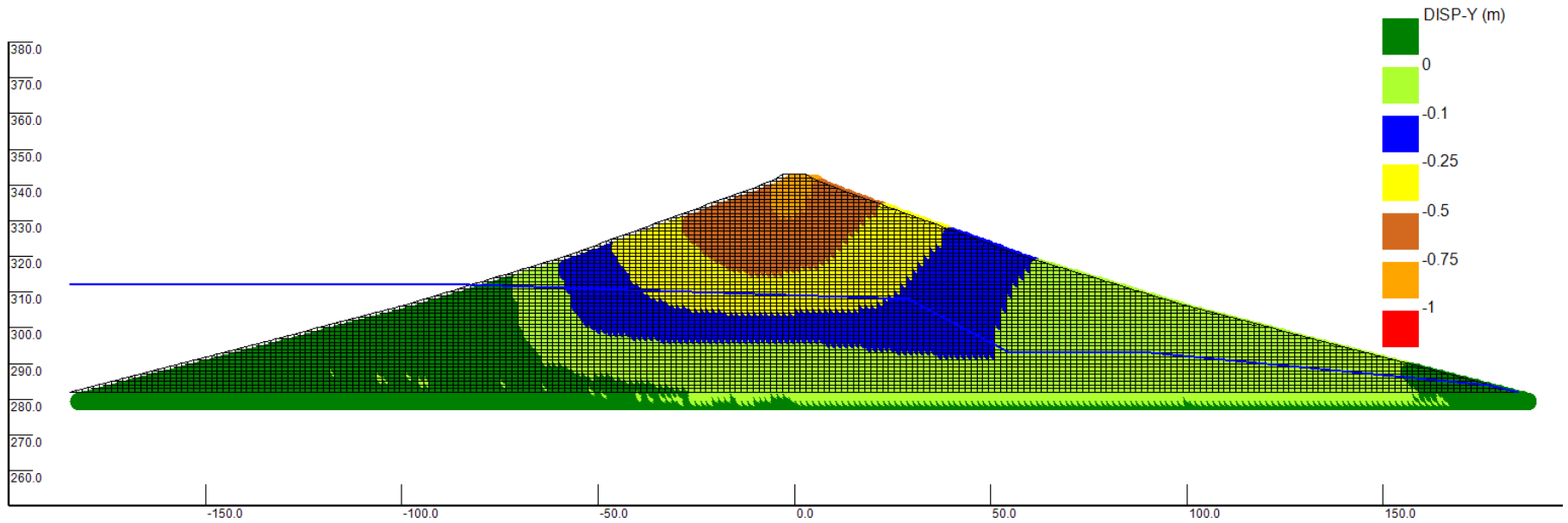


Fig. 12(b) Displacement Y for Case 1a



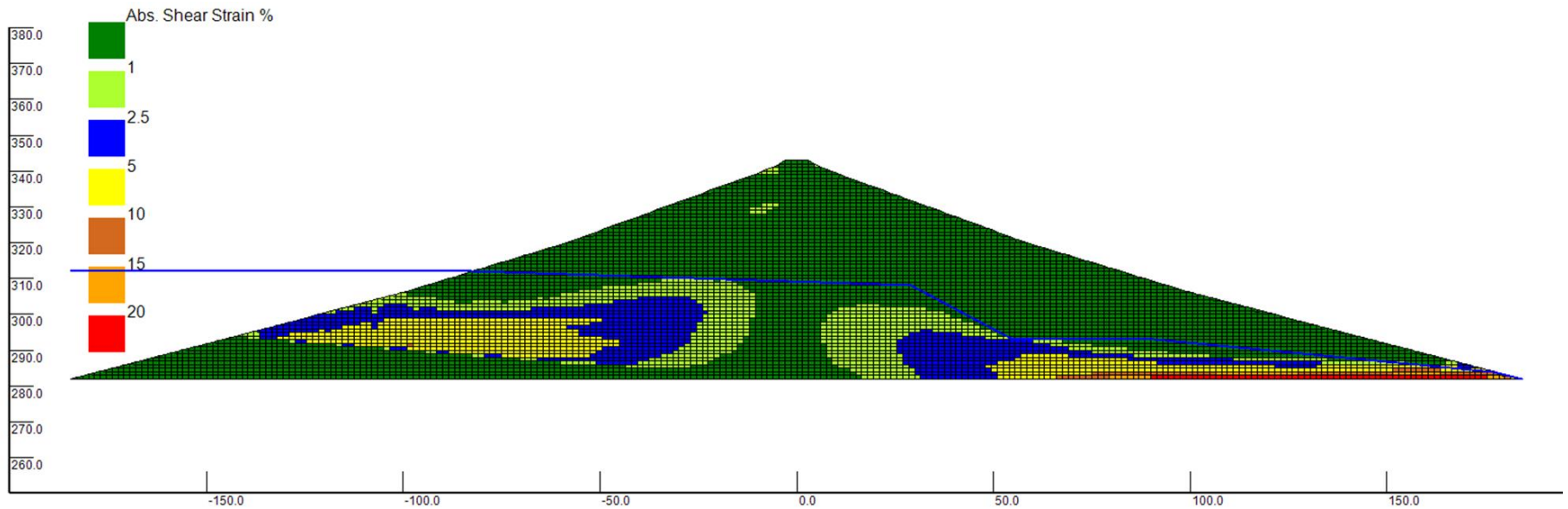


Fig. 13 Absolute of shear strains ( $\gamma_{xy}$ ) at end of earthquake shaking for Case 1a

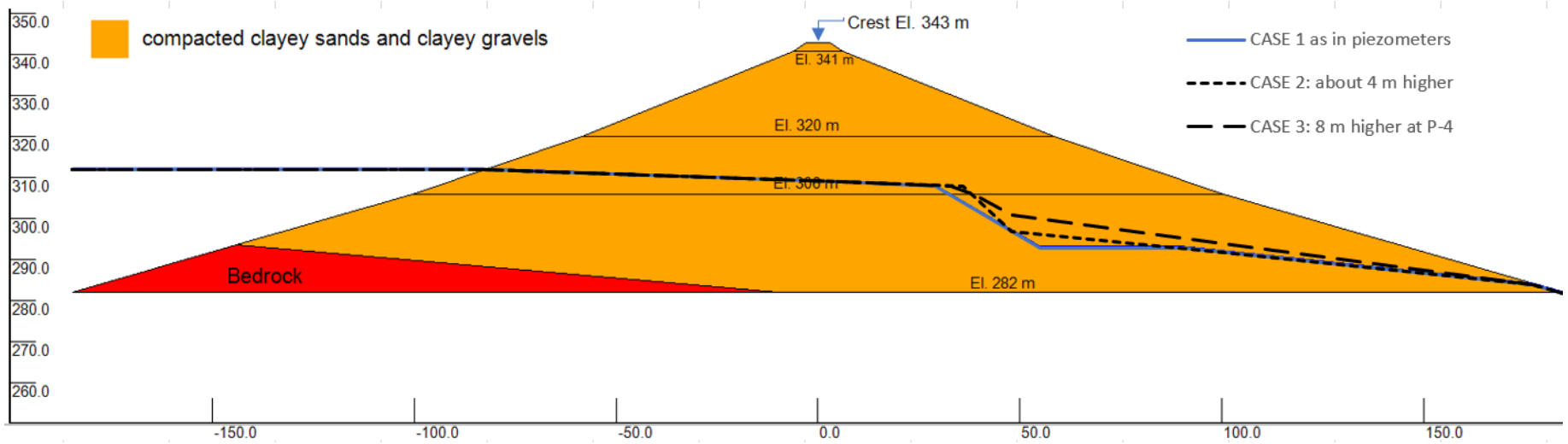


Fig. 19 Phreatic surfaces in the dam used in Cases 1, 2 and 3

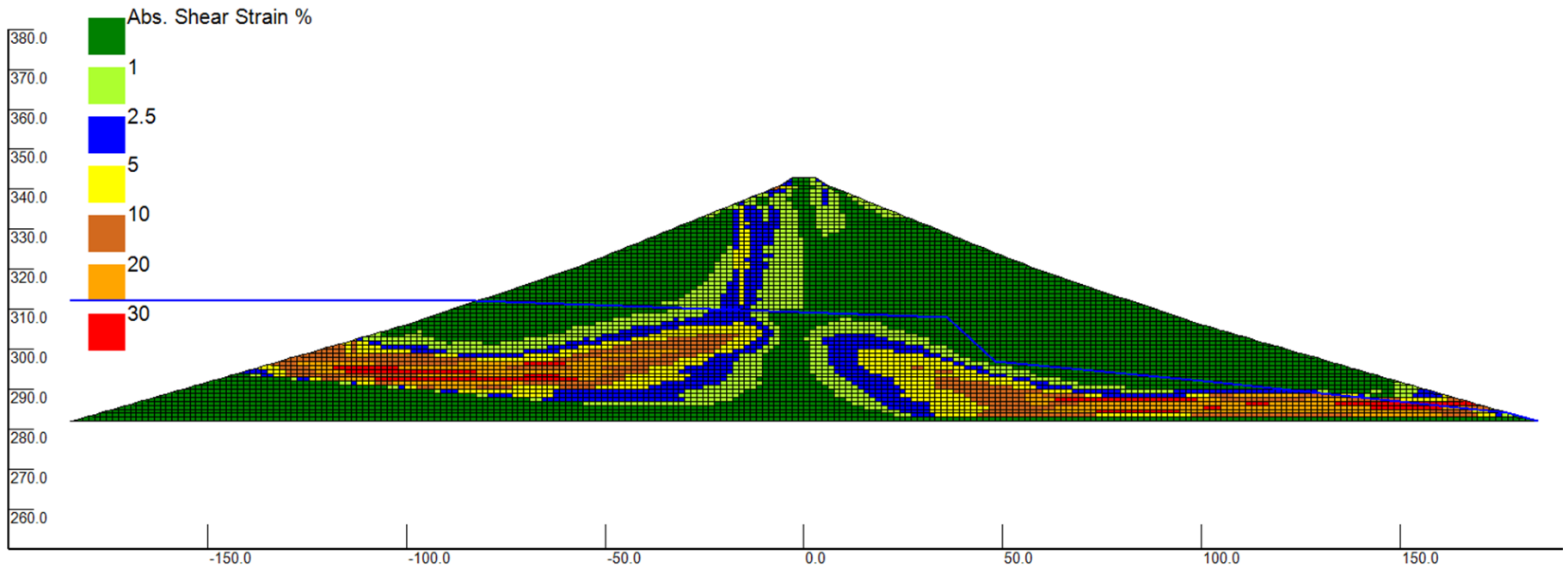


Fig. 21(a) Absolute of shear strains ( $\gamma_{xy}$ ) at end of earthquake shaking for Case 2b using c- $\phi$  approach

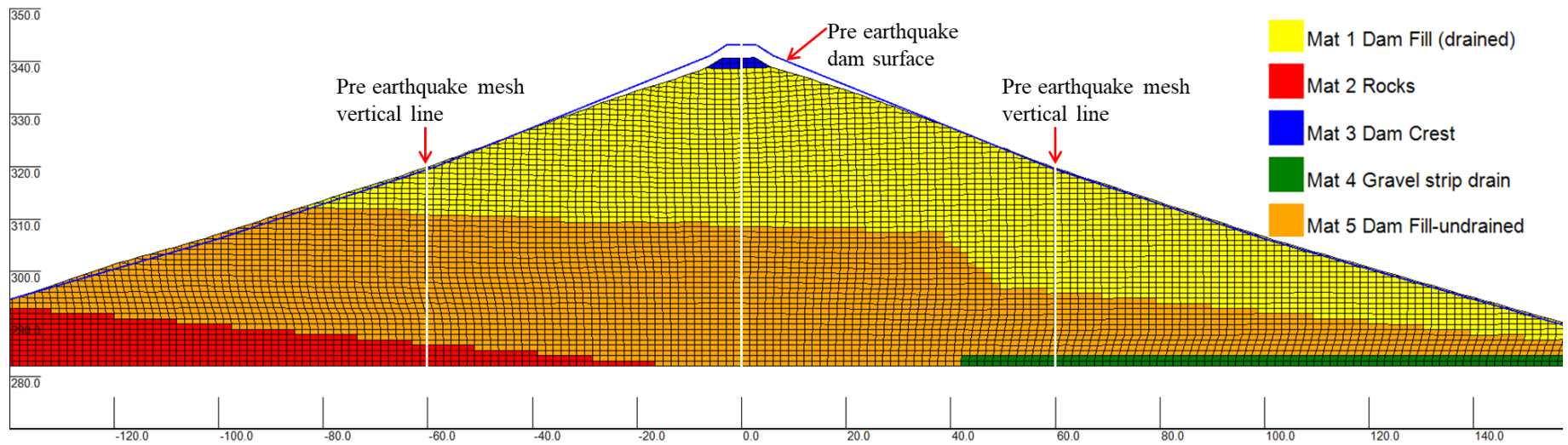


Fig. 21(b) Deformed dam at end of earthquake shaking for Case 2b using  $c-\phi$  approach (dam crest settlement of 2.4 m)